2014

Apelin Regulation of K-Cl Cotransport in Vascular Smooth Muscle Cells.

Neelima Sharma
Wright State University

Apelin Regulation of K-Cl Cotransport in Vascular Smooth Muscle Cells

A dissertation submitted in partial fulfillment of the
requirements for the degree of
Doctor of Philosophy

By

Neelima Sharma
M.A., Case Western Reserve University, 2006

2014
Wright State University

WRIGHT STATE UNIVERSITY
GRADUATE SCHOOL

May 27th, 2014

I HEREBY RECOMMEND THAT THE DISSERTATION PREPARED UNDER MY SUPERVISION BY Neelima Sharma ENTITLED Apelin Regulation of K-Cl Cotransport in Vascular Smooth Muscle Cells BE ACCEPTED IN PARTIAL FULFILLMENT OF THE REQUIREMENTS FOR THE DEGREE OF Doctor of Philosophy.

_____
Norma C. Adragna, Ph.D.
Dissertation Director

_____
Mill W. Miller, Ph.D.
Director, Biomedical Sciences
Ph.D. Program

_____
Robert E. W. Fyffe, Ph.D.
Vice President for Research and
Dean of the Graduate School

Committee on Final Examination

_____
Norma C. Adragna, Ph.D.

_____
Peter K. Lauf, M.D.

_____
Lawrence J. Prochaska, Ph.D.

_____
David R. Cool, Ph.D.

_____
Mauricio Di Fulvio, Ph.D.

ABSTRACT

Sharma, Neelima. Ph.D., Biomedical Sciences Ph.D. Program, Wright State University, 2014. Apelin Regulation of K-Cl Cotransport in Vascular Smooth Muscle Cells.

Atherosclerosis and high circulating levels of oxidized low density lipoproteins (oxLDL) are considered among the most important risk factors for the occurrence and development of cardiovascular disease (CVD). During the atherosclerotic lesion repair, phenotypic transition of vascular smooth muscle cells (VSMCs) from contractile to synthetic states plays a central role. In this process, enhanced proliferation/migration of VSMCs, from the *tunica media* to the *intima*, is required to sustain blood vessel endothelium integrity, and for inducing vessel wall remodeling in response to injury. At the molecular level, the activity of electroneutral potassium-chloride cotransporters or KCCs, is necessary to: a) allow changes in cell volume (key prerequisites to coordinate cell proliferation/migration) and b) sustain normal cardiovascular function. Stimulation of the adipokine apelin and its receptor APJ (apelin/APJ) signaling pathway has been shown to protect against atherosclerotic lesion formation by lowering blood pressure levels and promoting vasodilation. Upon binding to APJ, apelin promotes nitric oxide (NO)-mediated vasodilation, and cell proliferation via the PI3K/Akt and MAPK pathways. Apelin/APJ exert its action through the same

signaling pathways regulating the KCCs. However, the mechanisms of KCC regulation by apelin/APJ remain to be determined. Thus, we hypothesized that KCC expression and activity play an important role during VSMCs' phenotypic transition and could be involved in the apelin/APJ cardioprotective effects. In addition, it is possible that the apelin-mediated effect on KCC activity could also be dependent on factors affecting the transporter, such as, serum, ionic strength, osmolality, cell proliferation and migration.

This hypothesis will be tested using rat aortic VSMCs that were immunologically validated by specific markers. KCC activity was measured by atomic absorption spectrophotometry using rubidium as a potassium (K^+) congener. KCC expression and transport activity were characterized with respect to the VSMC phenotypes, in the presence or absence of apelin and corresponding inhibitors of the signaling pathways, oxLDL and as a function of the various aforementioned physiological factors.

While markers for the contractile VSMC phenotype are well known, they are less defined for the early and late synthetic ones. In the present study, we showed a decrease in expression levels of cytoskeletal proteins like α-actin, desmin and vimentin in late synthetic VSMCs compared to early states suggesting that the latter show similar characteristics to the contractile phenotype. In addition, KCC1 and KCC4 protein expression and overall KCC activity increased in late *vs* early synthetic VSMCs. The ion binding affinity (K_m) for late and early synthetic VSMCs was similar for K^+ whereas it decreased for Cl^-. Whether the increase in KCC activity in late synthetic VSMCs is due to turnover changes of pre-existing KCCs

or enhanced membrane trafficking/insertion of *de novo* synthesized KCC protein remains to be studied. Using selective inhibitors, we showed that apelin-mediated activation of KCCs occurs through the NO/sGC/PKG pathway in contractile, and by PI3K/Akt and MAPK dependent pathway(s) in synthetic VSMCs. Furthermore, apelin rescued the inhibition of KCC induced by oxLDL in contractile VSMCs. We also showed that the apelin-mediated activation of KCCs is dependent on extracellular sodium, osmolality, presence of serum in the growth media, VSMCs phenotype (contractile *vs* synthetic), and passage number. Altogether, our results identify apelin/APJ as an important modulator of KCC activity to sustain cell volume regulation and overall vascular function.

TABLE OF CONTENTS

LIST OF FIGURES

LIST OF TABLES

LIST OF ABBREVIATIONS

1^o	Primary
2^o	Secondary
ANOVA	Analysis of variance
APJ	Apelin receptor
APLN	Apelin gene
Ang II	Angiotensin II
AT_1	Angiotensin II receptor, type 1
ATP	Adenosine 5'-triphosphate
BSA	Bovine Serum Albumin
CCC	Cation-Chloride Cotransporter
CD-36	Cluster of Differentiation 36
COT	Cotransport / Cotransporter
cDNA	Complimentary DNA
DAPI	4',6'-diamidino-2-phenylindole
DMEM	Dulbecco's modified Eagle's medium
DNA	Deoxyribonucleic Acid
DTT	Dithiothreitol
EDTA	Ethylenediaminetetraacetic acid
EGF	Epidermal Growth Factor

eNOS	Endothelial Nitric Oxide Synthase
ERK	Extracellular Signal Regulated Kinase
FBS	Fetal Bovine Serum
FITC	Isothiocyanate form of fluorescein
GPCR(s)	G protein-coupled receptor(s)
HBS	HEPES buffered saline
HBSS	HEPES buffered saline solution
HEPES	N-2-hydroxyethylpiperazine-N'-2-ethanesulfonic acid
HDL	High Density Lipoprotein
hr	Hour
IgG	Immunoglobulin gamma
IGF	Insulin-like growth factor
kb	Kilobase
KCC	Potassium-Chloride Cotransport
KT5823	Inhibitor of protein kinase G (PKG)
LDL	Low Density Lipoprotein
LOX-1	Lectin-like oxidized low-density lipoprotein (LDL) receptor-1
LY294002	Potent inhibitor of phosphoinositide 3-kinases (PI3Ks)
MAPK	Mitogen-Activated Protein Kinase
MEK	MAPK kinase
min	Minutes
mM	Millimolar
mRNA	messenger RNA

mOSM	Milliosmoles
MOPS	3-Morpholinopropanesulfonic acid
Na/K	Sodium/Potassium Pump
NCBI	National Center for Biotechnology Information
NCC	Sodium-Chloride Cotransport
NKCC	Sodium-Potassium-Chloride Cotransport
NMDG	N-methyl D-Glucamine
NO	Nitric Oxide
NOS	Nitric Oxide Synthase
oGPCR	Orphan G Protein-Coupled Receptor
Osm	Osmolality
OSRI	Oxidative Stress-Responsive Kinase-1
oxLDL	Oxidized Low Density Lipoprotein
PBS	Phosphate Buffered Saline
PCA	Perchloric Acid
PCR	Polymerase Chain Reaction
PD98059	A potent and selective inhibitor of MAP kinase kinase
PKA	cAMP-dependent protein kinase A
PDGF	Platelet-Derived Growth Factor
pH	Log of the reciprocal of the hydrogen ion concentration
PKB	Protein Kinase B
PKG	cGMP-dependent protein kinase G
PI3K/Akt	Phosphatidylinositol 3-Kinase/Protein Kinase B

PP	Protein Phosphatase
RNA	Ribonucleic Acid
Rb^+	Rubidium
rpm	Revolutions Per Minute
sGC	Soluble Guanyl Cyclase
SLC	Solute Carrier Family
SD	Standard Deviation
SDS	Sodium Dodecyl Sulfate
SDS-PAGE	Sodium Dodecyl Sulfate-Polyacrylamide Gel Electrophoresis
sec	Seconds
SEM	Standard Error of Mean
Sf^-	Sulfamate
SMC	Smooth Muscle Cell
SPAK	STE20/SPS1-related proline/alanine-rich kinase
Ste20	Sterile 20
TBST	Tris buffered saline with Tween 20
TE	Tris EDTA
TM	Transmembrane
Tris	Trizma base
VSMCs	Vascular Smooth Muscle Cells
WB	Western blot
WNK	With no lysine kinase
x g	Centrifugal Force

ACKNOWLEDGEMENTS

I would like to recognize the tremendous amount of support and guidance that I received over the past years from my advisor Dr. Norma Adragna and co-advisor Dr. Peter Lauf. I am grateful for their incomparable mentorship and for letting me work in their laboratory, where I gained valuable knowledge on Cell Biophysics research.

I would also like to thank my committee members: Dr. Lawrence Prochaska, Dr. David Cool and Dr. Mauricio Di Fulvio for their insights and suggestions that contributed to the quality of this project. Special thanks to Ms. Kathleen Leonard for her technical assistance and training. In addition, I would like to acknowledge Dr. Gerald Alter, Dr. Mill Miller and Ms. Karen Luchin for their unwavering support and encouragement.

I am thankful for the funding support provided by the Biomedical Sciences Ph.D. program and to the department of Pharmacology and Toxicology and Graduate Student Assembly (GSA) for their resources and support.

I am grateful to my friends Khadijeh Alnajjar, Marjorie Markopoulos, Arathi Paluri and Ben Penry at Wright State University for their warm-hearted companionship. A heartfelt appreciation to Aunt Pamela Mackey, my sister and friend Chinyere

Amaefule, Betsy Salt and Mr. Charles Salt for their continuous motivation and blessings.

Finally, I am indebted to my late grandparents, parents, uncle and brothers for all their love, care, and inspiration in the pursuit of my educational goals. Special thanks to José Ponce for his moral support, encouragement and for instilling faith and confidence.

DEDICATION

I dedicate this dissertation to my family for their unconditional love and moral support. I love you all very much.

INTRODUCTION

Cardiovascular disease

Cardiovascular disease (CVD) is the leading cause of mortality worldwide (1-3). It has been estimated that CVD is responsible for over thirty percent of global deaths and billions of dollars are being spent on its prevention and treatment (4). CVD includes a number of health problems that affect heart and/or blood vessels function. Ischemic heart disease and stroke are among the most predominant CVDs. According to the World Health Organization (WHO), they are responsible for over 13 million deaths a year (5).

Among the several risk factors that lead to CVD, atherosclerosis (hardening and narrowing of the blood vessels) plays a pivotal role (6). In brief, endothelial dysfunction, loss of contractility of vascular smooth muscle cells (VSMCs) combined with improper handling of low density lipoproteins (LDL) and increased oxidative stress, result in luminal narrowing and concomitant inflammatory events. In sum, these processes trigger sub-endothelial accumulation of oxidized low density lipoproteins (oxLDL), macrophage infiltration and lesion formation (foam cell appearance and atherosclerotic plaques) (7) (**Figure 1**).

Since damaged endothelium of blood vessels plays a key role in the occurrence and developing of atherosclerosis, a brief description of blood vessels' architecture and VSMCs function will be provided.

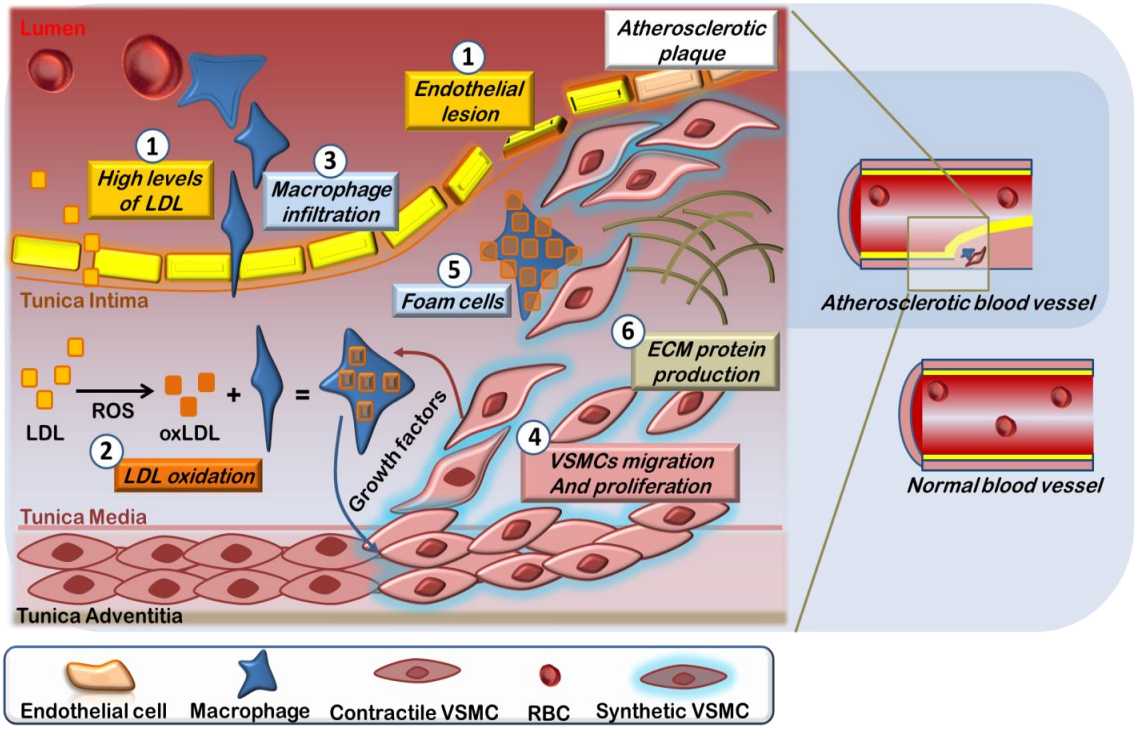

Figure 1. Events leading to atheroscleotic plaque formation. Atherosclerosis is the underlying cause of CVD resulting from processes involving endothelial dysfunction, accumulation of oxLDL, migration of VSMCs, and infiltration of macrophages among others. Figure modified with permission from (reference # 8, Madamanchi,N.R. 2005).

Blood vessels' architecture

Blood vessels are located throughout the body, and are hollow tubes that circulate blood to different organs. Functional blood vessels require the formation of endothelial tubes and recruitment of smooth muscle cells around these endothelial cells to form a multilayered vessel wall (9). Structurally, blood vessels are mainly composed of three concentric layers also called "*tunica*". The innermost layer is the "*intima*", the middle one is called "*media*" and the most exterior one called "*adventitia*". The intima outlines the lumen of the vessel wall. This layer is in direct contact with red blood cells and forms a slick surface to minimize friction against blood flow. The normal intima of large arteries, like the aorta, has a continuous endothelial monolayer seated on a basement membrane, separated from the media by the internal elastic lamina (10). The tunica media consists of VSMCs, macrophages, and fibroblasts (11). The media is very elastic and primarily composed of VSMCs arranged circumferentially. The muscle relaxes to vasodilate and contracts to vasoconstrict the vessel. This allows the regulation of blood flow. Outside of the tunica media is the adventitia that is separated from the media by the external elastic lamina. The outermost layer, adventitia, consists of connective tissue made up of fibroblasts and nerve fibers (12). The strong connective tissue supports and strengthens the vessel, connecting it to nearby structures (**Figure 2**).

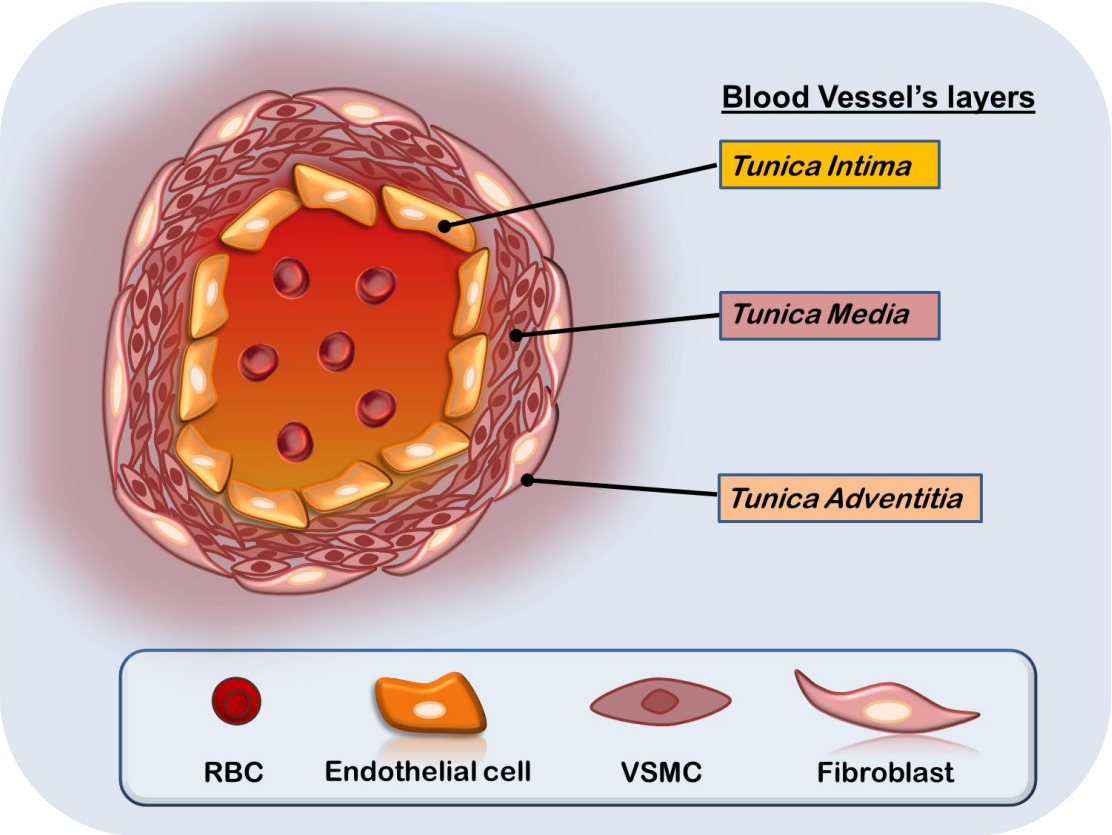

Figure 2. Composition of vascular wall. Functional blood vessels require the formation of endothelial tubes and recruitment of smooth muscle cells around these endothelial cells to form a multilayered vessel wall. The tunica *intima*, tunica *media*, and tunica *externa* (*adventitia*), are the three basic concentric layers of the arterial wall.

One important feature of the *tunica media* is its elasticity. When VSMCs relax/shrink, vasodilation is promoted, whereas when they contract/swell, vasoconstriction is sustained (13, 14). Regulation of cell volume is necessary to coordinate vasoconstriction/vasodilation events in order to sustain vascular tone and proper blood flow (**Figure 3**).

Vascular smooth muscle cells

VSMCs constitute the major component of the blood vessels' *tunica media*. By controlling changes in their cell volume; they are responsible for modulating vessel luminal diameters and thus vascular tone (**Figures 2 and 3**). The structural integrity of VSMC is maintained by various components. The plasma membrane contains multiple invaginations, called caveola. These caveolae enclose molecules essential for the initiation of signal transduction (15). Gap junctions in the periphery connect adjacent smooth muscle cells allowing the transmission of signals from cell to cell (16). A large portion of cytoplasmic volume is taken up by actin and myosin molecules, and the interactions of these filaments modulate the contraction of the smooth muscle. In VSMCs, α-actin is the prevalent actin filament isoform, a component of the contractile machinery (17, 18). Furthermore, intermediate filaments such as desmin and vimentin also play a key role in the coordinated relaxation and contraction of VSMCs (19). Thus, the coordinated interaction between the contractile machinery and cytoskeleton enables cells to elongate or shorten as needed.

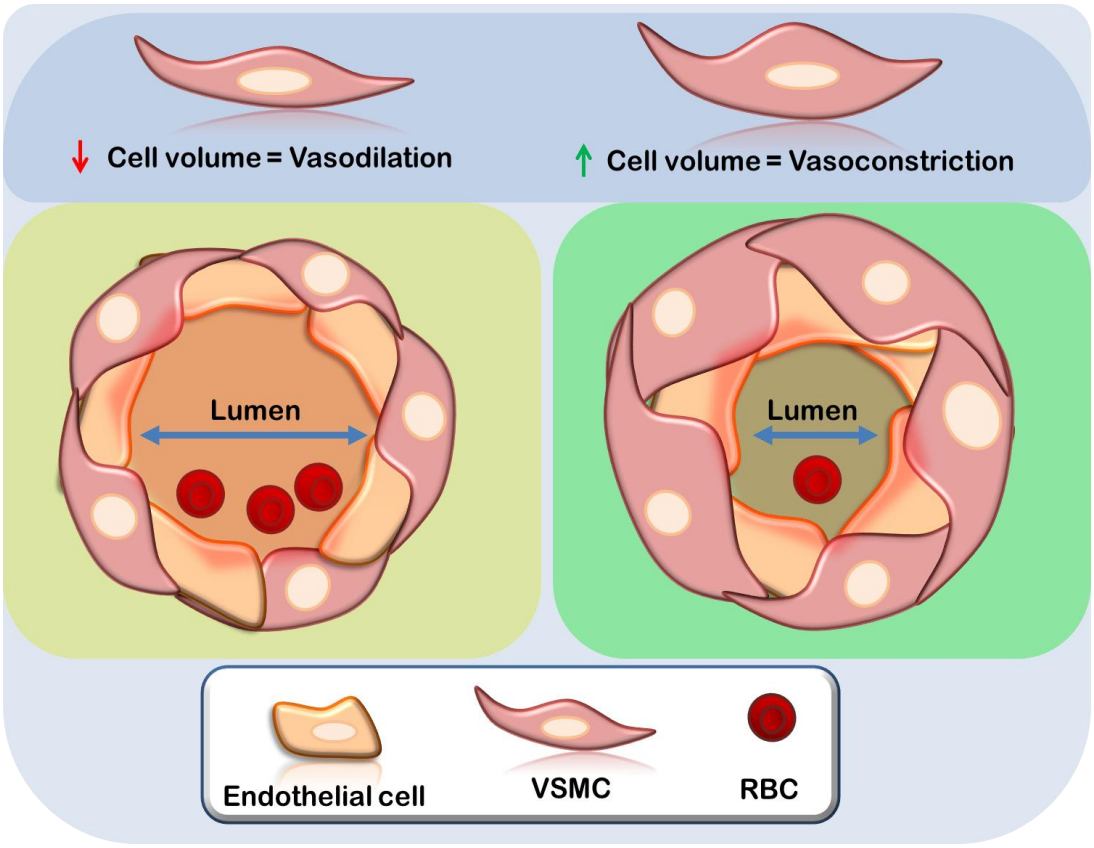

Figure 3. VSMCs regulate the vessel luminal diameter. VSMCs are elastic in nature and necessary for proper vascular tone (vasoconstriction/vasodilation) VSMCs are responsible for controlling the diameter of blood vessels by changes in their cell volume.

VSMCs participate in atherosclerotic lesions due to their remarkable capacity to migrate and proliferate. VSMCs uniqueness relies in their two extreme phenotypes: contractile and synthetic, with intermediate phenotypes in between (20-22). VSMCs undergo phenotypic modulation, especially during vascular injury (**Figure 1**). The contractile phenotype of VSMCs, which is required to allow vasodilation and vasoconstriction, is characterized by a robust NO-signaling casacade. It consists of the nitric oxide (NO)/soluble guanylate cyclase (sGC)/protein kinase G (PKG) pathway involved in vasodilation and vasoconstriction (23-25). In contrast, the synthetic phenotype, predominantly expressed in diseased blood vessels, is characterized by an impaired NO pathway and overexpression of the mitogen activated protein kinase (MAPK) and phosphatidylinositol-3-kinase (PI3K)/protein kinase B/Akt pathways both involved in cell proliferation. The differences in expression of protein markers, signaling molecules, and rate of proliferation and migration determine the VSMCs phenotypes (13). The transition from contractile to synthetic favors vascular remodeling and makes VSMCs an important model system to study atherosclerosis (23, 26, 27).

Due to their remarkable capacity to migrate, proliferate and differentiate into extreme different phenotypic states (contractile and synthetic); VSMCs also play an important role in the repairing of atherosclerotic lesions (20-22). When atherosclerotic lesions occur, transition from a “contractile” to a “synthetic state” facilitates proliferation and cell migration. Failure to switch back to a contractile state accelerates atherosclerotic lesion progression. The phenotypic transition in

VSMCs involves different protein expression profiles that are required to sustain and restore vascular function and cell contractibility (**Figure 1**). Under normal conditions, VSMCs can be found in a quiescent state and proliferate infrequently. Contractile VSMCs undergo phenotypic switching to synthetic states in response to hypertension, vascular damage, oxLDLs or atherosclerotic lesions (13, 28, 29).

To properly coordinate vasodilation/vasoconstriction events, contractile VSMCs rely on exquisite rearrangements of actin and myosin molecules along with intermediate filaments such as desmin and vimentin (17, 18).

The nitric oxide/soluble guanylate cyclase/protein kinase G signaling cascade (NO/sGC/PKG) is one of the most important regulators of the contractile machinery (30). When contractile VSMCs differentiate to synthetic states, (NO/sGC/PKG) becomes unresponsive and upregulation of signaling cascades involved in cell proliferation and migration takes place (MAPK and phosphatidylinositol-3-kinase (PI3K)/protein kinase B/Akt pathways) (13) (**Figure 4**). In addition, synthetic VSMCs exhibit high levels of production of extracellular matrix proteins needed for vascular remodeling during atherosclerotic injury (23, 26, 27) (**Figure 1**).

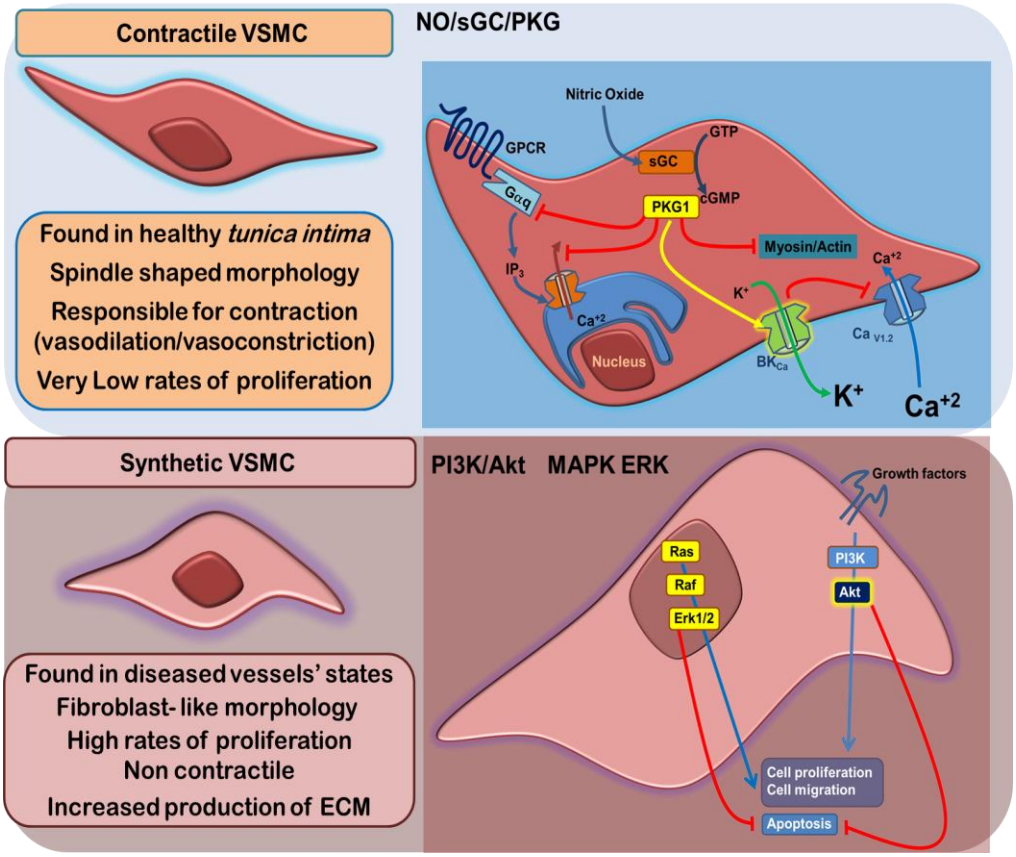

Figure 4. VSMCs phenotypic differentiation. VSMCs have two extreme phenotypes: contractile and synthetic. VSMCs in their contractile state have a spindle-like elongated morphology, express contractile proteins and regulate vascular tone. The Nitric oxide (NO)/sGC/PKG pathway is highly expressed in contractile VSMCs and is responsible for determining the vasodilation/vasoconstriction levels. Synthetic VSMCs display a fibroblast like morphology, exhibit high expression of extracellular matrix proteins (ECM) and are highly proliferative and mobile. PI3K/Akt and Ras/Raf/Erk1/2 MAPK pathways sustain cell proliferation and migration involved in the progression of atherosclerosis.

Given that high plasma levels of low density lipoproteins (LDLs) impair VSMCs' function and vasodilation of blood vessels, a brief discussion of their characteristics and their role in CVD will be presented.

Low density lipoproteins

LDLs are the principal particles to transport cholesterol and fat in the human body. They are sphere-like structures (18-25 nm in diameter), made basically of phospholipid monolayers and apolipoprotein B-100 (Apo B) (31, 32). The hydrophobic core of LDLs is the site where cholesterol molecules are carried. During cellular demand for cholesterol, Apo B on the surface of LDLs interacts with specific receptors and triggers endocytosis to facilitate uptake and utilization of lipids through lysosomal degradation (33).

Studies have shown that high circulating levels of LDL (over 160 mg/dL) facilitate cholesterol deposition in the *tunica intima* which, over time, promotes atherosclerotic plaque formation and lumen narrowing (34) (**Figure 1**). Thus, elevated levels of LDL have been implicated in coronary heart disease.

Oxidation of Low Density Lipoproteins

The oxidation of LDLs is considered one of the major culprits for the progression of atherosclerosis and occurrence of CVD (35-37). In brief, oxLDLs accelerate various pro-inflammatory and pro-atherogenic pathways (38). When LDLs are oxidized, they cannot be recognized by their “normal” LDL-receptors. Thus, in order to facilitate oxLDL uptake and its clearance from the *tunica media*, various scavenger receptors such as CD36 and LOX-1 are up-regulated (39, 40).

Reports have shown that there are abundant scavenger receptors in macrophages, endothelial cells and VSMCs. These scavenger receptors play a crucial role in the uptake of oxLDL. Uncontrolled uptake of oxLDL leads to morphology changes (appearance of foam cells: fat laden macrophages and VSMCs) (39, 41, 42). Besides changes in morphology, oxLDLs dramatically disturb cell function (**Figure 5**). They support recruitment of monocytes, facilitate macrophage infiltration, impair nitric oxide (NO) production/vasodilation and promote VSMCs differentiation, proliferation and migration. Altogether, oxLDLs profoundly impair normal vascular function and therefore contribute to the development of atherosclerotic lesions (39, 40).

As part of the repair mechanisms of atherosclerotic lesions; differentiation and migration of VSMCs is of crucial importance (43, 44). Because oxLDLs have shown to support the phenotypic transition of VSMCs, a more detailed examination of VSMCs’ role and function will be described below.

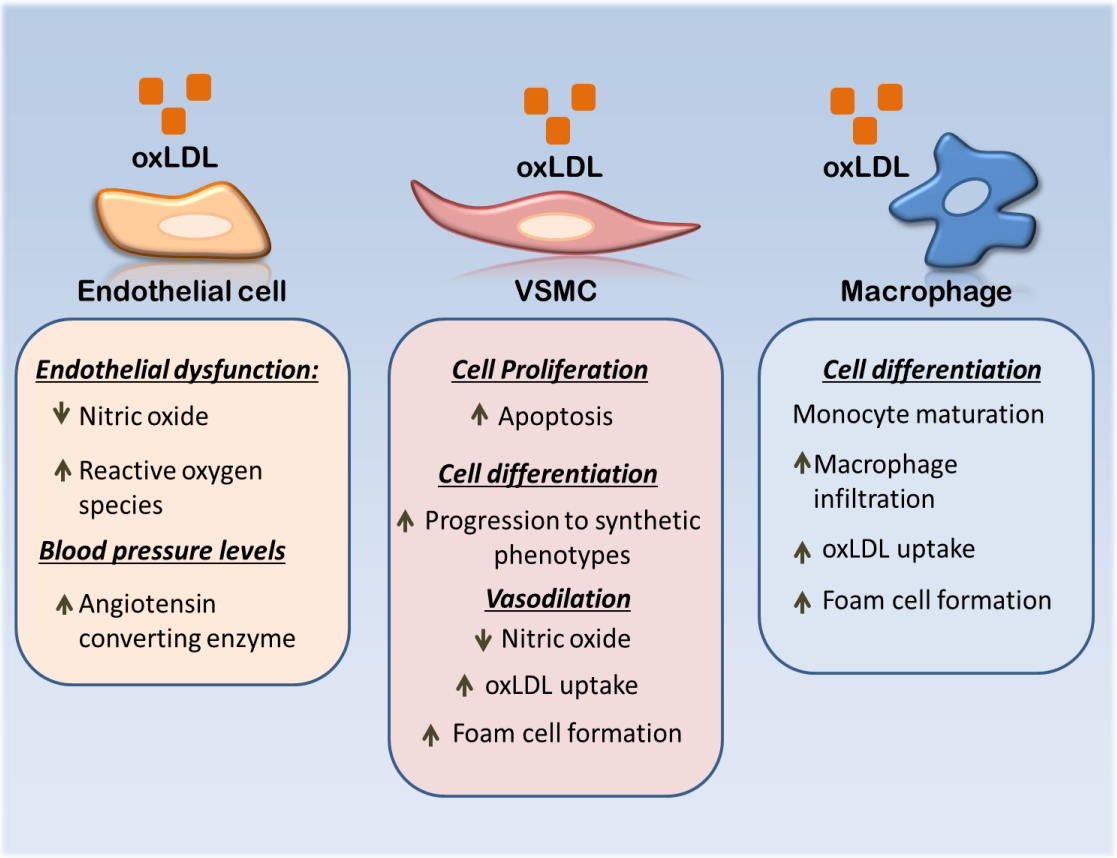

Figure 5. oxLDL atherogenic effects on cell function. oxLDL uptake by scavenger receptors expressed in endothelium, VSMCs and macrophages, promotes the occurrence and development of atherosclerosis by altering cell function.

In vitro primary cultures of VSMCs to study atherosclerosis progression

A time-dependent dynamic phenotyping switch in VSMCs was evident ever since they were first isolated and cultured *in vitro* (**Figure 4**). At initial stages of subculturing (passage # 1 to 4), cultured VSMCs display ribbon-like elongated shapes with high resemblance to the cells from intact tissue. Early *in vitro* VSMCs cultures exhibit high density of myosin filaments with close resemblance to contractile VSMCs *in vivo*. After several days in culture, the expression of myofilaments decreases, and the cells begin to resemble the “synthetic” cells seen during blood vessels’ regeneration and atherosclerotic plaques (45).

In vivo, contractile VSMCs undergo phenotypic switching due to stimuli like hypertension, vascular damage, exposure to oxLDLs or atherosclerotic lesions; *in vitro*, the phenotypic status of VSMCs is determined mainly by passage number or incubation with certain mitogens or growth factors (e.g., oxLDL, PDGF) (21, 22, 46-48). The possibility to obtain and track *in vitro* the transition of VSMCs to synthetic/diseased stages makes the usage of VSMCs extremely helpful in obtaining a better understanding of the progression of atherosclerotic lesions.

Apelin/APJ cardioprotective role

Recently, the signaling pathway (apelin/APJ), involving the adipokine apelin and its G-protein coupled receptor (APJ), has emerged as a potent regulator of cardiovascular function (49-51). Apelin, is generated *in vivo* as a 77 amino acid precursor (pre-proapelin) that is cleaved to generate functional shorter peptides,

(Apelin-13,-16,-17,-19 and 36) among which, apelin-13, exhibits the highest activity and concentration in the circulatory system (52-54) (**Figure 6**). Additionally, the apelin peptide undergoes posttranslational modification which results in the addition of pyroglutamate to the N terminus region producing (pyr^{1}) apelin-13 peptide. The pyroglutamation protects the peptide from exopeptidase degradation and preserves its biological activity (55).

APJ Receptor

The Apelin receptor (APJ) is a 7 transmembrane (TM) domain structure that belongs to the G-protein coupled receptor (GPCR) family. The receptor is expressed in numerous tissues, including heart, lung, liver, kidney, gastrointestinal tract, brain, adrenal gland, endothelium and smooth muscle. The gene encoding for APJ designated APLNR encodes for a 380-amino acid protein and is located on chromosome 11q12 (56, 57). APLNR is evolutionary conserved among species (57, 58). The APJ receptor shares 54% of identity in the TM region and 30% overall with the angiotensin II (Ang II) receptor, AT_1 (56). Even though there is high identity between the APJ and AT_1 receptors, the Ang II molecule does not bind to the APJ receptor (51).

Upon binding to its receptor, apelin-13 triggers a plethora of signaling cascades and changes in protein expression that have proven to be beneficial against CVD (52). Among its cardio-protective effects, scientific evidence highlights: strong anti-hypertensive and anti-atherogenic properties; all of them associated with several intracellular signaling cascades such as: a) NO/sGC/PKG pathway, b)

the PI3K/Akt, and c) the mitogen activated protein kinase MAPK signaling network Ras/Raf/Erk (51, 53, 59-63).

Apelin administration antagonizes the hypertensive effect of Ang II in vascular complications like atherosclerosis by increasing NO levels (51, 64, 65). Apelin also has ionotropic effects by increasing the heart rate and contractility of isolated and intact hearts of mice and rat (66, 67). Binding of apelin to APJ alleviates hypertension and has a protective effect in ischemic heart disease. Several *in vivo* and *in vitro* models have revealed a potential role of apelin in cardiovascular function, for instance, in knockout mice models for apelin, impaired cardiac contractility and occurrence of CVD have been observed (68). Studies have shown that apelin acts as a potent angiogenic factor promoting proliferation of VSMCs and endothelial cells (69-71). Consistent with its role promoting cell proliferation, apelin has proven to suppress via PI3K/Akt apoptotic cell death. Both apelin and APJ are needed for cardiovascular development and formation of heart morphology (65). Recent evidence has pointed out that apelin/APJ system plays a critical role in the homeostatic balances of numerous processes (58, 64, 72). Overall, increasing evidence points out the central role of apelin/APJ in cell function; placing it as a potential therapeutic target for the treatment of CVD (53, 73) (**Figure 7**).

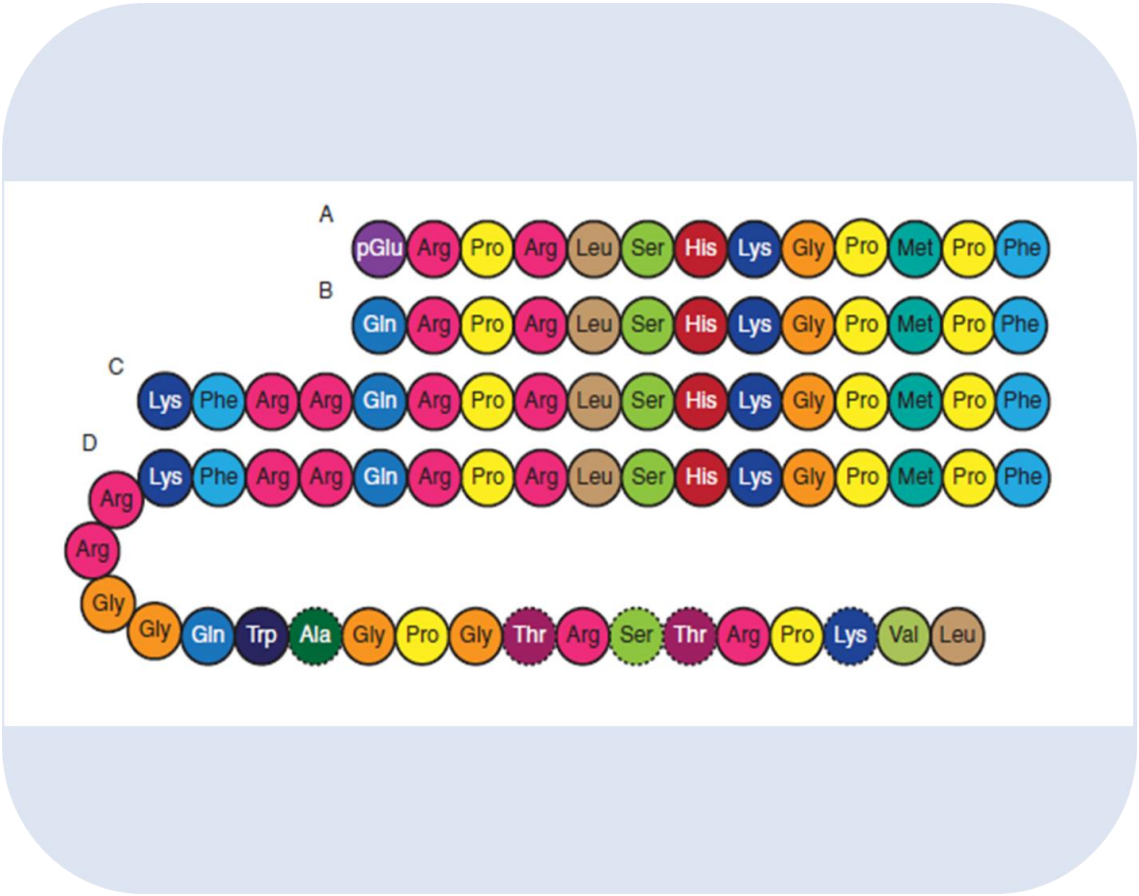

Figure 6. Apelin processing. Amino acid sequence of different apelin peptides isoforms. A. (pyr1) apelin-13, B. apelin-13, C. apelin-17 and D. apelin-36. Figure adapted with permission from (reference # 52, O'Carroll,A.M. 2013).

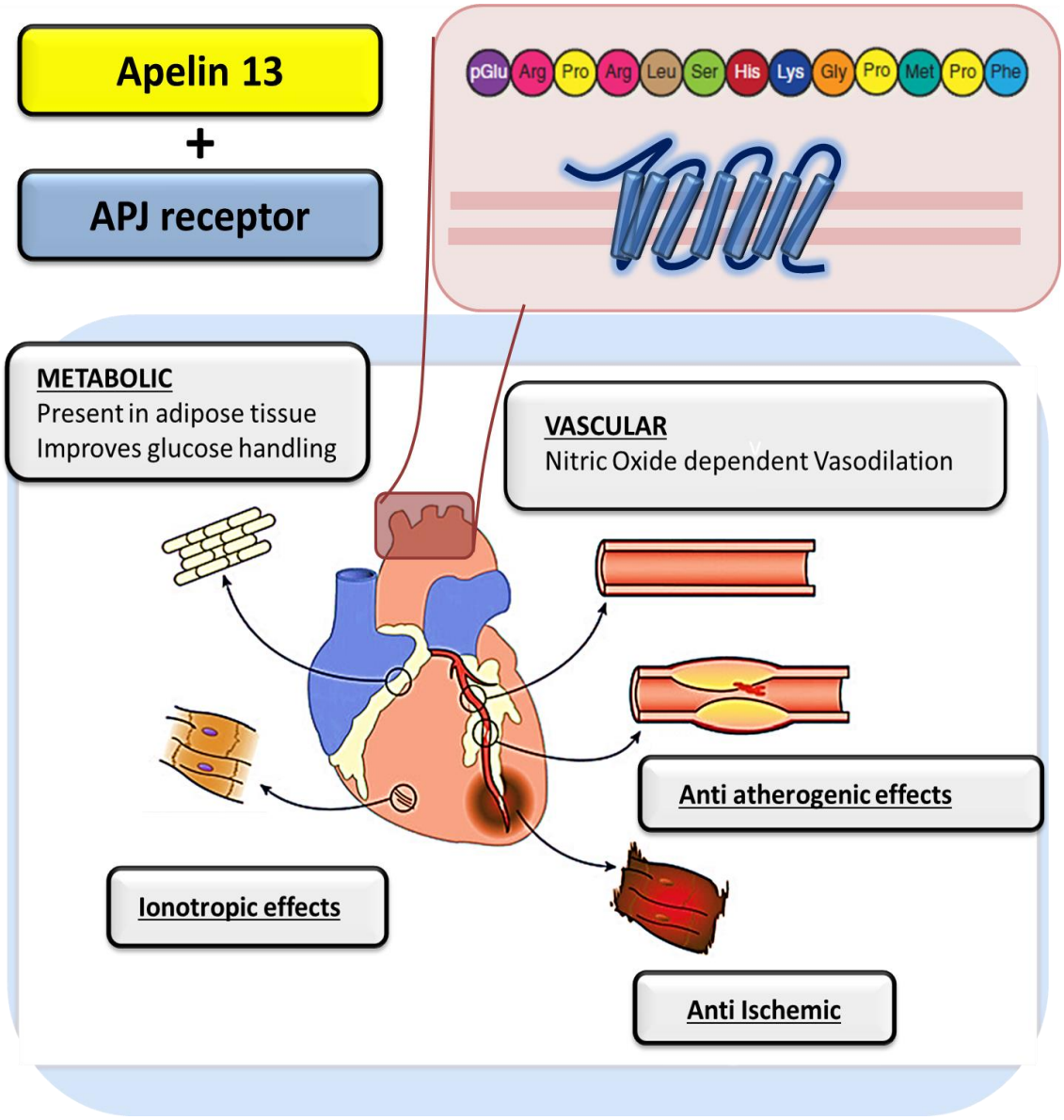

Figure 7. Cardioprotective effects mediated by apelin/APJ. Apelin and APJ signaling contribute to normal cell function in blood vessel and adipose tissue. Figure modified with permission from (reference # 74, Barnes,G. 2010).

As mentioned earlier, VSMCs differentiation, proliferation and migration are key during the repairing process of atherosclerotic plaques. At the molecular level, the coordinated activity of members of the solute carrier family 12A (SLC12A) is central to controlling cell volume and thereby cell proliferation and migration. Therefore in the following paragraphs the role and activity of SLC12A members will be discussed.

SLC12A-Cation Chloride Cotransporters

Members of the SLC12A are among the most important mechanisms to coordinate osmotic water influx and efflux. Based on homology and sequence identity, the *SLC12A* family is composed of at least eight cation chloride cotransporters (CCCs) members: three Na^+-dependent inwardly oriented (NCC, NKCC1 and NKCC2), four outwardly oriented K^+-dependent and Na^+-independent (KCC1 to 4), a cation chloride cotransporter interacting protein (CIP) and probably the polyamine transporter (CCC9) (75, 76) (**Figure 8**). Tight control of cell volume is of paramount importance to sustain normal cell function and survival (77).

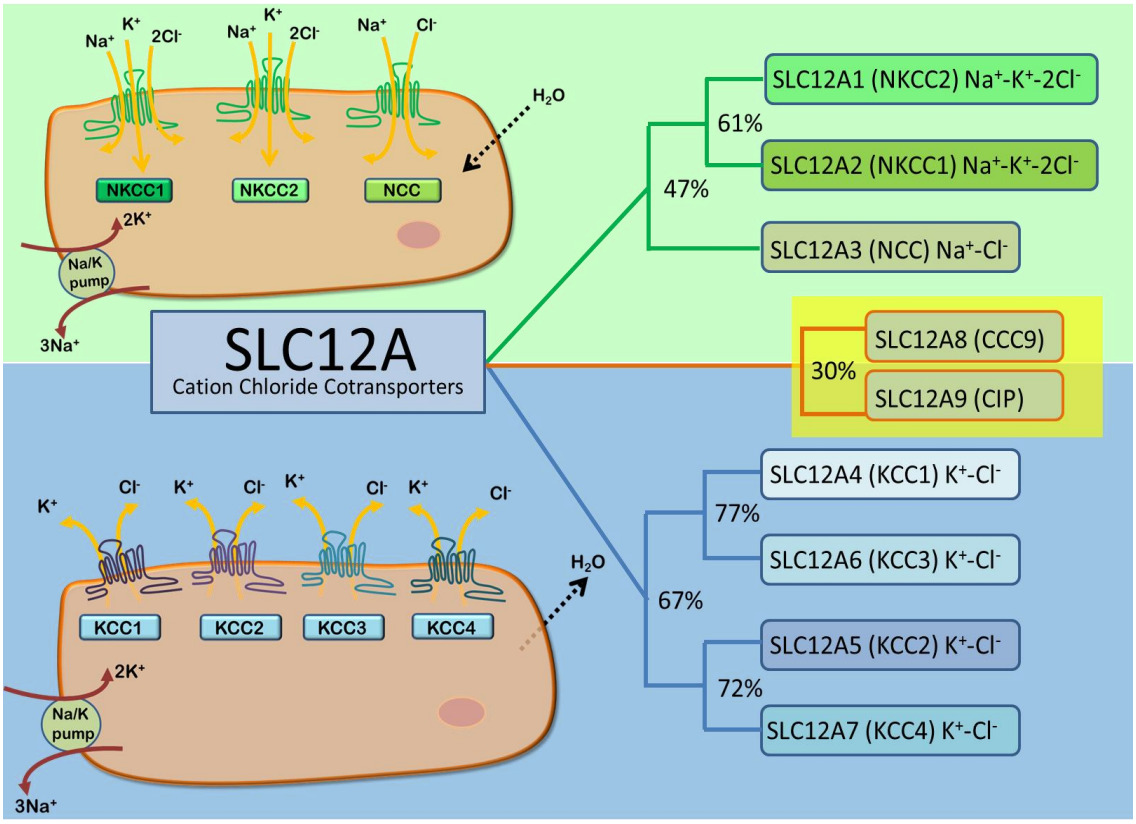

Figure 8. SLC12A family of cation chloride cotransporters. Schematic representation of SLC12A members of cation-chloride cotransporter. The potassium-driven chloride cotransporter (KCC1-4) mediate the efflux of chloride. NKCCs and KCCs participate actively in RVD and RVI by promoting the osmotic transport of water across the cell membrane.

When cell volume is perturbed, volume restoration mechanisms are activated in order to maintain cellular homeostasis. These mechanisms involve the coordinated function of CCC, channels, exchangers and sodium potassium ATPase (i.e. Na^+/K^+ pump) to change the intracellular concentration of organic and inorganic osmolytes and ultimately the osmotic influx/efflux of water.

Efflux of potassium (K^+), chloride (Cl^-) and organic osmolytes takes place to bring cell volume back to normal to counteract the exposure to hypotonic extracellular conditions that would lead to uncontrolled cell swelling. This volume restoration is achieved through stimulation of: K^+ and Cl^- channels, along with $\underline{K}^+$-$\underline{Cl}^-$ cotransporters (known collectively as KCCs). Altogether they mediate the exit of K^+ and Cl^- associated with water efflux (78-80). Similarly, when cells are exposed to hypertonic stimuli and as a way to prevent cell shrinkage, a series of events known as regulatory volume increase response (RVI) are triggered to increase the intracellular osmolyte concentration and water influx. RVI results in restoration of cell volume through activation of the sodium/potassium (Na^+/K^+) pump, sodium-potassium-two chloride (Na^+-K^+-$2Cl^-$) cotransporter (NKCC), along with chloride/bicarbonate (Cl^-/HCO_3^-) and sodium/proton (Na^+/H^+) exchanger (81, 82) (**Figure 9**).

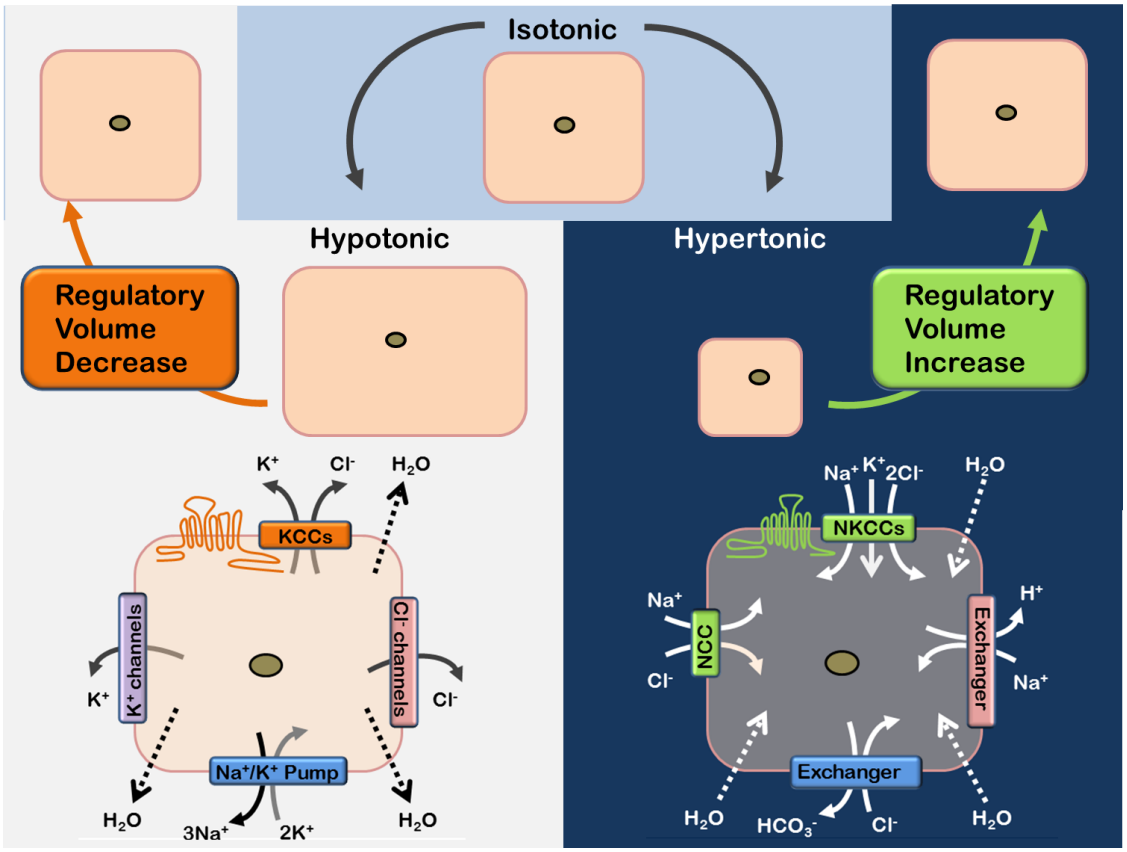

Figure 9. Regulatory mechanisms to keep cell volume constant. During hypotonic or hypertonic challenges, RVD or RVI response take place to prevent cell death by cell swelling or shrinkage. During RVD, KCCs' activity is upregulated to facilitate water osmotic efflux whereas NKCCs' activity is necessary to promote water influx during RVI.

The Cation-Chloride Cotransporters (CCCs) and the Na^+/K^+ pump

The CCCs are secondary active transporters, as there is no ATP utilization and therefore rely on the chemical gradient generated by the Na^+/K^+-ATPase to move Cl^- against its electrochemical gradient (83-86). Structurally, they are predicted to have 12 transmembrane segments and long intracellular amino and carboxy termini. Normally, NKCCs transport ions at a ratio of $1Na^+:1K^+:2Cl^-$, NCC at a ratio of $1Na^+:1Cl^-$, and KCCs at $1K^+:1Cl^-$ ratio. The stoichiometry for all CCC results in electroneutral movement as the net charge traversing the plasma membrane is zero and thus, they are classified as electroneutral cation-coupled-anion transporters (76, 87). These cotransporters share a 47-60 % identity in amino acids among each other (88).

In VSMCs, expression of several members of the SLC12A has been reported (89-91). NKCC1, KCC1, 3 and 4 actively participate in several cellular processes such as regulation of cell volume, differentiation, motility and proliferation (91). NKCC1 is a protein of 1212 amino acids, encoded by the SLC12A2 gene located on chromosome 5q23 (92). NKCC1 exhibits ubiquitous expression and is target of tissue specific posttranslational modifications (glycosylation) that result in proteins ranging from 135 kDa to 195 KDa (93). NKCC1 is known to function as a homodimer and is predicted to have a hydrophobic core of 12 TMD and long N- and C-terminal cytoplasmic domains. They bear a long hydrophilic extracellular loop (ECL) between TMD 7 and TMD 8 which is target for glycosylation (92, 94-96). NKCC1 activity can be inhibited by loop diuretics bumetanide and furosemide. To date, the precise binding site for bumetanide has not been

resolved. Using chimeric protein approaches and point mutation strategies, it is believed that they are localized across the hydrophobic core of the TM domain. Cation binding is primarily localized on TM2 domain, Cl^- binding involves TM4 and TM7 domains, and bumetanide binding includes multiple domains comprising TM2, TM7, TM11 and TM12. The N- and C- termini do not participate in ion binding (97-99).

NKCC1 activity is tightly linked to its phosphorylation state. Phosphorylation of three N- terminal threonine residues (Thr-184, 189 and 202) and Thr-1114 on the C-terminal regions have been identified as modulators of NKCC1 trafficking and activity (93-95, 100).

These sites are phosphorylated via two serine threonine kinases: the Ste-related proline-alanine-rich kinase (SPAK) and the oxidative stress response 1 kinase (OSR1). Protein phosphatase 1 (PP1) removes these phosphates and inactivates the cotransporter. These protein kinases and phosphatases physically interact with NKCC1 through overlapping binding motifs within NKCC1 N-terminal region, highlighting a coordinate modulation of the NKCC1 activity (**Figure 10**) (101).

Besides NKCC1, VSMCs highly express several KCCs (KCC1, 3-4) and very low levels of KCC2, which actively participate in modulating cellular volume and ionic homeostasis (102-105). Apelin relevance in regulating the three signaling pathways described in the preceding sections lies in the fact that the newly discovered ion transporter, KCC was initially co-discovered and characterized in

detail by Drs. Peter Lauf and Norma Adragna from our laboratory in the US and by Drs. Clive Ellory and Philip Dunham in the United Kingdom (90).

The KCC share roughly 30 % identity in amino acids with other CCCs family members. Their primary structure is predicted to be of 12 trans-membrane (TM) domains with both N and C termini located in the cytoplasm and a glycosylated extracellular loop between TM 5 and TM 6 (76, 88, 106-108). The 12 TM segments are highly-conserved regions, and the C-terminus domain is even more conserved compared to the N-terminus domain. The cation binding sites in TMD2 have been established through chimera work, whereas, the anion binding sites are less defined, involving several domains of the molecule (88, 97). Both N and C-termini domains have consensus phosphorylation sites for kinases and phosphatases and are involved in signal transduction (**Figure 10**) (76). The transporter is highly selective for K^+ and Cl^- ions, possesses asymmetric kinetics in ion binding, mediates the electroneutral transport of ions and is important in cell volume regulation (109, 110).

The modulation of KCC activity involves dephosphorylation of serine/threonine residues located within the amino and carboxy termini. Thus, the coordinated activity of kinases and phosphatases is important to sustain normal KCC function (111). Protein phosphatase 1A and 2B along with members of the “with no lysine” (WNKs) and STE20 (SPAK) serine kinase family are important modulators of the activity of KCCs and NKCCs (112-115). These proteins and kinases reciprocally regulate KCC and NKCC activity (116, 117)**.** Coordinated modulation of NKCC

and KCC by these kinases and their involvement in controlling in cell volume is summarized in (**Figure 10**).

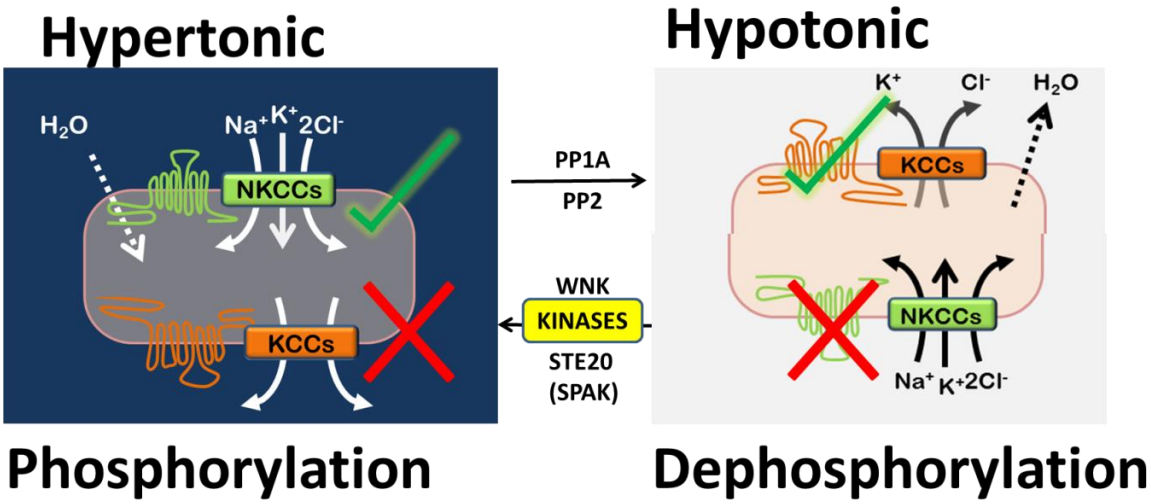

Figure 10. Coordinated regulation of K-Cl cotransporters (KCCs) and Na-K-2Cl cotransporters (NKCCs). Phosphorylation/dephosphorylation events control the activity of NKCCs and KCCs during changes in osmolarity. PP1A/PP2 mediated dephosphorylation inhibits NKCC and activates KCC. The serine threonine kinases WNK and SPAK phosphorylate NKCCs and promote their activation.

KCC is a ouabain- and bumetanide-insensitive transporter that mediates coupled K^+ and Cl^- bidirectional transport across the membrane (107-110). Although the transporter functions bi-directionally, under physiological conditions, KCC is mainly directed outward (118).

An important feature of KCC is its ability to be stimulated by cell swelling or by treatment with *N*-ethylmaleimide (NEM) (84, 119, 120). KCC activation by hypotonicity was initially observed in red blood cells and then later discovered in different cells of various species (120). In various cell systems, NEM selectively activates KCC (121, 122, 122-124). Both NEM and hypotonicity-stimulated cell swelling have been used as diagnostic criteria to identify the functional presence of KCC.

To date, four KCC isoforms have been identified: KCC1, KCC2, KCC3 and KCC4 with their distinct tissue specific expression. KCC1 and KCC3 share 75 % identity in their amino acids; whereas, KCC2 and KCC4 share 72 % identity in their amino acid residues (125, 126). Additionally, these isoforms are also capable of interacting with each other or one another resulting in the formation of homo-oligomers or hetero-oligomers, respectively, most likely involving the last C-terminal residues (127-129).

KCC1 is encoded by the *SLC12A4* gene located on chromosome 16q22 (88). The expression of KCC1 is ubiquitous (housekeeping isoform) and plays a role in cell volume regulation acting in reverse direction of NKCC1. While NKCC1 plays a role in RVI when the external osmolarity increases, KCC1 plays a role in RVD

by enabling K^+ and Cl^- to exit the cell (88, 130, 131). The predicted structure of KCC is similar to NKCC except that the extracellular hydrophilic loop containing glycosylation sites are linked to TMD5 and TMD6.

The KCC2 transporter was originally cloned from a mouse brain cDNA library (106). The protein is composed of 1116 amino acids residues and this isoform is encoded by the *SLC12A5* gene located on chromosome 20q13. Although initial findings suggested localized expression in CNS due to a neuronal-restrictive silencing element (NRSE), recent evidence has shown its expression in metastatic processes and minimal mRNA expression documented in VSMCs (75, 88, 104, 106, 125, 132, 133, 133-138). Unlike KCC1, KCC2 activity is not sensitive to cell volume and thus, is not stimulated upon cell volume. KCC2 function in conjunction with NKCC1 and KCC3 to maintain neuronal excitability by regulating intracellular Cl^- concentration. Due to differential expression of NKCC1 and KCC2 during the development of the central nervous system; in embryonic immature neurons, intracellular [Cl^-] is high due to increase in activity of NKCC1. As the neurons undergo maturation, the expression of NKCC1 declines and is switched by KCC2 that extrudes Cl^- (139). This switch allows operation of γ-aminobutyric acid (GABA) receptors to induce depolarization in developmentally immature neurons and hyperpolarization in mature adult neurons. KCC2 knockdown models display epilepsy (140, 141).

KCC3 consists of 1150 amino acids residues and is encoded by the *SLC12A6* gene located on chromosome 15q13-14 (135). The isoform is fairly expressed in

brain, muscle, kidney, liver, lung and heart. KCC3 mutations have been associated with Anderman's disease. KCC4 is encoded by SLC12A7 gene that is located on chromosome 5p15.3 and is mainly expressed in kidney, heart, smooth muscle cells and to a slighter extent in the brain. KCC4 has been linked to inner ear function (125).

The broad arrays of the physiological roles of each of the KCC isoforms have been studied by gene disruption in mice and the resulting phenotypes observed were linked to various human diseases. KCC1 and KCC3 are implicated in hemoglobinopathies. KCC3 is implicated in hypertension, KCC2 is associated with epilepsy, and KCC4 is linked to hearing disorders (76, 137, 142-145). The functions of each of the isoforms are shown in **Table 1**.

VSMCs have three of these four isoforms: KCC1, KCC3 (splice variants KCC3a and KCC3b), and KCC4 (102, 103). KCC2a but not KCC2b, which is neuron specific KCC2 has been documented as fairly expressed in VSMCs and lens epithelial cells (132, 138). It is possible that the expression of different isoforms in VSMCs varies in quantity in pathological conditions.

Gene Name	SLC12A4	SLC12A5	SLC12A6	SLC12A7
Protein	KCC1	KCC2	KCC3	KCC4
Human gene locus	16q22	20q13	15q14	5p15
Tissue expression	Ubiquitous	Neurons, tumor	Extensive	Extensive; limited in brain
Ion co-transport coupling	$1K^+$-1 Cl^-	$1K^+$-1 Cl^-	$1K^+$-1 Cl^-	$1K^+$-1 Cl^-
Isoforms		KCC2a KCC2b	KCC3a KCC3b	
Amino acids Residues	1085	1075 1115	KCC3a: 1150 KCC3b: 1099	1083
Direct disease association	-	-		
KO phenotype	No phenotype	Death due to lack of respiratory drive, epilepticus	Deafness, hypertension, tumor biology	Sensorineural deafness and renal tubular acidosis
Direct disease association			ACCPN (Andermann syndrome)	
Role in complex disease	Sickle cell anemia	Epilepsy	Renal tubular acidosis, sickle cell anemia, epilepsy	Renal tubular acidosis, sickle cell anemia, epilepsy
Phosphorylation sites	-	-	T991, T1048	-

Table 1. Summary of KCC isoform-specific distribution and function (76, 118, 146)**.**

KCC and signaling pathways in relation to CVD

A substantial body of evidence suggests a role of KCC in general cellular homeostasis, hypertension, blood pressure regulation and cell proliferation stressing the need to study KCC in relation to CVD and cellular homeostasis (75, 89, 118, 134, 145, 147).

Important modulators of the expression and activities of KCC involve the NO/cGMP/PKG pathway (75, 102-105, 148). In addition, PDGF uses PI3K/Akt-mediated pathway in vascular smooth muscle cells (VSMCs) to regulate KCC (149, 150). Furthermore, KCC1 and KCC3 are regulated via the phosphoinositol/PKC pathway in low-K sheep red cells (151). The NO/cGMP/PKG pathway leads to vasodilation and activates KCC, which in turn, plays an important role in blood pressure regulation, as shown by a hypertensive phenotype in mice with deletion of the KCC3 isoform (KCC3 -/-) (89, 102, 137, 145, 145, 145, 152).

In addition to regulating KCC, the NO-mediated pathway regulates VSMC proliferation, migration, apoptosis, extracellular matrix protein formation, and relaxation (153-155). The NO-pathway is also important in preventing atherosclerosis lesions and is activated only if VSMCs are contractile *in vitro*, i.e. before passage 4 given that PKG expression diminishes after this passage (22, 25). The activators of the pathway, such as sodium nitroprusside (SNP), NONOates (NO donors), YC-1 (NO-independent activator of sGC), 8 Br-cGMP (soluble substrate of PKG) and inhibitors such as LY83583 (for sGC) and

KT5823 (for PKG), stimulate and inhibit KCC activity, and mRNA and protein expression, respectively (89, 102-105, 137, 137, 152). Additionally, our laboratory has shown an association between KCC and atherosclerosis using the synthetic VSMCs as a model system, where the MAPK and PI3K/Akt signaling pathways play a prominent role (149, 150).

Regulation of KCC by the PI3K/Akt pathway has been documented by our laboratory. Platelet derived growth factor (PDGF), a serum mitogen, has a regulatory role in the pathogenesis of atherosclerosis. In addition, PDGF stimulates KCC through PI3K/Akt and protein phosphatase 1 (PP-1) and induces VSMC proliferation (149, 150). The stimulation of KCC was blocked by a selective inhibitor of the pathway, suggesting regulation of KCC by the PI3K/Akt pathway (75, 149, 150). Finally, regulation of KCC by MAPK, initially documented in sheep red blood cells and was later confirmed in successive studies on cervical carcinoma (134, 151, 156, 157). In these studies, KCC stimulation was blocked by PD98059, a MEK selective inhibitor, and furthermore, knockdown of KCC decreased cervical cancer proliferation and activation of the MAPK signaling cascade suggesting an interdependent relationship between the MAPK pathway and KCC (151, 158-160).

KCC in cell proliferation/migration

Several studies have suggested serum as an important modulator of ion channels and transporters (150, 161, 162). Serum contains mitogens and growth factors that have been shown to regulate activity of channels and transporters in

various cultured cells. Evidence from our laboratory and others has also shown regulation of KCC by growth factors or mitogens that is involved in cell proliferation. Serum factors were essential for basal KCC activity maintenance (150). Serum deprivation for twenty four hours abolished KCC activity; however, the effect was recovered after serum addition. PDGF (platelet derived growth factor), a major mitogen/growth factor for cells of mesenchymal origin present in serum, is also prevalent in atherosclerotic lesions. PDGF, a potent chemo-attractant induces cell proliferation in VSMCs during atherosclerosis. In cell culture, PDGF utilizes a MAPK pathway to initiate cell proliferation. Our laboratory has demonstrated that PDGF activates KCC in a time- and dose-dependent manner: both acutely and chronically via a PDGF receptor (149, 150). Primarily, PDGF increases overall protein content in cultured VSMCs demonstrating the effect of PDGF on cell proliferation, which is an important mechanism observed during atherosclerosis. Since VSMCs migration is an initial step in formation of atherosclerotic lesions, evidence of KCC in cell migration has been documented in studies involving various models.

Cell migration is important in several physiological and pathophysiological processes including cell volume regulation, embryogenesis, tumor metastases, wound healing, inflammation, immune defense, atherosclerosis and tissue remodeling (163). Several lines of evidence have demonstrated KCC playing a vital role in cell migration (163-165).

Previous research has shown an interrelationship between cell migration and KCC activity studies using cancer cell lines showed. An insulin-like growth factor-1 (IGF-1) receptor has been shown to regulate KCC production by activating PI3K and Erk1/2 MAPK pathways in cancerous cells (133, 157, 164). Knockdown of KCC significantly reduced cell migration. This indicates the importance of KCC to modulate IGF-1-dependent cell migration and invasion in cancer.

KCCs and apelin

Noteworthy, similar and overlapping regulatory networks converge to regulate apelin-mediated effects and potassium-chloride cotransport by KCCs, the latter being ultimately determined through phosphorylation /dephosphorylation events. For instance, high levels and dysregulated oxLDL uptake by the fatty acid translocase CD36 (atherosclerosis hallmark), result in pronounced upregulation of KCC1 (166). At the molecular level, KCCs activity has been shown to be modulated by the NO, PI3K/Akt and MAPK/ERK1/2 signaling networks, through which apelin elicits its cardioprotective effects (89, 137, 145, 152). Altogether, the evidence presented in this thesis suggests a strong link between apelin-mediated cardioprotective effect and KCC activity (**Figure 11**). Since KCC activity has proven to be required for controlling cell volume, migration, proliferation and vascular remodeling, we endeavor in establishing a connection between apelin and KCC function.

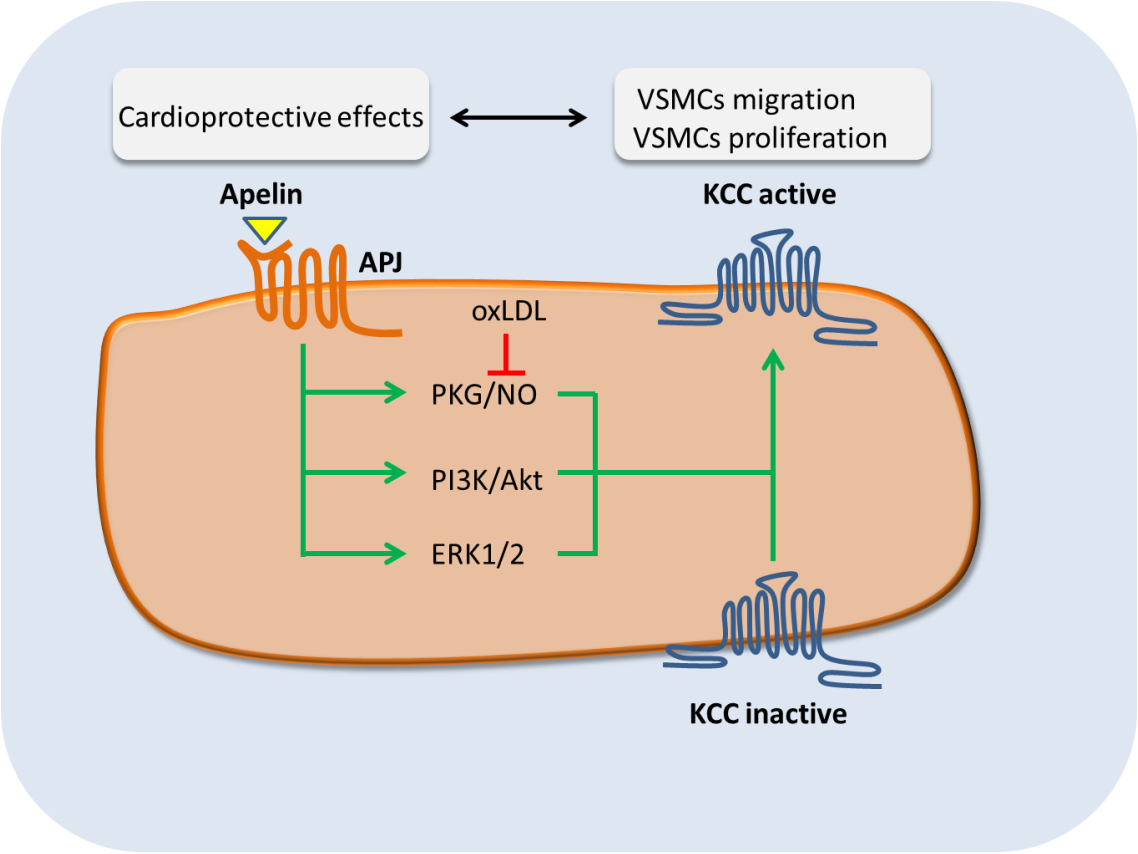

Figure 11. SLC12A family of Cation Chloride Cotransporters. Overlapping signaling cascades regulate the activity of K^+-Cl^- cotransporters and apelin cardioprotective effects.

DEVELOPMENT OF THE HYPOTHESIS

Apelin/APJ is an important modulator of fluid homeostasis and cell volume. Its stimulation displays important cardio-protective functions by reducing blood pressure levels and counteracting the effect of oxLDL. In atherosclerosis, VSMCs migration/proliferation in combination with high circulating levels of oxLDL accelerates atherosclerosis progression and blood vessels lesion formation. Since cell migration/proliferation and cell volume are tightly linked to K-Cl activity, and extensive overlap exists between the apelin-mediated signaling pathways (NO, PI3K/Akt, MAPK) and K-Cl cotransport mode of regulation: **I hypothesize that oxLDL and apelin/APJ are important modulators of K-Cl activity to sustain cell volume regulation, and normal cardiovascular function. In addition, because K-Cl cotransport activity is dependent on several factors, such as, serum, ionic strength, osmolality, cell proliferation and migration, it is possible that the apelin-mediated effect on K-Cl cotransport could also be dependent on the aforementioned factors.**

GOAL: To obtain a better understanding of K-Cl cotransport activity in VSMCs and to establish whether apelin/APJ exerts an effect on K-Cl cotransport activity and whether this effect is modulated by other physiological factors.

SPECIFIC AIMS

***Specific Aim 1*:** To characterize K-Cl cotransport in VSMCs and to examine a possible link to VSMCs phenotype.

Since synthetic VSMCs are highly proliferative and cell migration/proliferation strongly relies on K-Cl cotransport and dynamic rearrangements of cytoskeletal proteins, it is likely that during VSMCs' dedifferentiation, changes in K-Cl cotransport expression and activity, and expression of cytoskeletal markers take place to sustain VSMCs' transition to synthetic states.

***Specific Aim 2*:** To determine the acute and chronic effect of apelin on K-Cl cotransport activity in VSMCs. To establish the involvement of NO, PI3K/Akt and MAPK signaling pathways in the regulation of the transporter.

***Specific Aim 3*:** To assess the factors, such as, serum, osmolality, ionic strength, VSMCs phenotypes on apelin-mediated effect on K-Cl cotransport activity. The above factors will shed light on possible variability in the apelin response on K-Cl activity.

MATERIALS AND METHODS

Chemicals. Rubidium chloride (RbCl, 99.8 % purity metal basis) and amidosulfonic acid (99.99 % purity, metal basis) were purchased from Alfa Aesar (Ward Hill, MA). Potassium chloride (KCl), sodium hydroxide (NaOH), magnesium chloride ($MgCl_2$), 2-[4-(2-hydroxyethyl)piperazin-1-yl] ethanesulfonic acid (HEPES), Tris, D-glucose, sucrose, calcium chloride ($CaCl_2$), calcium gluconate, N-methyl D-Glucamine (NMDG), Minimum Essential Medium (MEM) Alpha Medium, low glucose Dulbecco's Modified Eagle's culture medium (DMEM), fetal bovine serum (FBS), 0.25 % trypsin, Western blot gel loading buffer (10X), molecular weight protein ladder, and 70 % perchloric acid (PCA) were procured from Thermo Fisher Scientific (Waltham, MA). Penicillin (10,000 units/mL), streptomycin (10,000 µg/mL) and cesium chloride (CsCl) were acquired from Life Technologies (Carlsbad, CA). Magnesium gluconate, 3-[*N*-morpholino] propane sulfonic acid (MOPS), and bovine serum albumin (BSA) were purchased from Sigma-Aldrich (St. Louis, MO).

Bicinchonic acid (BCA) protein kit, mammalian protein extraction reagent (M-Per), radioimmunoprecipitation assay (RIPA) buffer, Halt protease inhibitor and enhanced chemiluminescence (ECL) substrate were from Pierce (Rockford, IL). Ouabain octahydrate was purchased from EMD Millipore (Billerica, MA).

Bumetanide was acquired from MP Biomedicals (Solon, OH). Apelin-13 (catalog # 60833) was acquired from Anaspec (Fremont, CA). Inhibitors of the PKG, PI3K/Akt and MAPK signaling pathways (KT5823 (catalog # 420321), LY294002 (catalog # 19-142) and PD98059 (catalog # 513000), respectively) were purchased from Calbiochem (Billerica, MA). oxLDL (catalog # STA-214) was purchased from Cell BioLabs (San Diego, CA). Collagenase type II (catalog # 171049-019) was purchased from GIBCO BRL (San Francisco, CA).

Antibodies. Polyclonal rabbit anti-PKG antibody was purchased from BioVision (San Francisco, CA). Mouse (ms) anti-α-actin and rabbit (rb) monoclonal anti-vimentin were from Cell Signaling (Danvers, MA). ms anti-β-actin was acquired from Santa Cruz (Dallas, TX), and ms anti-desmin was procured from BD Pharmigen Co (San Jose, CA). Rabbit polyclonal anti-apelin receptor (APJ) was purchased from EMD Millipore (Billerica, MA). Rabbit polyclonal KCC4 antibody was purchased from Chemicon International. KCC1 non-commercial antibody was generated by traditional rabbit immunization procedures developed by Gagnon and Lauf (167). Epitope used to raise KCC1 antibody corresponded to sequences within third extracellular loop (ECL3) (167).

***Extraction of primary cultures of VSMCs*.** Enzymatic dispersion of rat aortic VSMCs was performed as previously described (150). Aortas from Sprague Dawley rats (150-200 g) were washed three times in Minimum Essential Medium (MEM) alpha medium. Then, aortas were mechanically stripped of fat and connective tissue and treated with collagenase II for 30 min at 37 °C. After

mechanically removing the tunica adventitia, tissue was cut into smaller segments and incubated at 37 °C with a trypsin and collagenase II solution until a single cell suspension was obtained (**Figure 12**). Cells were centrifuged and resuspended in DMEM medium containing 10 % fetal bovine serum (FBS), and diluted to obtain a final concentration of 4 x 10^5 cells/mL. Finally, cells were plated into 75 cm^2 tissue culture flasks (T-75) and grown in DMEM containing 10 % FBS and supplemented with penicillin (50 units/mL) and streptomycin (50 µg/mL) at controlled atmosphere of 95% O_2/ 5% CO_2 at 37 ^oC. Growth media was replaced every two days until cells were 100 % confluent. Standard trypsinization was performed to split cells (1:4 ratio) into new T-75 flasks or 12-well plates, depending upon the experimental requirements. Cells at passages 1-4 were considered as contractile VSMCs, whereas passages 6-75 were used as synthetic VSMCs based on previous phenotype characterization reports as discussed in the result section.

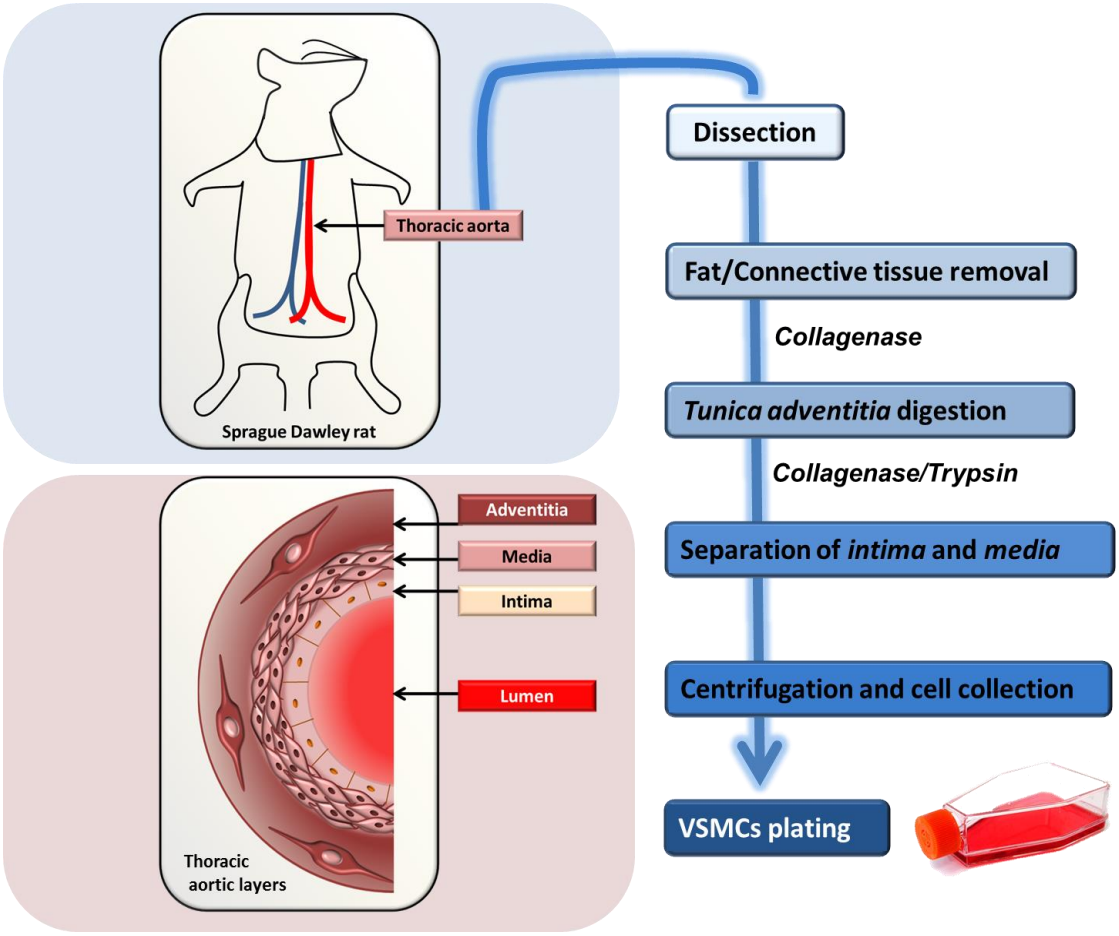

Figure 12. VSMCs isolation from Sprague Dawley's thoracic aorta. Single VSMCs were isolated by incubating aorta with a collagenase and trypsin solution.

Solutions used for Rubidium (Rb^+) transport studies.

Several buffers were used during the transport studies to determine K-Cl cotransport activity. Examination of Rb^+ transport under isotonicity was performed by incubating VSMCs in a balanced salt solution (BSS-NaCl) composed of 20 mM HEPES-Tris buffer (pH 7.4 at 37 ^oC) containing (in mM): NaCl (130), KCl (5), $CaCl_2$ (2), $MgCl_2$ (1), glucose (10). The preincubation solution contained 0.1 % BSA in BSS. The flux solution replaced 5 mM K^+ with 10 mM Rb^+.

The Cl^--free media contained sulfamate (Sf^-) in the K^+, Rb^+, and Na^+ salts, and gluconate in Mg^{+2} and Ca^{+2} salts. Na^+-free media contained: NMDG in Cl^- or Sf^- salts. A wash buffer to terminate Rb^+ uptake was composed of 10 mM MOPS-Tris, $MgCl_2$ of pH 7.4 (300 mOsM). Osmolality was changed by varying the ionic strength of the solution with variable amounts of NaCl, NaSf, NMDGCl or NMDGSf salts while keeping the other ions constant. In some experiments, osmolality was increased by using sucrose maintaining the constant ionic strength. Osmolality (in mOsm/kg H_2O) of the hypotonic, isotonic and hypertonic solutions were 120, 300 and 450, respectively. Ouabain (2 mM) and bumetanide (2-30 µM) was used to fully inhibit Rb^+/K^+ fluxes by the Na^+/K^+ pump and the sodium-potassium-two chloride cotransporter (Na^+-K^+-$2Cl^-$) activities, respectively (Figure 13).

All stock salt solutions were prepared in deionized water. Stock solutions of the drugs: 400 mM ouabain, 400 µM bumetanide and 0.1 M NEM, KT5823,

LY294002, PD98059 were prepared in DMSO as solvent. The osmolalities (osmol/kg H_2O) of the salt solutions were measured with Advanced Micro-Osmometer (Norwood, MA).

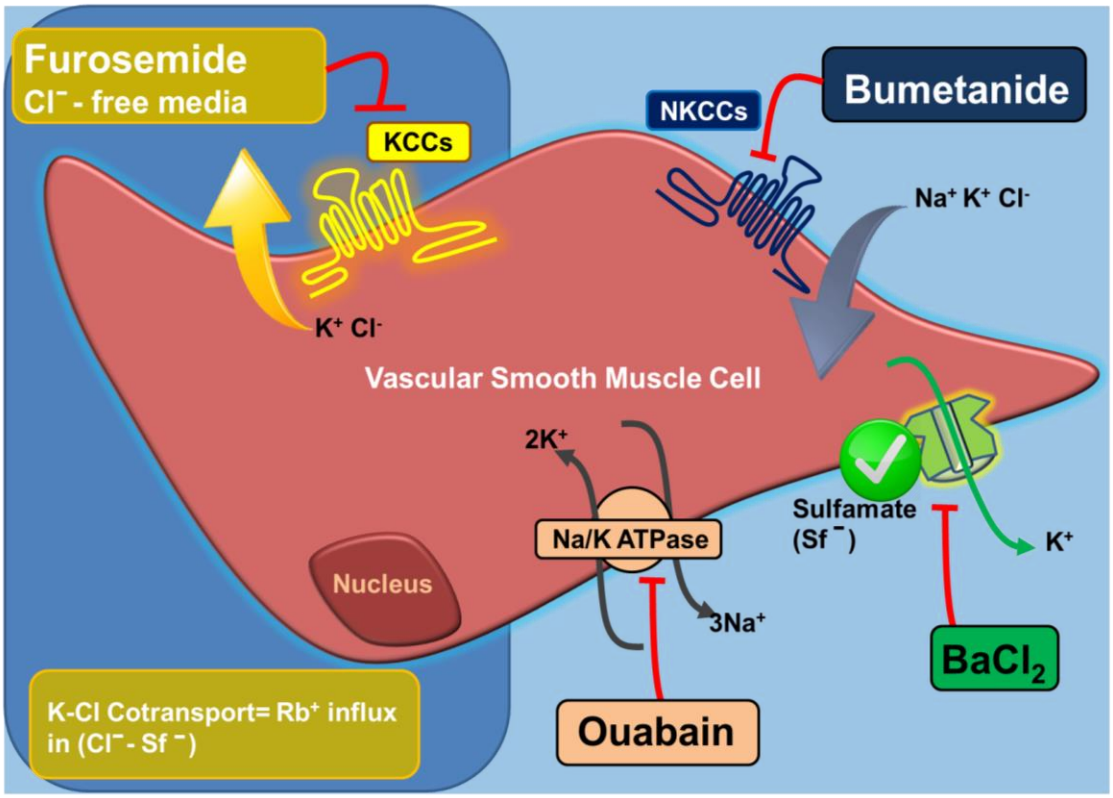

Figure 13. Schematic representation of various K^+ transport mechanisms in VSMCs. Potassium chloride cotransport (KCCs) can be inhibited by furosemide or chloride (Cl^-)-free media. In our experimental design, the anion sulfamate (Sf^-) was used to study the "leak" pathway represented by other K^+ channels that might be present in VSMCs. K-Cl Cotransport corresponds to the differences in Rb^+ influx in Cl^- and sulfamate (Sf^-) media in the presence of ouabain and bumetanide to inhibit the Na^+/K^+ pump and NKCC activity, respectively.

Rb^+ transport studies. K-Cl cotransport activity was measured using previously established protocols in VSMCs with slight modifications (150, 152). Confluent monolayers of VSMCs grown into 12 well plates were rinsed three times with BSS and then equilibrated for 10 min in preincubation media. Several flux timeframes (from 0-40 min) were used to determine K-Cl cotransport activity, which was normalized to protein concentration. Addition of ouabain and bumetanide during preincubation and flux periods prevented K^+/Rb^+ movement mediated by Na^+/K^+ pump and Na^+-K^+-$2Cl^-$ cotransporters, respectively. Rb^+ flux was terminated by washing cells with ice cold 10 mM MOPS-Tris, $MgCl_2$. Intracellular Rb^+ was released from cells by incubating them in 5 % PCA-4 mM CsCl 15 min at 4 ^oC and measured by using a Perkin-Elmer 5000 Atomic Absorption Spectrophotometer (AAS) in the emission mode (148, 150). Next, cells were solubilized with 1N NaOH for 30 min at room temperature and protein concentration was determined using BCA protein assay. Quantification of protein was performed using Labsystems Multiskan MCC/340 plate reader following manufacturer's guidelines (Figure 14). The difference between Rb^+ transport in the presence of Cl^- and Sf^- was used to determine Cl^--dependent Rb^+ influx (i.e. K-Cl cotransport activity).

Apelin studies. Previously described Rb^+ flux studies were performed with minor changes: When required, VSMCs were serum deprived for 24 h at sub-confluence prior to an experiment. Apelin (1 µM) was added either during flux and/or in the growth media based on the experimental goals and design (see result section).

Solutions for Rb^+ transport studies (e.g., Na^+ containing solution)

Initial wash solutions

Balanced salt solution (BSS-NaCl): 20 mM Hepes-Tris, 5 mM KCl, 2 mM $CaCl_2$, 1 mM $MgCl_2$, 10 mM glucose and NaCl, pH 7.4, 37 ^oC, 300 mOsM.

BSS-NaSf: 20 mM Hepes-Tris, 5 mM KSf, 2 mM calcium gluconate, 1 mM magnesium gluconate, 10 mM glucose and NaSf, pH 7.4, 37 ^oC, 300 mOsM.

Preincubation solutions

BSS-NaCl-BSA: 20 mM Hepes-Tris, 5 mM KCl, 2 mM $CaCl_2$, 1 mM $MgCl_2$, 10 mM glucose, 0.1% BSA and NaCl, pH 7.4, 37 ^oC, 300 mOsM.

BSS-NaSf-BSA: 20 mM Hepes-Tris, 5 mM KSf, 2 mM calcium gluconate, 1 mM magnesium gluconate, 10 mM glucose, 0.1% BSA and NaSf, pH 7.4, 37 ^oC, 300 mOsM.

Flux solutions

BSS-RbCl-NaCl-BSA: 20 mM Hepes-Tris,10 mM RbCl, 2 mM $CaCl_2$, 1 mM $MgCl_2$, 10 mM glucose, 0.1% BSA and NaCl, pH 7.4, 37 ^oC, 300 mOsM.

BSS-RbS-NaSf-BSA: 20 mM Hepes-Tris, 10 mM RbSf, 2 mM calcium gluconate, 1 mM magnesium gluconate, 10 mM glucose, 0.1% BSA and NaSf, pH 7.4, 37 ^oC, 300 mOsM.

Final wash solution

10 mM MOPS-Tris, $MgCl_2$, pH 7.4, 4 ^oC, 300 mOsM.

Rb^+ extraction

5% perchloric acid (PCA), 4 mM CsCl

Protein extraction

1M NaOH

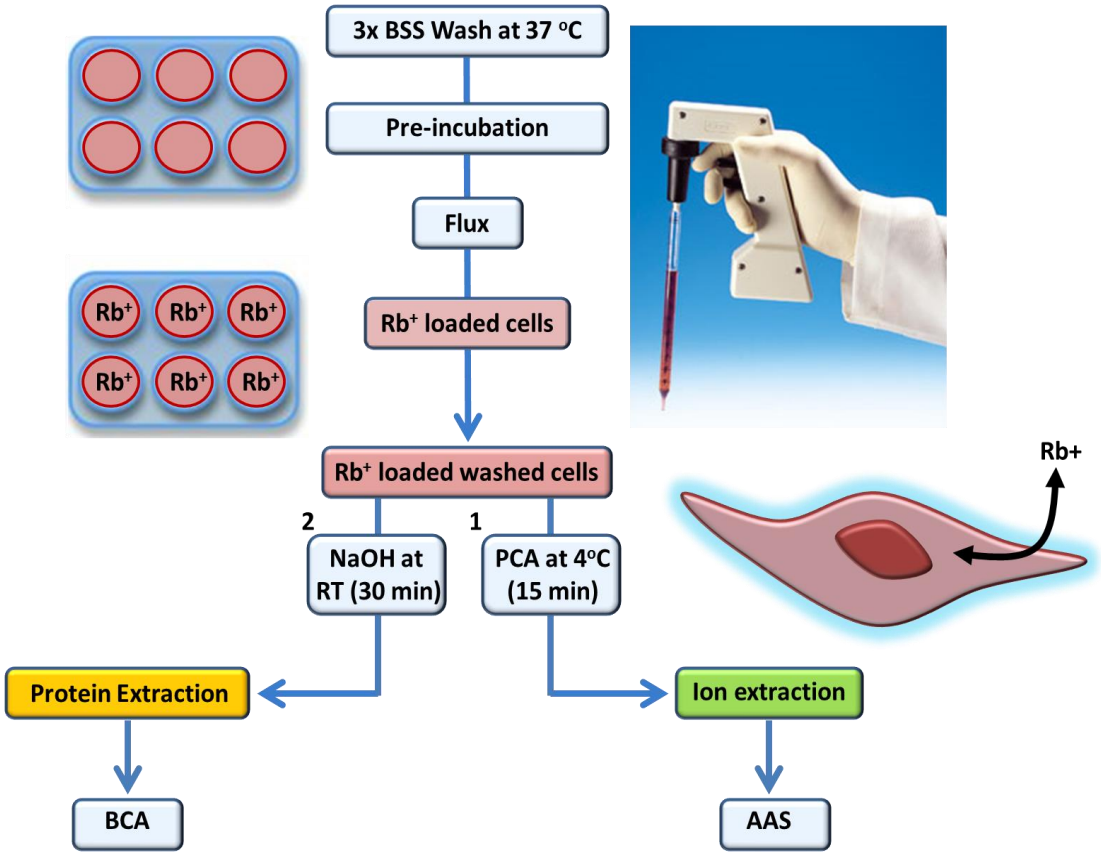

Figure 14. Summary of steps for assessing Rb^+ influx in VSMCs. Washed VSMCs were loaded with Rb^+ (5-40 min), then Rb^+ ion was extracted by PCA and ion concentration was measured by AAS. Protein was solubilized by 1 N NaOH and the content was determined by BCA protein assay.

Protein extraction. Total extracts from VSMCs were obtained using either M-PER and/or RIPA lysis and extraction buffers (Pierce Biotechnology). In all cases manufacturer's guidelines were followed accordingly. VSMCs were grown into 100 mm petri dish. Confluent monolayers were rinsed with cold PBS and resuspended in lysis buffer at 4 ^{o}C in the presence of protein-phosphatase and protease inhibitors. Total cellular protein extracts were obtained using a cell scrapper, then sonicating 5 pulses for 5 seconds followed by centrifugation at 14,000 g for 10 min. The protein concentration of the supernatant was determined according to the BCA protein assay. Protein samples were stored at -20 ^{o}C until used for Western blot analysis.

Western blot (WB) analysis. Standard Western blot procedures were performed as described elsewhere with slight modifications (148, 149). Equal amount of proteins of contractile and/or synthetic VSMCs were resolved by 7.5 and/or 8.5 % SDS-PAGE and transferred to polyvinylidene difluoride (PVDF) membranes using a semidry system. Membranes were blocked with 10 % nonfat dry milk and/or 5 % BSA in Tris-buffered saline and 0.05 % tween 20 (TBS-T) for 1h at room temperature (RT). Membranes were then exposed overnight at 4 ^{o}C to primary antibodies against: mouse (ms) anti-α-actin (1:1000), rabbit (rb) anti-vimentin (1:1000), ms anti-desmin (1:1000), rb anti-KCC1 (1:250), rb anti-KCC4 (1:500), and polyclonal rb anti-APJ (1:1000). Similar protein loading was verified by probing membranes with ms anti-β-actin (1:1000). PVDF membranes were then washed extensively in TBS-T and incubated for 2 h with the appropriate horseradish peroxidase-conjugated secondary antibodies, donkey anti-rb

(1:3000) and/or donkey anti-ms (1:3000) in 10 % nonfat dry milk in TBS-T. Prior to detection, membranes were washed three times in TBS-T and enhanced chemiluminescence (ECL) was used for visualization of immunocomplexes using a high resolution Fuji LAS3000 CCD camera. Band densitometry was performed by computer software attached to a Kodak camera and/or ImageJ software to determine the changes in protein expression.

Immunofluorescence. The immunofluorescence procedure was described elsewhere (137, 138). Here with slight protocol modifications, protein localization patterns for α-actin, PKG and APJ receptor were determined from contractile and/or synthetic VSMCs at 25 % confluency. VSMCs were seeded in 8-well chamber slides (Lab-Tech; NUNC) at a density of 8 x 10^4 cells/well, washed with ice cold 1X PBS, fixed with 0.5 mL/well of 4 % paraformaldehyde (± saponin) for 30 min at 4 ^oC, then incubated in 0.5 mL/well 3 % of normal goat/donkey serum (NGS/NDS) for 1h at 4 ^oC to block non-specific immune staining. After serum removal, cells were incubated with corresponding primary antibodies at the following concentrations: ms monoclonal anti-α-actin (1:250) in 3 % NGS, rb polyclonal anti-APJ (1:100) in 3 % NDS and rb anti-PKG (1:100) in 3 % NDS overnight at 4 ^oC. Samples incubated with only primary or secondary antibodies were used to assess specificity of the antibodies used. Cells were then washed twice with ice cold PBS followed by incubation with anti-ms IgG-FITC (1:1000), or anti-rb FITC (1:100), or donkey anti-rb Cy3 (1:200) for 1 to 2 h at room temperature (RT). Finally, cells were washed in cold PBS and with deionized water. The cells were co-labeled with 4',6-diamidino-2-phenylindole (300 nM

DAPI) to visualize cell nuclei. Slides were imaged with an inverted Nikon E400 fluorescent microscope using 100X to 400X (oil) magnification and then superimposed using GIMP software.

Statistical analysis. Graphs were generated using Origin 7.0 (Origin Labs, Northampton MA) and STATISTIX 7 software (Analytical software, Tallahassee FL). Most results shown are product of at least two independent experiments with multiple determinations per condition. Data are reported as mean ± SD or SEM. Unpaired *t-test* or One-way ANOVA was performed using Graph pad Prism 5 software (La Jolla, CA). A p value of < 0.05 was considered statistically significant.

RESULTS: Specific Aim 1

Growth rate of VSMCs with passage number and according to the phenotype (contractile and synthetic).

This study utilizes cultured VSMCs as a model system to provide insight into a better understanding of the differences between VSMCs phenotypes (28). Several reports correlate VSMCs passage number with their respective phenotypes. VSMCs at passages 0-4 have been defined as predominantly contractile, at passage 5 intermediate, and at passages 6 and later as synthetic (25, 168, 169). Thus, an important factor in characterizing VSMCs properties is the time for them to proliferate in culture. When seeded at a constant density, an inverse correlation between time to reach confluence and VSMCs passage number was observed. For the purpose of comparison, the synthetic VSMCs populations were grouped based on their passage number: early (6-15); medium (30-45); and late (70-80). Contractile VSMCs (passages 0-4) required 10-14 days to reach confluence, whereas, early synthetic phenotype cells achieved maximum confluence in 4-6 days, and medium and late synthetic phenotype cells consistently reached confluence in 2-3 days (**Figure 15**).

VSMC phenotypic determination by specific markers

The phenotypic transition of VSMCs from contractile to synthetic can be studied using specific protein markers (*e.g.*, α-actin, myosin, desmin, vimentin, osteopontin, and others) that are either up- or down-regulated depending upon the differentiation state of the cells (17-19). Thus, the phenotypic identity of the *in vitro* cell populations with antibodies against specific contractile protein markers was confirmed using SDS-PAGE and Western blotting.

In late synthetic VSMCs phenotype (passage ≥ 70), there was a 60 % reduction in α-actin (**Figure 16A**), a 25 % reduction in vimentin (**Figure 16B**), and a 90 % reduction in desmin protein expression (**Figure 16C**). Consistent with the decrease in α-actin seen in **Figure 16**, immunofluorescence labeling of α-actin expression in early and late synthetic VSMCs showed an abundance of filamentous α-actin in the cytoplasmic compartment of early passage VSMCs (**Figure 17A**), whereas in higher passages, α-actin was redistributed or rearranged in a punctate fashion (**Figure 17B**).

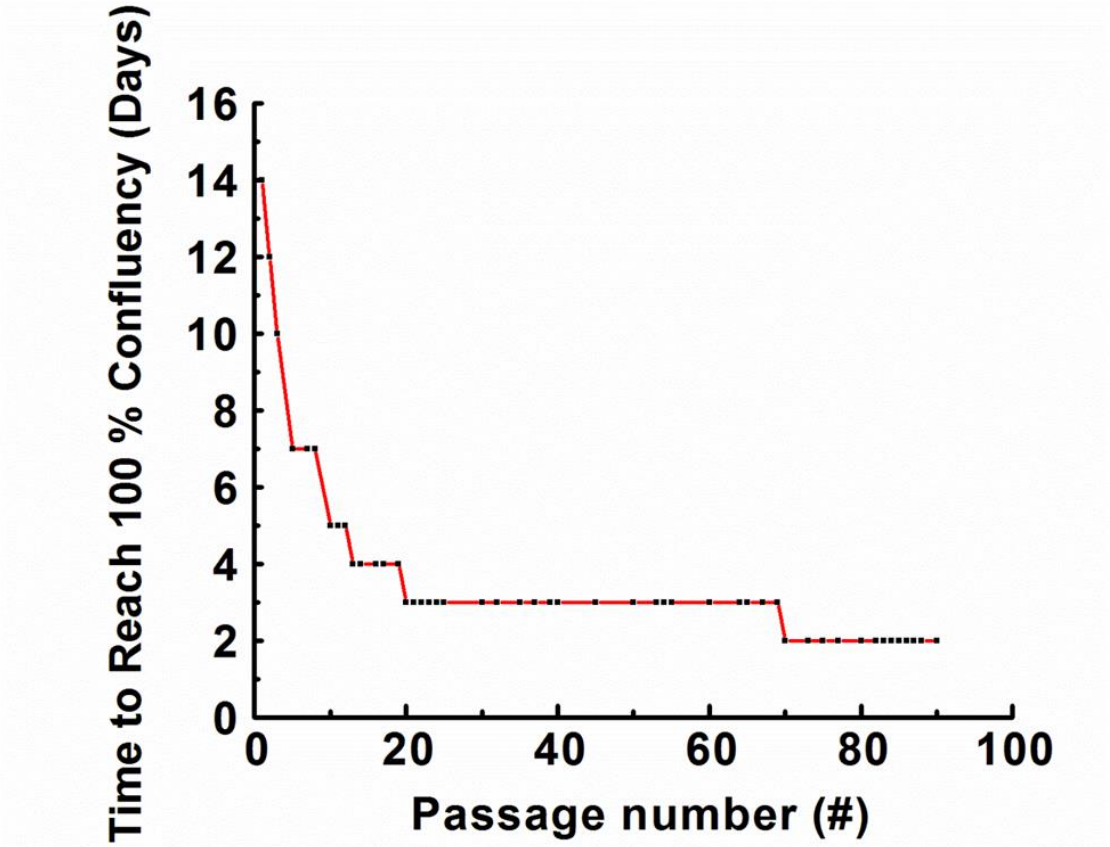

Figure 15. Time to reach confluency of vascular smooth muscle cell (VSMC) cultures as a function of passage number. VSMCs at various passages (0 – 90) were seeded in T-75 flasks at constant seeding density of 5 x 10^5 cells/mL per flask. Y-axis shows time (days) to reach confluence in culture and in the X-axis the passage number. VSMCs at earlier passages (passage 0-4) were predominantly contractile whereas those at higher passages (≥ 6) corresponded to increasing populations of synthetic VSMCs.

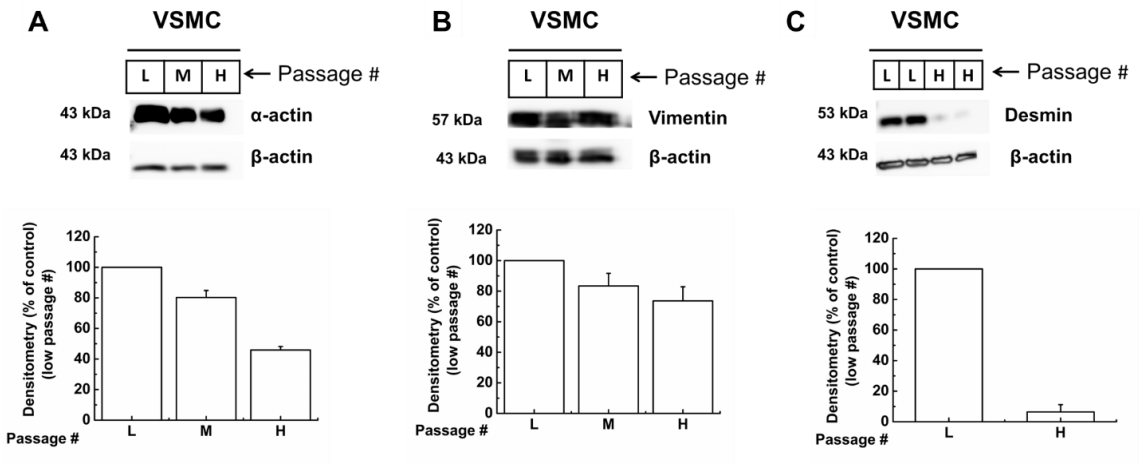

Figure 16. Characterization of VSMCs phenotypes in culture with respect to specific protein markers. Western blots of a representative experiment for low (L, passage 6), medium (M, passage 38) and high (H, passage 74) passage VSMCs. **Panel A**. ~ 43 kDa α-actin. **Panel B.** ~ 57 kDa vimentin. **Panel C.** ~ 53 kDa Desmin. Densitometric quantitation of the protein bands shown in A-C were normalized to β-actin (internal control), and then the quantified protein bands of M and H passages were normalized to basal expression levels (L as a baseline control). Densitometry analysis represents mean ± range of two experiments.

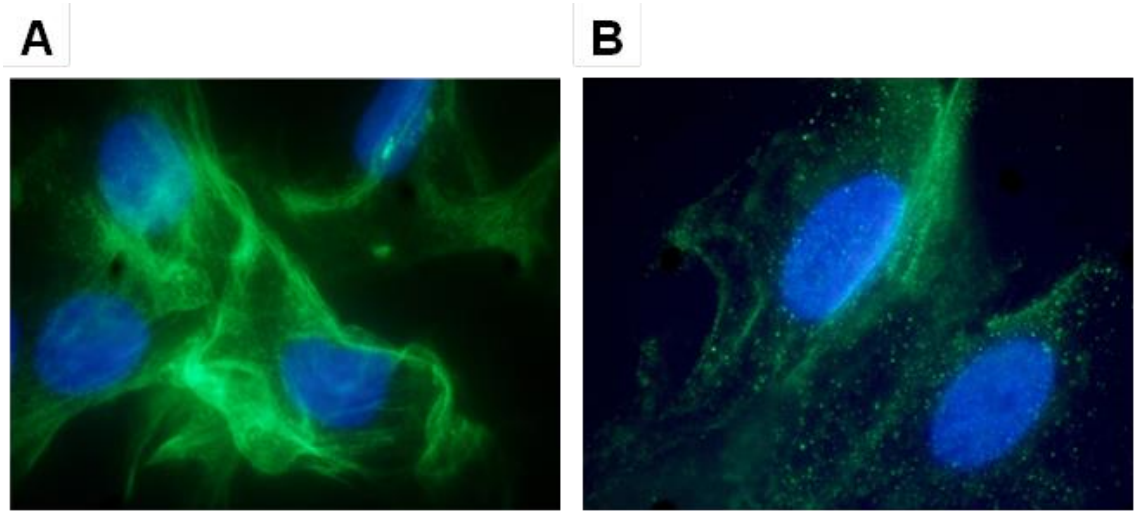

Figure 17. Immunolocalization and distribution of α-actin contractile protein marker in early and late passage synthetic VSMCs. Immunofluorescence of FITC-labeled α-actin and DAPI-labeled nuclei in early (Panel A, passage 6) and late passage (Panel B, passage 89) VSMCs.

K^+ influx pathways in VSMCs

Non-radioactive rubidium ($^{85}Rb^+$) has been used as a potassium congener in previous ion flux studies (110, 110, 150, 170, 171). In order to isolate the portion of Rb^+ influx that moves through KCC, three Rb^+ uptake components were measured: (1) the total Rb^+ uptake in the absence of inhibitors (T), (2) in the presence of ouabain (oua), and (3) in the presence of ouabain and bumetanide (oua + bum) as described elsewhere (171). Rb^+ uptake through the ouabain-sensitive Na^+/K^+ pump, the ouabain-insensitive and bumetanide-sensitive NKCC, and [ouabain + bumetanide]-insensitive K^+ "leak" component containing the KCC and K^+ channels, were calculated as a function of time. Initial rates for Na^+/K^+ pump and NKCC were linear up to 5 min. The remaining ouabain- and bumetanide-insensitive portions of Rb^+ influx were linear up to 15 min (**Figure 18**). In addition, percent Rb^+ uptake-mediated by NKCC was higher than transport via the Na^+/K^+ pump. Higher transport velocity of NKCC suggests that in VSMCs, there are more copies of NKCC with higher turnover rate, or they are mostly activated by phosphorylation. For both the pump and NKCC, the equilibration was achieved by 20 min (**Figure 19**).

To study in greater detail KCC in VSMCs, the concentration of ouabain and bumetanide to block the Na^+/K^+ pump and NKCC were optimized. First, we determined the ouabain concentration at which complete inhibition of Rb^+ transport via the Na^+/K^+ pump occurs in VSMCs (**Figure 20**). In order to achieve that, Rb^+ influx was measured from confluent VSMCs incubated with ouabain concentrations up to 4 mM. Ouabain was present throughout the whole course of

the experiment (preincubation and flux; 15 min), or only during flux time period (5 min). Data revealed a 45 % and 65 % reduction in total Rb^+ transport when ouabain concentrations (≥ 2 mM) were present during flux or throughout the whole course of the experiment. Notably, higher ouabain concentrations were required to inhibit Na^+/K^+ pump activity compared to previous reports using different cell types (eg. Human lens epithelial cells (HLEC), human embroyonic kidney (HEK-293) cells, etc.) (171, 172). Since the alpha subunit of the Na^+/K^+ pump is targeted by ouabain, and differences in ouabain sensitivity have been reported among isoforms ($\alpha1<\alpha2<\alpha3$); it is possible that alpha 1 isoforms with low ouabain affinity are highly and predominantly expressed in VSMCs (173, 174).

After determining the optimal ouabain concentration to inhibit the Rb^+ mediated flux via the Na^+/K^+ pump, similar studies including bumetanide at concentrations up to 20 μM were carried out to further dissect the KCC-mediated Rb^+ transport fraction. As seen in **Figure 21**, 80 % inhibition of Rb^+ transport was obtained when bumetanide (>1 μM) and ouabain (2 mM) were present during preincubation and flux time periods. In VSMCs, the IC_{50} for bumetanide was 0.1 μM. Interestingly, bumetanide concentrations in the nanomolar range displayed a stimulatory effect on Rb^+ influx. To date, the mechanisms behind this initial and transient stimulation of Rb^+ transport remains unclear.

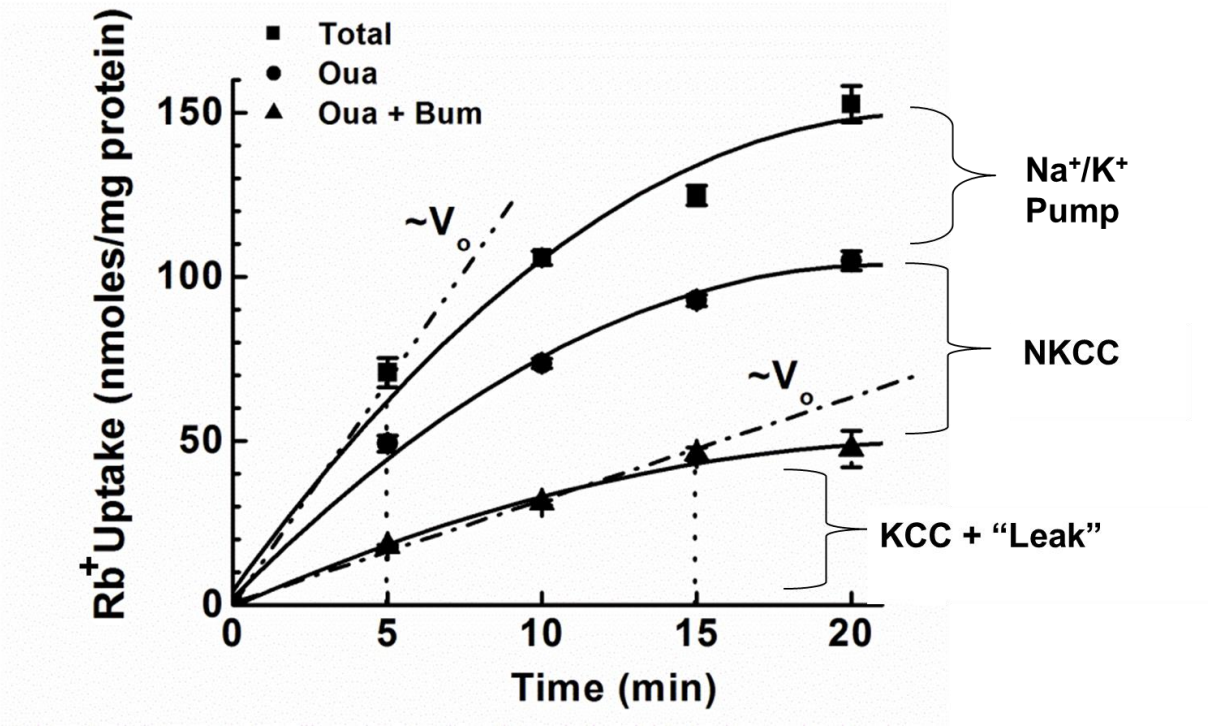

Figure 18. Characterization of Rb^+ uptake in VSMCs via various K^+ transport pathways. Rb^+ uptake (nmoles/mg protein) as a function of time (min) was tested under isotonic (300 mOsM) conditions. Total Rb^+ uptake was measured in the absence of inhibitors (Total, squares), in the presence of ouabain (1mM) (Oua, circle), and in the presence of ouabain (1 mM) and bumetanide (10 µM) (Oua + Bum, triangle). Na^+/K^+ pump is the difference between Rb^+ uptake in the absence of inhibitors (Total) and in the presence of ouabain (Oua). NKCC is the difference between Rb^+ transport in the presence of ouabain (Oua), and ouabain + bumetanide (Oua + Bum). Finally, KCC and "leak" mediated by K^+ channels is Rb^+ transport in the presence of ouabain and bumetanide (Oua + Bum). Data shown is a representation of three independent experiments. Data are expressed as mean ± SD (n= 4 per condition).

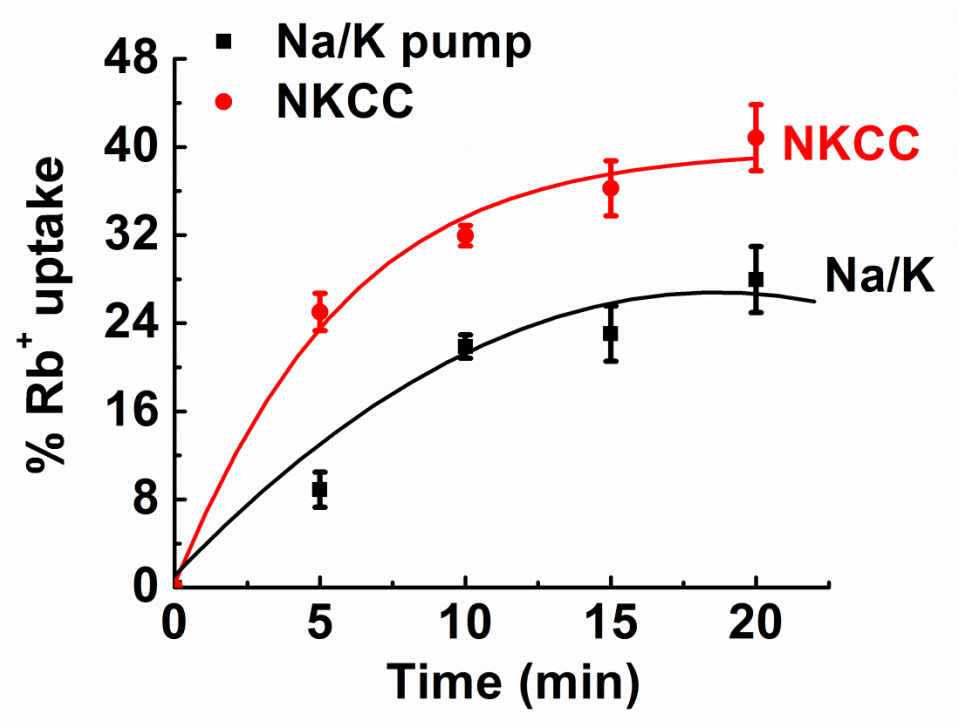

Figure 19. Percent Rb^+ uptake-mediated via NKCC and Na^+/K^+ pump in VSMCs. Rb^+ uptakes-mediated by NKCC and Na^+/K^+ pump were normalized to that of total uptake in the absence of any inhibitors. NKCC and Na^+/K^+ pump-mediated uptakes were calculated as described in Material and Methods and previous section. Normalized Rb^+ uptake increased parabolic with time for NKCC and Na^+/K^+ pump and equilibrated at 20 min. Data shown is a representative experiment done in triplicates. For each condition, data reported is mean ± SD (n = 4 per condition).

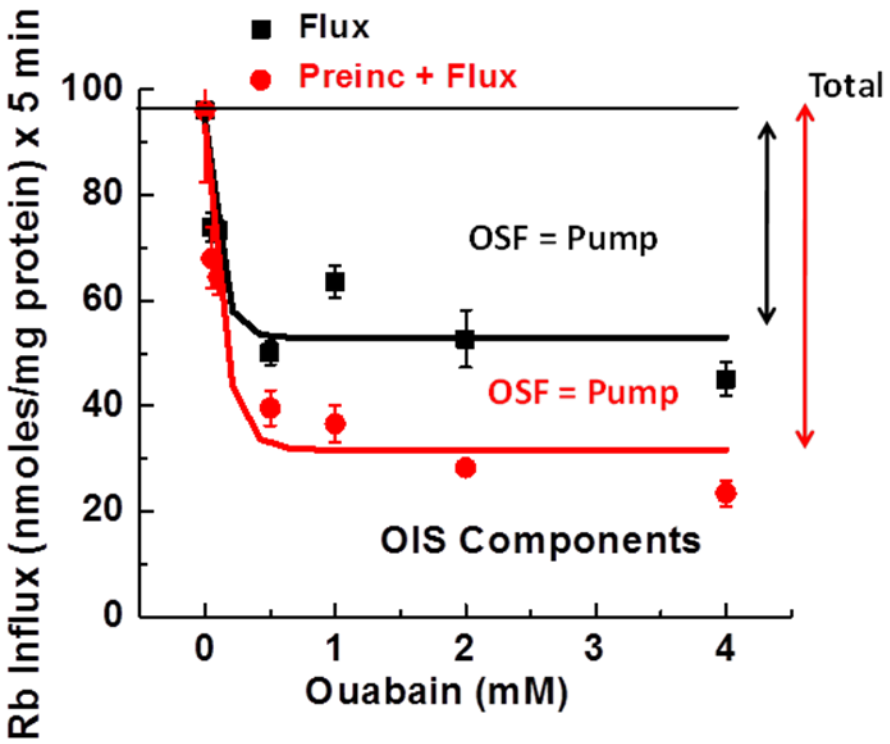

Figure 20. Determination of ouabain concentration optimally inhibiting the Na^+/K^+ pump in VSMCs. VSMCs were grown up to confluence and washed three times with BSS as described in Materials and Methods. The ouabain-sensitive flux (OSF) was calculated as the difference between Rb^+ influx in the presence and absence of ouabain and is plotted here as function of ouabain in flux only (filled squares) or with combination in preincubation and flux (filled circles). Data fitted with Boltzmann function revealed that ouabain concentrations ≥ 2 mM, when present during flux periods resulted in a 45 % of reduction in Rb^+ transport (filled squares). Further inhibition of Rb^+ transport (up to 65 %) was attained when ouabain was present during preincubation and flux periods (filled circles). Data shown are mean ± SD of a representative experiment done in triplicates. For each condition, n = 4.

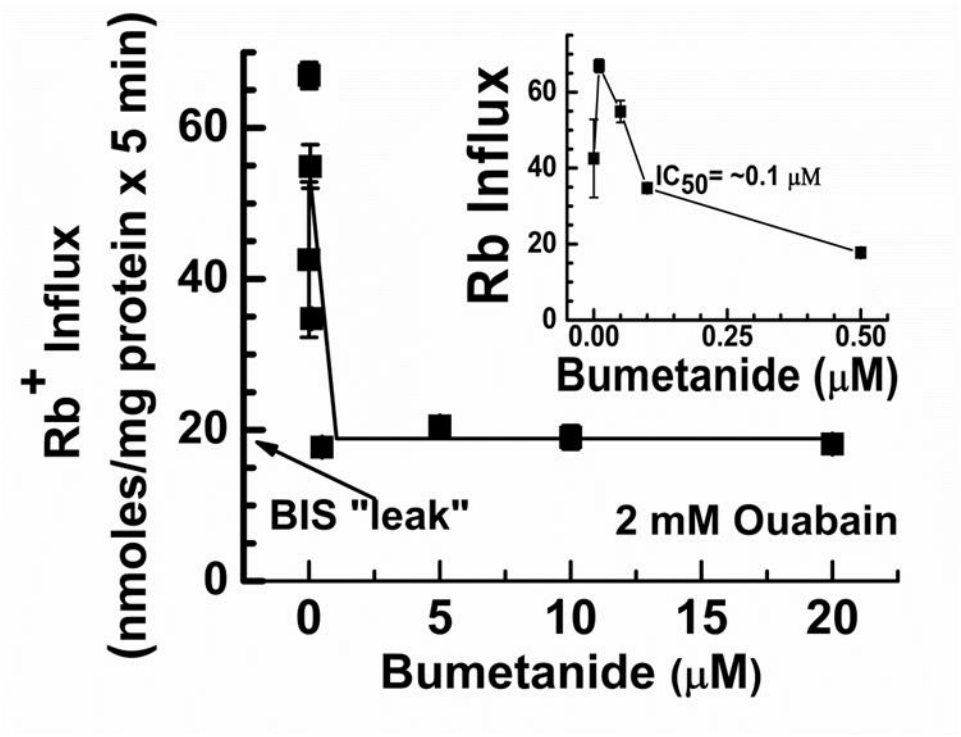

Figure 21. Bumetanide dose-response curves in rat aortic VSMCs. Rb^+ influx was determined in the presence of ouabain (2 mM) and bumetanide (0-20 μM). With increasing bumetanide concentrations and in the presence of 2 mM ouabain, NKCC- and Na^+/K^+ pump- mediated transport mechanisms are removed and KCC activity can be further dissected. Bumetanide concentrations above 1 μM in combination with 2 mM ouabain resulted in 80 % inhibition of Rb^+ influx. The IC_{50} for bumetanide was found at 0.1 μM. Rb^+ influx linear between 1 and 20 μM bumetanide is the to bumetanide-insensitive (BIS) "leak" pathway attributed to KCC + K^+ channels. Data represents mean ± SD. For each condition, n = 4.

Functional characterization of K-Cl cotransport in VSMCs

KCC anion preference (Cl^- >Br^- >SCN^- >I >$NO3^-$ >$MeSO4^-$) was previously established by Lauf and Theg 1980, and Ellory et al 1982 in erythrocytes (84, 121, 175) and later in VSMCs (150). Consistent with previous findings from our laboratory in VSMCs (149, 150), **Figure 22** shows KCC activity, calculated as the difference of Rb^+ uptake in Cl^- and Sf^-, maintained linearity up to 30 min. To determine an optimal extracellular $[Rb^+]_o$, that would saturate KCC, the activity of KCC was measured with respect to $[Rb^+]_o$ and the findings are shown in **Figure 23**. KCC saturation was achieved at a concentration of 20 mM $[Rb^+]_o$. Therefore in subsequent experiment, $[Rb^+]_o$ lower than 20 mM within K_m value range (10 mM Rb^+) were used to assess KCC activity.

Additionally, KCC activity was tested using known stimulators of the system (hypotonicity and NEM) as shown in **Figure 24.** Similar findings have been previously reported (75, 89, 90, 151, 152) and the effect was reproduced under the present conditions. KCC activity under hypotonic stimulus was increased by 80 % (with respect to isotonic). The NEM concentration of 0.05 mM has been used to see the stimulatory effect (90). Our studies showed NEM (0.05 mM) increased KCC activity by 2-fold. This mode of activation has been a hallmark of KCC regulation, which suggested that Rb^+ influx was indeed mediated by thiol group modification as originally proposed by Lauf and Theg (84, 176) (**Figure 24**).

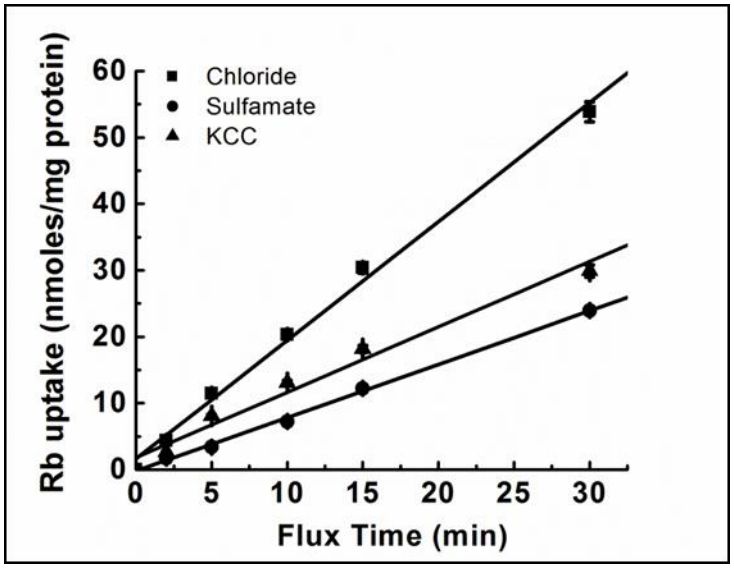

Figure 22. Rb+ uptake as a function of time was measured under isotonic condition in Cl^- and Sf^- media. Rb^+ uptake as a function of time was measured in the presence of Cl^- and Sf^-, respectively. Ouabain (2 mM) and bumetanide (2 µM) were present during the preincubation and flux. Rb^+ uptake via KCC was calculated as the difference in Rb^+ uptake in Cl^- and Sf^-, and was linear up to 30 min. For each time point, n = 4 and values expressed are mean ± standard error.

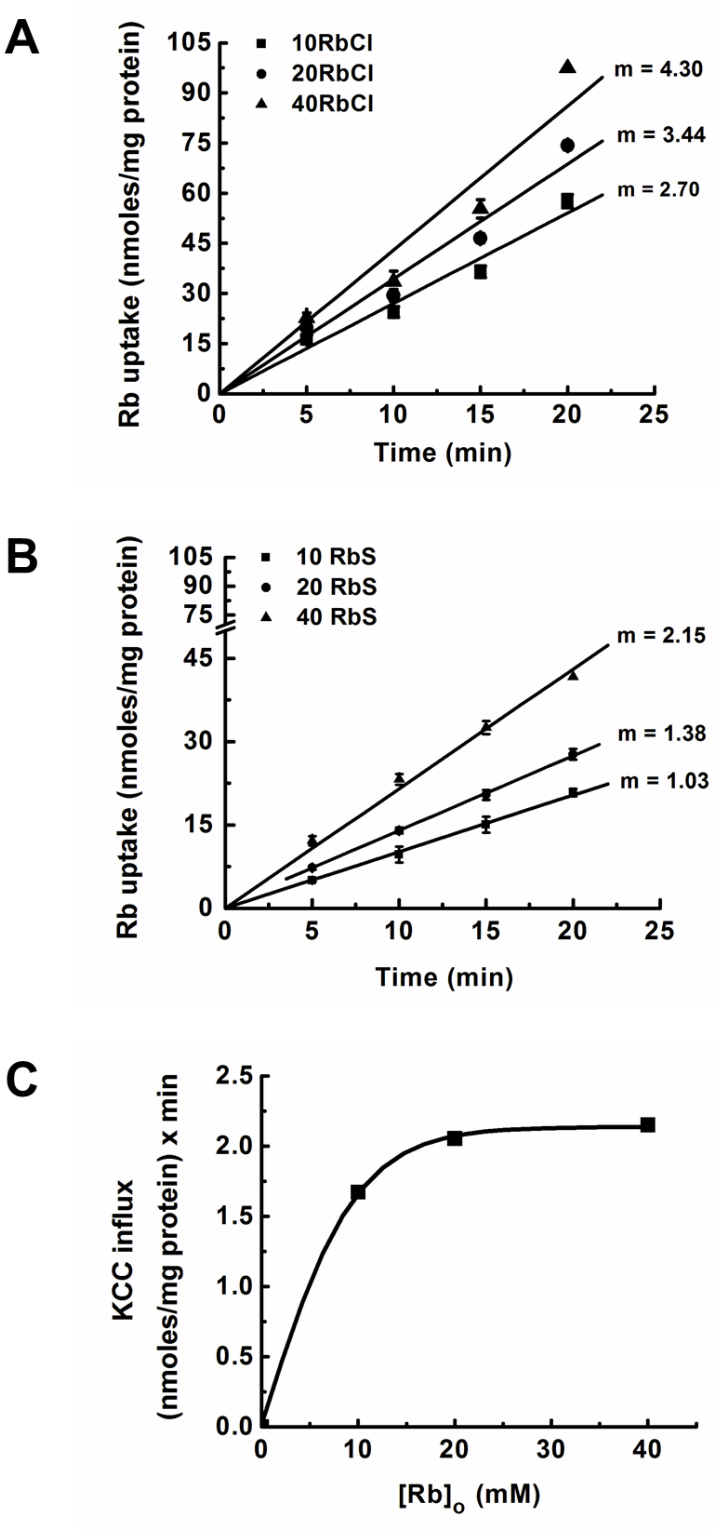
A
Rb uptake (nmoles/mg protein)
105
90
75
60
45
30
15
0
10RbCl
20RbCl
40RbCl
m = 4.30
m = 3.44
m = 2.70
0
5
10
15
20
25
Time (min)
B
Rb uptake (nmoles/mg protein)
105
90
75
45
30
15
0
10 RbS
20 RbS
40 RbS
m = 2.15
m = 1.38
m = 1.03
0
5
10
15
20
25
Time (min)
C
KCC influx
(nmoles/mg protein) x min
2.5
2.0
1.5
1.0
0.5
0.0
0
10
20
30
40
[Rb]o (mM)

Figure 23.

Figure 23. KCC as a function of varying $[Rb^+]_o$. Rb^+ uptake was measured in the presence of increasing concentrations of RbCl between 0 and 40 mM (Panel A) or RbSf (Panel B) at various time points. The slope "m" of the straight lines represents the Rb^+ influx in Cl^- and Sf^-. The difference between the slopes represents the Cl^--dependent Rb^+ influx (KCC) (Panel C). VSMCs at passage 37 were used for this study. For each time point, n = 4 and the data represent mean ± SD.

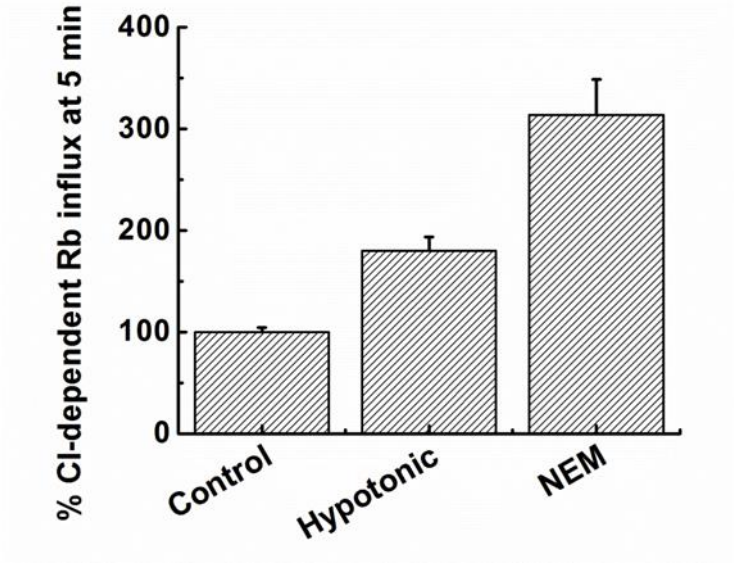

Figure 24. Activation of KCC by hypotonicity and NEM. Percent (%) Cl^--dependent Rb^+ influx (KCC) was calculated at 5 min in isotonic (control, 300 mOSM), hypotonic (120 mOSM) and in the presence of the thiol-modifying agent N-ethylmaleimide, NEM (isotonic, 300 mOSM). NEM (final concentration 0.05 mM) was present in the preincubation media as described in Material and Methods. NaCl was used to increase the osmolality to 300 mOsM. Ouabain (2 mM) and bumetanide (2 µM) were present in both preincubation and flux solutions to inhibit Na^+/K^+ pump and NKCC, respectively. For each condition, n = 6, and values are mean ± standard error.

KCC kinetic parameters in low and high passage synthetic VSMCs

To determine a potential relationship between K-Cl cotransport activity and VSMCs' phenotypic transition, we compared the Cl^--dependent Rb^+ flux in low and high passage synthetic cells. In order to characterize KCC activity in early and late passage VSMCs, Rb^+ influx was measured as a function of $[Rb^+]_o$ at fixed Cl^- concentration ($[Cl^-]_o$ ~ 145 mM) (**Figure 25**) or as a function of varying $[Cl^-]_o$ at fixed $[Rb^+]_o$ (10 mM) (**Figure 26**). Both curves show that transport of Rb^+ across the cell membrane required presence of both external Cl^- and Rb^+. At maximal concentration of these ions, saturation was achieved as described by the Michaelis-Menten equation. The transport velocity reached a plateau at a certain substrate concentration and above which there was no substantial increase in uptake velocity (**Figure 25A and Figure 26 A-B**). The apparent binding affinity for Rb^+ was higher than that of Cl^- (**Figure 25B *vs* Figure 26B**). The maximal rate of Rb^+ uptake was similar for both conditions (**Figures 25B and Figure 26B**). The Hill coefficient "n" for both ions was close to unity (~ 1) suggesting there is only one binding site for each ligand. Whether, the binding of each ligand appears to be independent of a previous or subsequent ligand binding to the same site, i.e. random order of binding, cannot be determined from these studies (107, 110).

In low passage VSMCs, similar experiments demonstrated that the Cl^--dependent Rb^+ transport activity through KCC in the presence of $[Rb^+]_o$ (10 mM) or $[Cl^-]_o$ (145 mM) resulted in a significant 50 % reduction in maximal velocity as compared to high passage VSMCs (**Figure 25D-F, Figure 26D-F and Table 2**).

The binding affinity (K_m) for Rb^+ at the external site of KCC was higher than the apparent binding affinity for Cl^- (**Figures 25-26 B *vs* E**). The Hill coefficient "n" was 1 for both Rb^+ and Cl^- implying presence of one binding site for each ion as stated earlier (**Figures 25-26 B *vs* E**). **Table 2** summarizes the average of several experiments for early and late synthetic VSMCs with respect to the ionic ligands. As shown in **Table 2**, the V_{max} with respect to external Rb^+ and Cl^- was twice for late synthetic, the K_m for Rb^+ at external KCC binding sites were consistent in both groups. Apparent affinity for Cl^- was higher (low K_m value) in late synthetic VSMCs compared to earlier stages (**Table 2**).

KCC expression during VSMCs phenotypic switching

During VSMCs' phenotypic switching, increased motility and proliferation rates are tightly linked to synthetic states of VSMCs. Additionally, precise control of cell volume and thus K-Cl cotransport activity is required to allow changes in cell volume and sustain cell proliferation and motility. With that in mind, we wondered if changes in KCC protein expression could be associated to VSMCs' dedifferentiation processes. As can be seen in **Figure 27** KCC1 and KCC4 total protein levels, assessed by Western blot, were increased in later synthetic states. Interestingly, upregulation of KCC4 seemed to occur earlier compared to KCC1 (**Figure 27A *vs*. Figure 27B**). Maximal KCC1 upregulation was observed in VSMCs cultures at passage 74 (High) whereas KCC4 highest protein levels were detected at passage 38 (Med). The observed increase in KCC1 and KCC4 expression is in accordance with higher motility and proliferation rates seen in synthetic VSMCs populations.

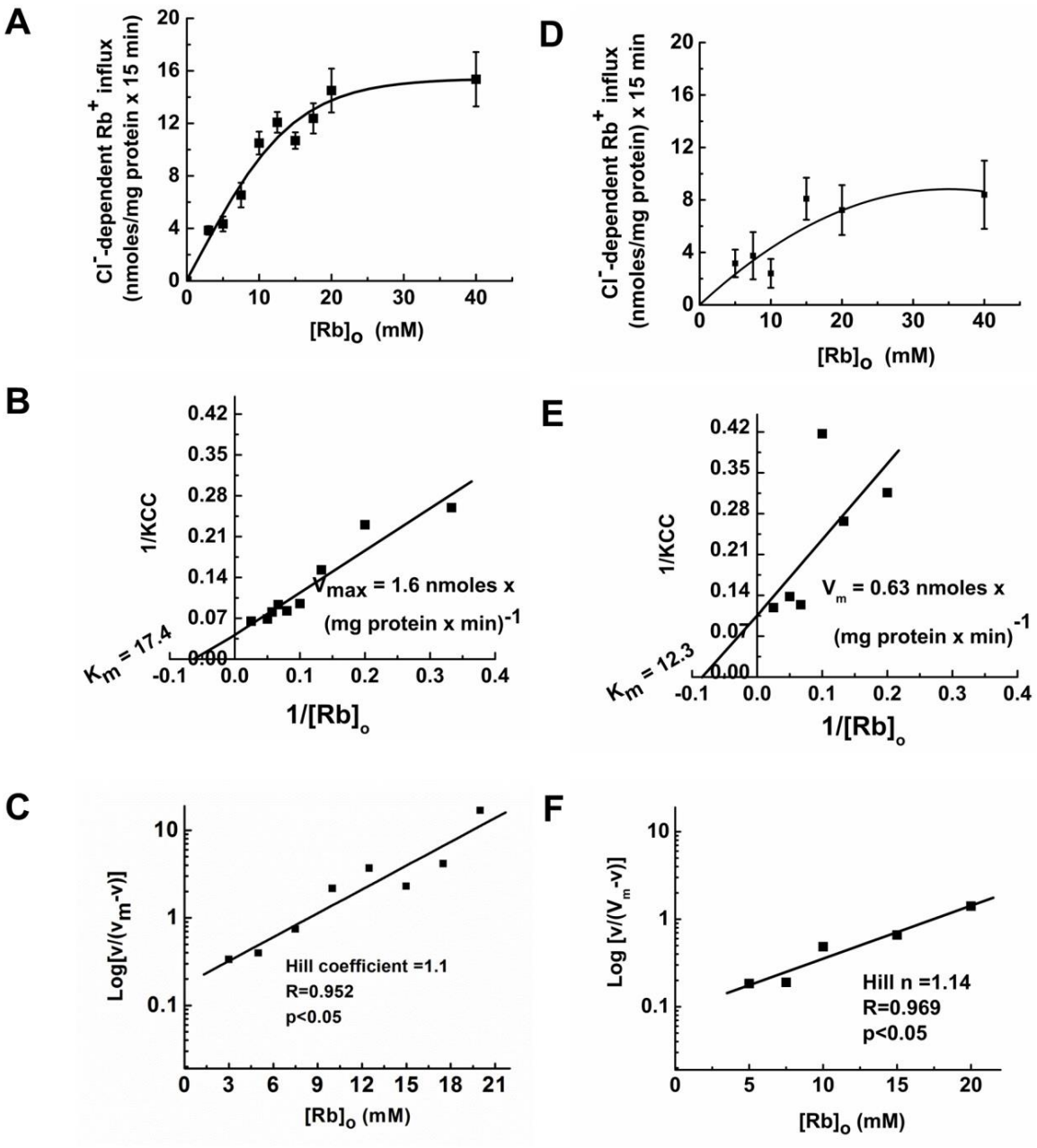
A
Cl⁻-dependent Rb⁺ influx (nmoles/mg protein x 15 min)
[Rb]o (mM)
D
Cl⁻-dependent Rb⁺ influx (nmoles/mg protein) x 15 min
[Rb]o (mM)
B
1/KCC
Vmax = 1.6 nmoles x (mg protein x min)⁻¹
Km = 17.4
1/[Rb]o
E
1/KCC
Vm = 0.63 nmoles x (mg protein x min)⁻¹
Km = 12.3
1/[Rb]o
C
Log[v/(Vm-v)]
Hill coefficient =1.1
R=0.952
p<0.05
[Rb]o (mM)
F
Log [v/(Vm-v)]
Hill n =1.14
R=0.969
p<0.05
[Rb]o (mM)

Figure 25.

Figure 25. Characterization of KCC kinetics in high passage (P 42) and low passage (P 8) VSMCs with respect to the external Rb^+ concentration. Panels A-C show kinetics data for high passage and panels D-F are for low passage VSMCs. (A and D) Cl^--dependent Rb^+ influx through KCC. KCC activity was calculated as the difference between the Rb^+ influx in Cl^- and Sf^-. (B and E) Lineweaver-Burke plot of data in (A and D) to calculate the maximal rate of Rb^+ uptake (V_{max}) by KCC, and the binding affinity (K_m) for Rb^+. (C and F) Hill plot showing the degree of co-operativity "n". Data shown is a representative experiment done in quadruplicates. Data calculated is mean ± standard error (n = 4).

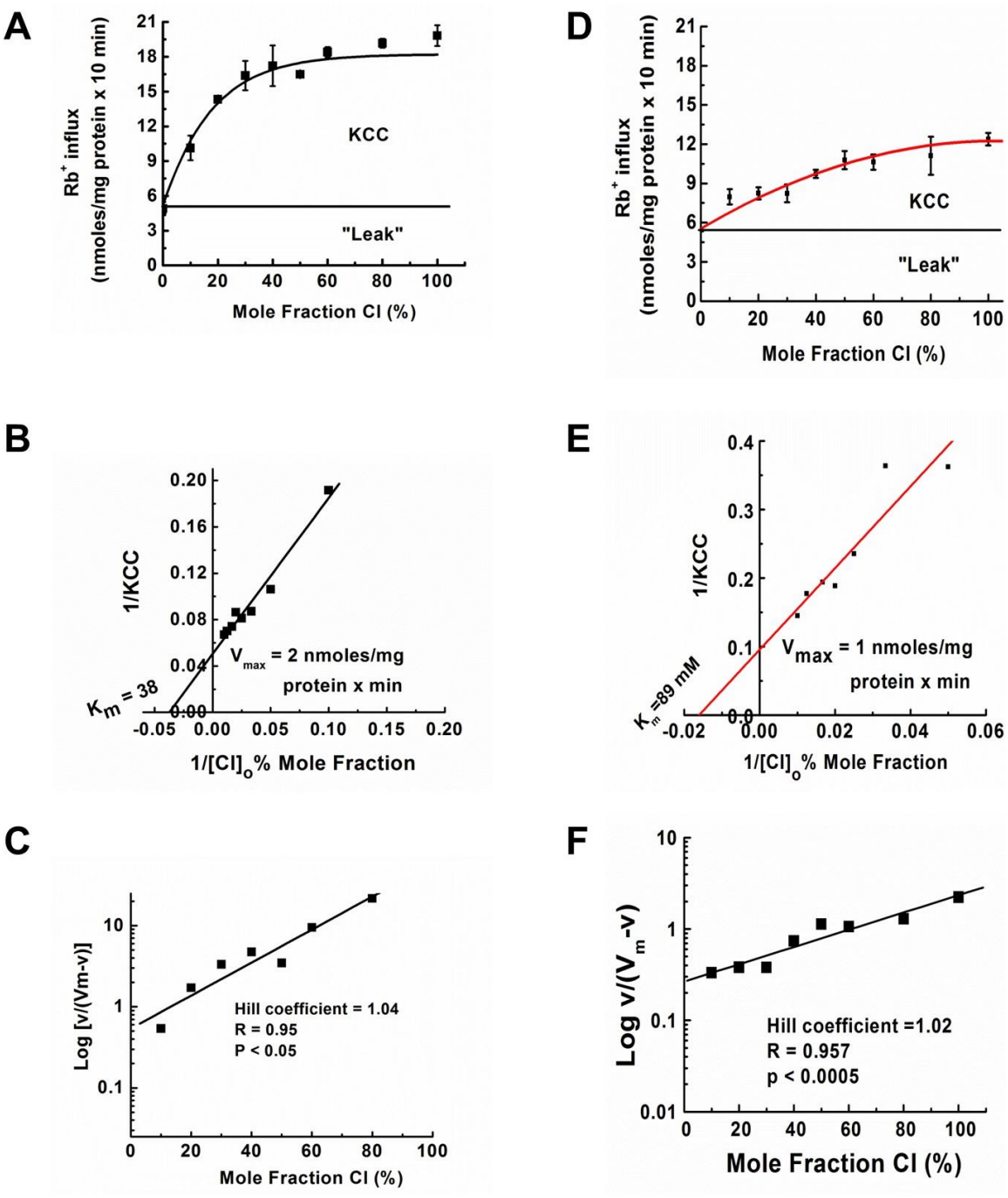
A
Rb+ influx
(nmoles/mg protein x 10 min)
KCC
"Leak"
Mole Fraction Cl (%)
D
Rb+ influx
(nmoles/mg protein x 10 min)
KCC
"Leak"
Mole Fraction Cl (%)
B
1/KCC
Vmax = 2 nmoles/mg
protein x min
Km = 38
1/[Cl]o % Mole Fraction
E
1/KCC
Vmax = 1 nmoles/mg
protein x min
Km =89 mM
1/[Cl]o % Mole Fraction
C
Log [v/(Vm-v)]
Hill coefficient = 1.04
R = 0.95
P < 0.05
Mole Fraction Cl (%)
F
Log v/(Vm -v)
Hill coefficient =1.02
R = 0.957
p < 0.0005
Mole Fraction Cl (%)

Figure 26

Figure 26. Characterization of KCC kinetics in high passage (P 39) VSMCs and low passage (P 6) with respect to the $[Cl^-]_o$. Panels (A-C) are kinetic data for high passage and panels (D-F) are for low passage VSMCs. (A) KCC activity was calculated as the difference between the Rb^+ influx in Cl^- minus Sf^- ("Leak"). KCC saturation was achieved at maximum chloride concentration (145 mM). (B) Lineweaver-Burke plot showing the apparent binding affinity of the external binding site of KCC for Cl^-, and the maximal rate of Rb^+ uptake (K_m and $V_{max,}$ respectively). (C) Hill plot showing degree of co-operativity "n". (D) KCC influx was decreased compared to high passage VSMCs. (E) Lineweaver-Burke plot showing apparent binding affinity of Cl^- and maximal rate of Rb^+ uptake. The K_m was increased (low affinity) as compared to Panel B. The V_{max} was decreased by half as compared to Panel B. (F) Hill plot showing degree of co-operativity "n" = 1, which is similar to high passage VSMCs. The data shown is a representative experiment with quadruplicate measurements and the values are mean ± standard error (n=4).

VSMC Passage	V_m (nmol Rb/mg protein x min)		K_m (mM)		Hill coefficient	
	$f[Rb]_o$	$f[Cl]_o$	$[Rb]_o$	$[Cl]_o$	$f[Rb]_o$	$f[Cl]_o$
Low	0.67 ± 0.05	1.0	8.3 ± 4.0	89	1.1 ± 0.05	1.02
High	2.0 ± 0.4	1.99 ± 0.3	14.4 ± 2.95	48.6 ± 8.5	1.2 ± 0.1	1.03 ± 0.01

Table 2. Summary of KCC functional properties in low and high passage synthetic VSMCs. The maximal velocity, V_m of Rb^+ influx was calculated in the presence of external Rb^+ and Cl^- (second column). The apparent binding affinity, K_m for Rb^+ and Cl^- on KCC binding site was calculated from Lineweaver Burk plot (third column). The Hill coefficients for both Rb^+ and Cl^- were close to unity ~ 1 (fourth column). Data shown are average of two independent experiments each done in quadruplicates (n=8) with respect to external Rb^+ and three independent experiments each done in quadruplicates (n=12) with respect to external Cl^- for high passage VSMCs.

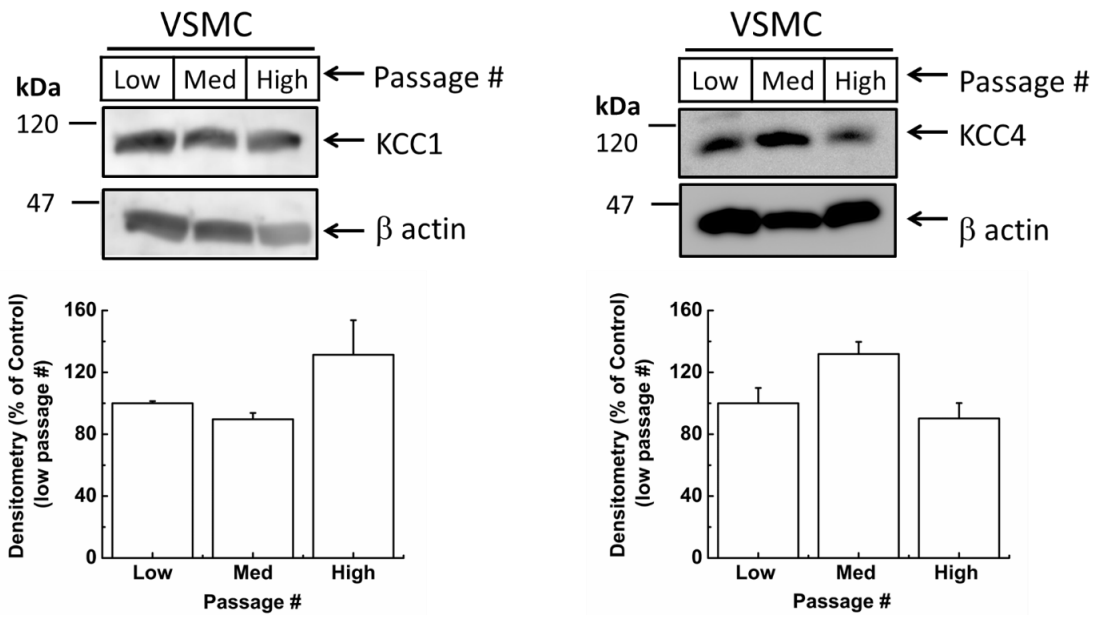

Figure 27. KCC protein expression is increased in late synthetic VSMCs.

VSMCs total extracts from cell cultures at different passage numbers (Low: passage 6, Med: passage 38, and High: passage 74) were obtained and separated by SDS-PAGE. Panel A. Normalized KCC1 expression increased in passage number 74. Panel B. Normalized KCC4 expression was increased in passage number 38. Densitometric quantitation of the protein bands were normalized to β-actin (internal control), and then the quantified protein bands of M and H passages were normalized to basal expression levels (L as a baseline control). Western blot shown is a representative experiment and densitometry quantification represents mean ± SD of two experiments for KCC1 and mean ± SD of three experiments for KCC4.

DISCUSSION: Specific Aim 1

For long, studying VSMCs' phenotypic switching has helped to obtain a better understanding of atherosclerosis progression and occurrence. Here, cultured VSMCs were used to investigate proliferation rates during their *in vitro* aging process. Additionally, we determined differences in cytoskeletal protein marker expression that facilitate VSMC phenotypic identification. Finally, K-Cl cotransport activity, important in cellular homeostasis and for controlling cell volume and migration, was characterized and optimized conditions for its study were established.

Due to different gene expression profiles, contractile VSMCs (passages 0-4) are mostly non-proliferative and thus, replication rates in monolayer cultures are significantly longer than in synthetic populations (≥ passage 6) (**Figure 15**) (13, 177). As VSMCs transition to a synthetic state, changes in expression and reorganization of cytoskeletal proteins are evident (30). Immunofluorescence of α-actin revealed dramatic changes in expression and subcellular distribution between contractile and late synthetic VSMCs (**Figure 17**). Furthermore, significant decreases in protein expression levels of α-actin, desmin and vimentin were observed in late synthetic VSMCs compared to early states. Notably, desmin total expression was reduced by 90 % in late passage synthetic VSMCs (**Figure 16**). These results are consistent with previous findings

where expression of cytoskeletal proteins and contractile machinery decreased during VSMCs' transition to synthetic states. Similar results have been reported in blood vessel intimal thickening due to atherosclerotic lesion formation (178, 179).

Initial attempts to characterize the electroneutral K-Cl cotransport in VSMCs involved the finding and establishment of optimal conditions in which no other potassium transport mechanism was present. To achieve that, ouabain and bumetanide dose response curves were performed to allow identification of conditions at which complete ablation of Na^+/K^+ pump and NKCC activities could be obtained. Based on our results, and in accordance with previous reports showing that rodent Na^+/K^+ pump is predominantly composed of low ouabain affinity α1 subunits (O'Brien, WJ et al. 1994; Juhaszova, M. 1997); it is likely that in VSMCs, α1 subunits are predominantly expressed since higher ouabain concentrations (up to 2 mM) and longer incubation periods (preincubation and flux) were required to fully inhibit the Na^+/K^+ pump.

Additionally, we characterized the K-Cl cotransport in VSMCs with respect to early and late synthetic phenotypes. K-Cl cotransport activity was assessed with respect to its known ligands [Rb^+ and Cl^-]. VSMCs of late synthetic passage had different transport activities and apparent affinities for Cl^- as compared to early synthetic VSMCs (**Figures 25-26, and Table 2**). Rb^+ transport via KCC required simultaneous presence of both Cl^- and Rb^+ ions externally. The maximal transport velocity of Rb^+ (V_{max}) increased by 2-fold in late synthetic cells. Whether

this increase is due to turnover changes of pre-existing KCCs or enhanced membrane trafficking/insertion of *de novo* synthesized KCC proteins, remains to be studied. In late synthetic VSMCs, the apparent affinity for Cl^- increased, while the affinity for Rb^+ remained fairly constant. It is possible that conformational changes due to KCC isoform assembly or posttranslational modifications might be responsible for increased Cl^- affinity. Interestingly, in both early and late synthetic VSMCs, KCC activity showed an obligatory coupled movement of Rb^+ and Cl^- in 1:1 stoichiometry ratio, as suggested by Hill coefficient of 1. This observation indicates that this mode of cotransport is electroneutral, and is in agreement with previously reported models (87, 180, 181). Whether, the binding of each ligand appears to be independent of a previous or subsequent ligand binding to the same site, i.e. random order of binding, cannot be determined from these studies (107, 110).

Shedding light onto K-Cl cotransport regulation is of considerable importance since several lines of evidence have highlighted KCC activity in sustaining human health and during the occurrence of pathophysiological conditions (75, 133, 137, 145, 158, 160, 181). Stimulation of K-Cl cotransport activity during hypotonicity and NEM treatment, constitute original hallmarks of this mode of electroneutral ionic transport. Consistent with previous findings, hypotonicity and NEM treatment resulted in significant stimulation of K-Cl cotransport. Therefore, it is likely that common signaling pathways and regulatory mechanisms are conserved among cell types (**Figure 20**) (84, 122, 180, 182-184). Previous studies have suggested that during both, hypotonicity- and NEM-treatment; KCC

upregulation is due to dephosphorylation of key serine and threonine residues within its C-terminus. It is likely that inhibition of kinase activities such as WNK and Ste20, in combination with activation of protein phosphatases like PP1/2, results in concomitant KCC de-phosphorylation and thus activation (185-187).

Changes in KCC activities observed in **Figures 25 and 26** could be explained by re-distribution of cytoskeletal proteins that would promote their trafficking to the cell membrane and recruitment of regulatory proteins (91). As cytoskeletal proteins regulate intracellular signaling cascades their distribution and location may be important for determining VSMC phenotype. Thus, any reorganization of the cytoskeleton or signaling molecules could affect VSMCs phenotypic modulation (30). Moreover, several cell culture models suggest that the cytoskeleton machinery is linked to cell migration (91, 188, 189). Further evidence also indicates emerging roles of ion channels and transporters playing a significant role in cell migration (163, 190, 191). During the cell migratory process, there is polarized distribution of ion channels or transporters due to structural reorganization of the cytoskeleton. Based on our findings, it is plausible that as VSMCs undergo phenotypic transformation; decreased interaction between KCC and cytoskeletal proteins could enhance membrane trafficking and increases in transport activity (137).

We also demonstrated that during VSMCs dedifferentiation or phenotypic switching, KCC1 and KCC4 expression is increased. These results further support the notion that high levels of K-Cl cotransport activity are necessary to attain a better control of cell volume and proliferation/migration processes.

Importantly, our results suggest that up regulation of different KCC isoforms could be passage number-dependent. It remains to be determined whether changes in expression of other KCC isoforms (KCC2 and KCC3) occur during the studied conditions. Since KCC1 up regulation occurred at later states (passage 74), in which KCC4 protein levels were comparable to the ones seen at passage number 6; it is possible that mutually exclusive gene-expression profiles occur in VSMCs. In sum, at late VSMCs' passage numbers, K-Cl cotransport activity is enhanced by both, and increase in enzyme kinetics (ion affinity and V_{max}) and KCC protein levels.

It is possible that the numbers of KCCs transporters do not change in the plasma membrane or that new KCCs are synthetized as cells undergo cell division. Furthermore, kinases could be involved in KCC regulation and change their expression pattern. In addition, it is likely that expression patterns are changing and those changes are responsible of the overall observation. Our data also showed that the transition of the VSMCs phenotype is linked to the expression and activity of KCC. Likewise, KCC regulation could lead to a VSMCs phenotypic transition with enhanced migration and proliferation. Recent studies have correlated the expression of KCC isoforms in embryogenesis and dedifferentiated cancerous cells linking KCC to tumorigenesis, cell proliferation, and migration (133, 134, 158-160). Similarly, VSMCs synthetic phenotypic transition is also linked to cell proliferation and migration (192). Thus, KCC activity and expression could be an important modulator of VSMCs transiting to synthetic phenotypes.

SUMMARY

The main finding of this study is that concomitant with the process of VSMCs' transition from early to late synthetic phenotype, there is an increase in KCC functional properties. Additionally, KCC1 and KCC4 protein levels were up-regulated, whereas considerable reductions of cytoskeletal proteins were found. Altogether our results suggest a link between KCC activity/expression and VSMC's phenotypic switching.

SPECIFIC AIM 2

To determine the acute and chronic effect of apelin on K-Cl cotransport activity in VSMCs. To establish the involvement of NO, PI3K/Akt and MAPK signaling pathways in the regulation of the transporter.

RESULTS: Specific Aim 2

Apelin receptor is expressed in VSMCs

To establish whether the most abundant and potent form of apelin (apelin-13) might affect K-Cl cotransport via its membrane receptor APJ (predicted MW 42.35 kDa), western blot analyses using total lysates from contractile and synthetic VSMCs were performed using the validated commercial antibody against APJ (**Figure 28A**). Since APJ protein expression has been previously reported and extensively studied in central nervous system, brain extracts were used as control for APJ immunodetection (52, 193). As shown in **Figure 28A**, differences in APJ protein expression were observed between brain samples and among VSMC phenotypes (contractile *vs* synthetic). First, there was a difference in size of APJ compared to predicted molecular weight between brain (~55 kDa) and VSMCs (~60 kDa). These differences in APJ molecular size suggest possible tissue-specific post-translational modifications/processing that would require further detailed examination. Second, in contrast to brain samples, strong APJ bands were detected from VSMCs samples at around 120 kDa indicating either nonspecific antibody binding or possible APJ oligomerization. Lastly, densitometric analysis of total APJ (monomeric and dimeric) normalized to b-actin, revealed a decreasing trend in APJ protein expression corresponding to

VSMCs' phenotypic states. Total extracts of late synthetic VSMCs (passage number 41) revealed a possible reduction (30 %) in APJ expression compared to contractile or early synthetic VSMCs (passage numbers 2 and 9 respectively) (**Figure 28B**). In addition, APJ immunolabeling revealed differences in its subcellular localization among VSMCs' phenotypes. In synthetic VSMCs (passage number 17), the majority of APJ expression was homogeneously distributed along the cytoplasm (**Figure 28C**), whereas a more localized perinuclear immunolabelling pattern was detected in contractile states (passage number 2) (**Figure 28D**). These observed differences in protein expression levels, oligomerization and subcellular localization of APJ could result in variability of the apelin-mediated effects in different VSMCs' phenotypes. To confirm primary antibody specificity, VSMCs were incubated in its absence (**Figure 28C and D**).

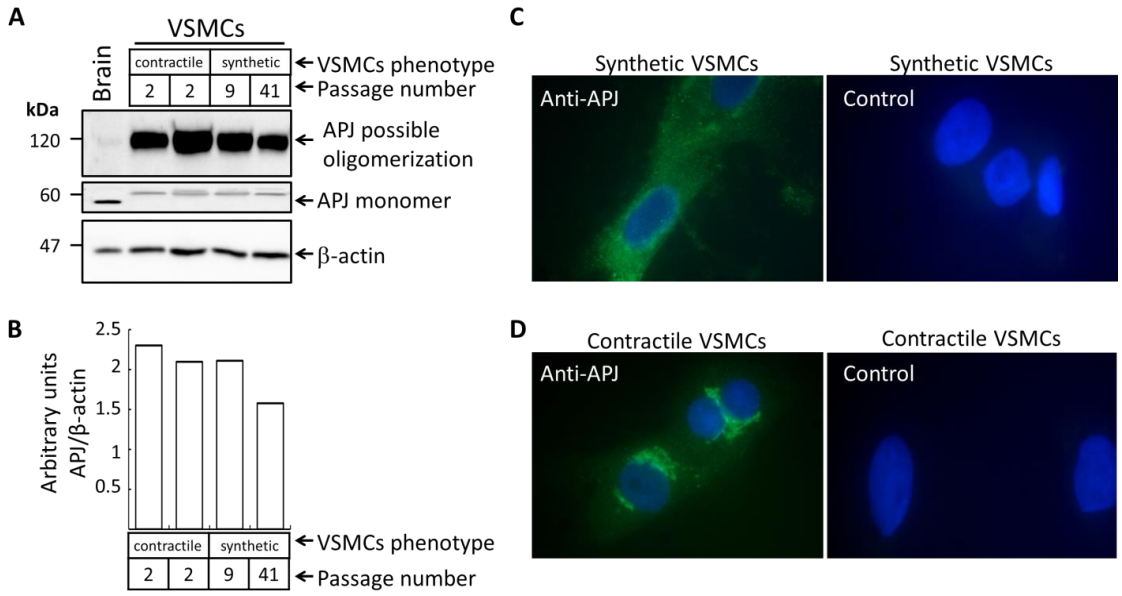

Figure 28. APJ protein expression. (A) Protein extracts (40 μg/lane) from brain and VSMCs primary cultures (synthetic and contractile) were separated by SDS-PAGE and subsequent immuno-detection of APJ was performed. APJ monomer conformation was detectable around 60 kDa. Interestingly, the APJ signal from VSMCs was slightly different in size when compared to brain total protein extract. Strong immuno-detection at 120 kDa was detected in VSMCs protein extracts as well as weakly in brain tissue suggesting SDS resistant oligomerization. Anti-APJ primary antibody (1:1000) and β-actin (1:2000) was used as an internal control. (B) Densitometric analysis of total APJ (monomeric and dimeric) relative to β-actin in VSMCs from a representative experiment. (C) Immuno-labeling of APJ in synthetic VSMCs. (D) Immunolabeling of APJ in contractile VSMCs. In both cases, VSMCs were fixed, permeabilized, and incubated with anti-APJ antibody (1:100); (FITC)-conjugated secondary antibody was used against anti-APJ

(1:100). As a negative control; synthetic (C) and contractile (D) VSMCs were incubated with a 3% normal goat serum (NGS) and (FITC)-conjugated secondary antibody (1:100).

Once evidence was gathered suggesting APJ protein expression in VSMCs, we determined the timeframe in which apelin-13 treatment would act upon the linear behavior on K-Cl cotransport activity. Cl^--dependent Rb^+ uptake from untreated and apelin-treated VSMCs was assessed from 0 to 40 min. K-Cl cotransport from 1 µM apelin-treated VSMCs, was linear up to 40 min (**Figure 29**). Thus, subsequent determinations of K-Cl cotransport activity were performed within the aforementioned timeframe.

Acute apelin regulation of K-Cl cotransport in serum-starved VSMCs

Apelin regulation of K-Cl cotransport by the NO-mediated signaling pathway and the role of oxLDL

Previous studies have shown that the guanyl cyclase PKG is one of the most important regulators of K-Cl cotransport and determinant of VSMCs contractile phenotype (22, 103, 148). In order to establish a direct link between the apelin effect and the NO-mediated regulation of KCC, immuno-labeling of PKG was performed in contractile VSMCs. As can be seen in **Figure 30A**, clear immuno-detection of PKG was observed. Primary antibody specificity was determined in the absence of PKG antibody (**Figure 30**). All slides were counterstained with 4′,6-diamidino-2-phenylindole (DAPI) to visualize cell nuclei (**Figures 28C-D and 30B**).

To further assess whether apelin regulates K-Cl cotransport through the NO/cGMP/PKG pathway, VSMCs were used at ≤ passage 4, when they are in the contractile state, to ensure PKG is present. VSMCs were cultured until sub confluence and then serum deprived for 24 h prior to flux measurement. Cells

were then incubated with 2.5 µM KT5823, a potent inhibitor of PKG for 10 min in preincubation media followed by additional 30 min during flux in the presence and absence of apelin (1 µM). The experimental outcomes of each condition were normalized relative to the control. As shown in **Figure 31A**, the inhibitor alone did not affect the basal K-Cl cotransport activity. Apelin treatment of serum-starved contractile (PKG positive) VSMCs resulted in a significant increase of 87.3 % (*$p < 0.05$) compared to the basal K-Cl cotransport activity. Importantly, when contractile VSMCs were incubated in the presence of KT5823, the apelin-mediated increase in K-Cl cotransport was prevented suggesting that apelin uses NO pathway to regulate K-Cl cotransport activity.

Because oxLDL modulate progression of atherosclerosis by impairing the NO-mediated pathway in contractile VSMCs (194, 195), we tested whether oxLDL might affect K-Cl cotransport activity, which was shown to be modulated by apelin. Rb^+ influx was measured in contractile VSMCs (passage 4) treated for 24 h ± 8 µg/mL oxLDL and then followed by a 40 min incubation of 4 µM apelin. Cl^--dependent Rb^+ influx for each condition were normalized to the baseline control. Apelin treatment resulted in an increase in K-Cl cotransport by 2-fold (* $p < 0.05$); whereas the baseline KCC was inhibited significantly by oxLDL by over 70 % (* $p < 0.05$). The oxLDL-mediated inhibition of KCCs was restored by apelin treatment and importantly, similar fold of apelin-mediated activation was obtained from untreated VSMCs (**Figure 31B**). This suggests that oxLDL and apelin have a counter-regulatory action in the regulation of K-Cl cotransport activity in VSMCs.

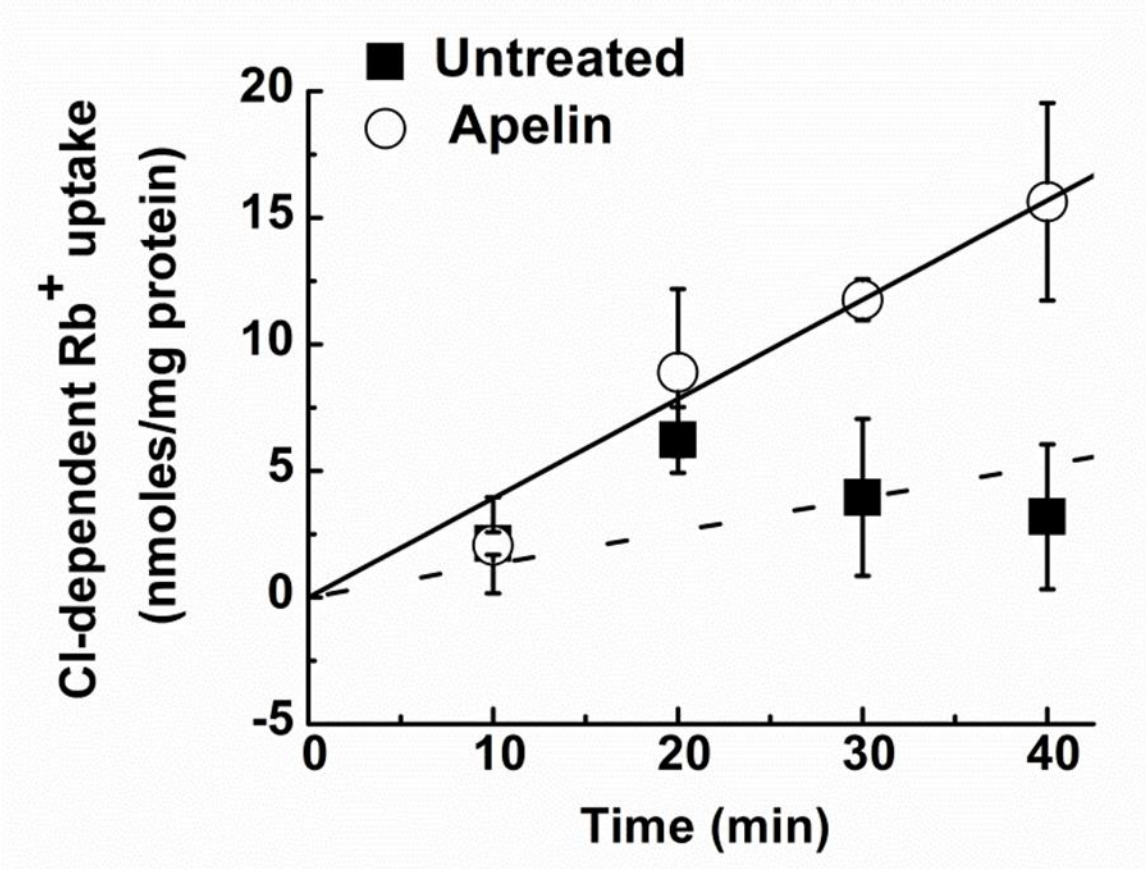

Figure 29. Cl^--dependent Rb^+ uptake as a function of time in the presence of apelin. Cl^--dependent Rb^+ uptake was measured as a function of time from 24 h-serum deprived VSMCs. Untreated VSMCs: (filled squares). VSMCs treated with 1 µM apelin for 40 min incubation time (open circles). Rb^+ uptake was measured in the presence of ouabain (2 mM) and bumetanide (2 µM) for 10-40 min at 37 ^oC. For each conditions, n = 4 and values are reported as mean ± SD.

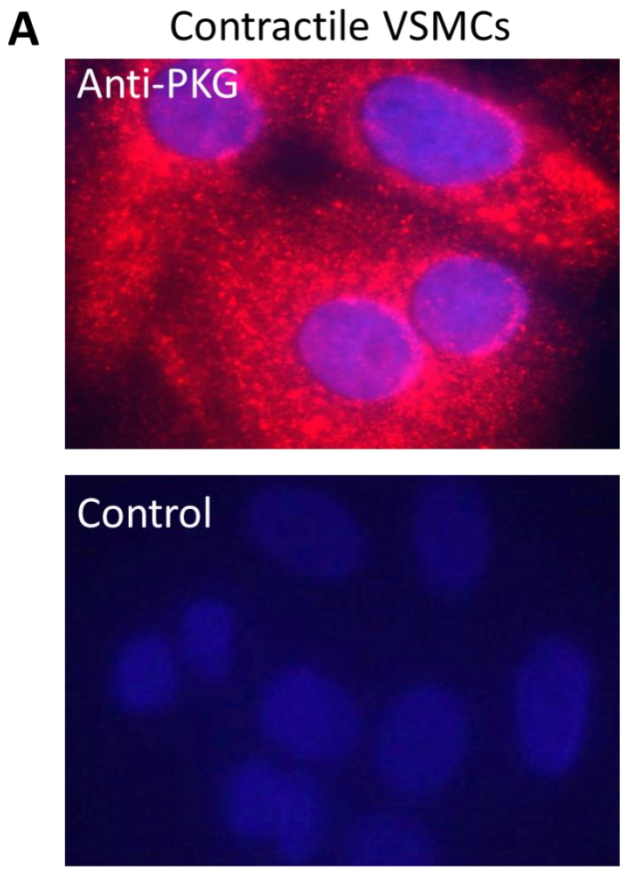

Figure 30. Immunolabeling of PKG in contractile VSMCs. Contractile VSMCs (passage 3) were fixed, permeabilized and incubated with anti-PKG 1 antibody. Cy3-conjugated secondary antibody was used against anti-PKG 1. In negative control VSMCs were incubated with a 3 % normal goat serum (NGS) and Cy3-conjugated secondary antibody.

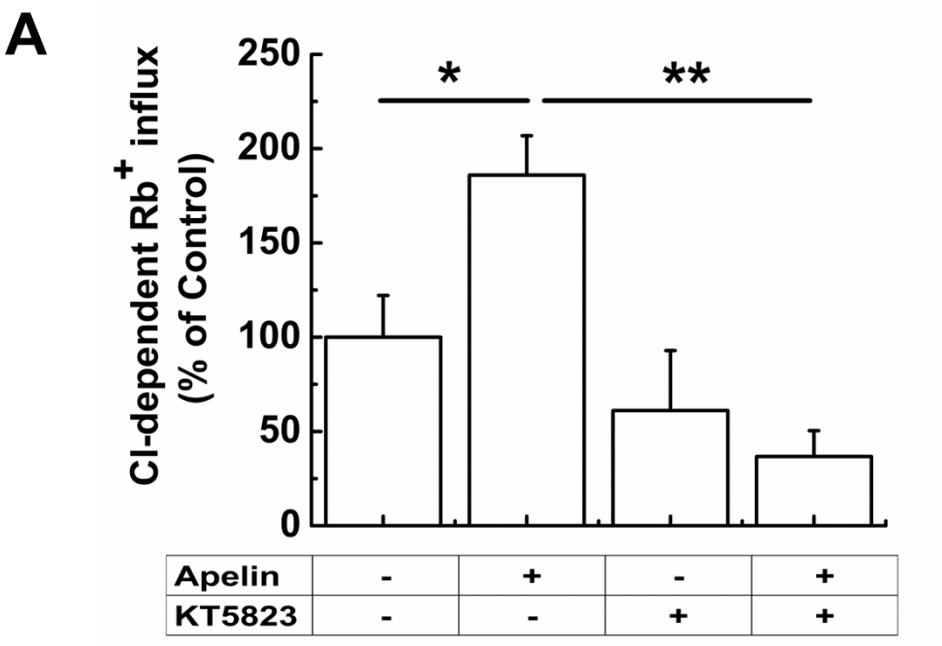
A
Cl-dependent Rb+ influx
(% of Control)
250
200
150
100
50
0
*
**
Apelin - + - +
KT5823 - - + +

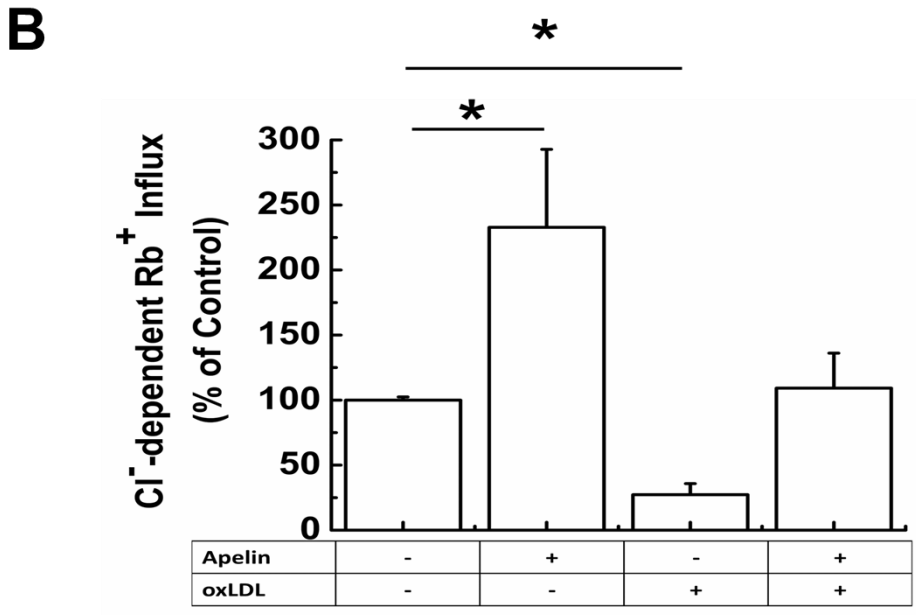
B
Cl--dependent Rb+ Influx
(% of Control)
300
250
200
150
100
50
0
*
*
Apelin - + - +
oxLDL - - + +

Figure 31.

Figure 31. Apelin effect on K-Cl cotransport by the NO-mediated pathway. (A) KCC-mediated Rb^+ uptake from 24 h-serum deprived contractile VSMCs was measured in the presence or absence of 1 µM apelin and 2.5 µM of KT5823, an inhibitor of PKG. The experimental outcomes were normalized relative to the baseline control. Data represent means ± standard errors of two independent experiments each done in triplicates, n = 6 per conditions. *p<0.05 *vs* control group. (B) Apelin rescues oxLDL-mediated inhibition of KCC activity. KCC-mediated Rb^+ uptake, from 24h-serum deprived contractile VSMCs, was measured in the presence or absence of 4 µM apelin and 8 µg/mL oxLDL. Subconfluent cells were incubated oxLDL in serum free media for 24 h. Cells were then washed with BSS and Rb^+ influx assay was carried out as described in Materials and Methods. Apelin was added during flux to see an acute effect on oxLDL-treated cells. Data represents mean ± standard error, n = 3 per conditions. *p<0.05 *vs* control group.

Apelin regulation of K-Cl cotransport by PI3K/Akt and MAPK-mediated signaling pathways

VSMCs motility and proliferation have been tightly linked to the activation of PI3K/Akt and MAPK signaling pathways that are important for vascular remodeling and repair. Similarly, apelin effects on motility involve stimulation of the aforementioned signaling cascades. Therefore, we assessed the effect of selective inhibitors of the PI3K/Akt and MAPK pathways on K-Cl cotransport activity in the presence or absence of apelin. Sub confluent synthetic VSMCs (passages 6-8) were serum starved for 24 h prior to flux measurement. Cells were then incubated for 10 min with 10 μM of either LY294002 or PD98059, selective inhibitors of PI3K/Akt and ERK1/2, respectively. Then cells were further incubated with these inhibitors for additional 40 min during flux in the presence or absence of apelin. The outcomes of each experimental condition were normalized to the baseline control. As can be seen in **Figure 32A and 32B**, acute apelin treatment resulted in activation of K-Cl cotransport in synthetic VSMCs by 142% (*$p < 0.05$). Baseline activity was not affected by neither of the inhibitors used. However, VSMCs incubated with the inhibitors were no longer responsive to apelin-mediated activation of K-Cl cotransport activity. These results point out apelin/APJ regulates KCC via PI3K/Akt and MAPK pathways. A summary of the signaling pathways that result in K-Cl cotransport upregulation by apelin and the usage of selective inhibitors are displayed in **Figure 33**. Inhibitors, KT5823, PD98059 and LY294002 blocked the activation of K-Cl cotransport in

the presence of apelin. OxLDL inhibitory effect on K-Cl cotransport activity was rescued to the baseline levels by apelin (**Figure 33**).

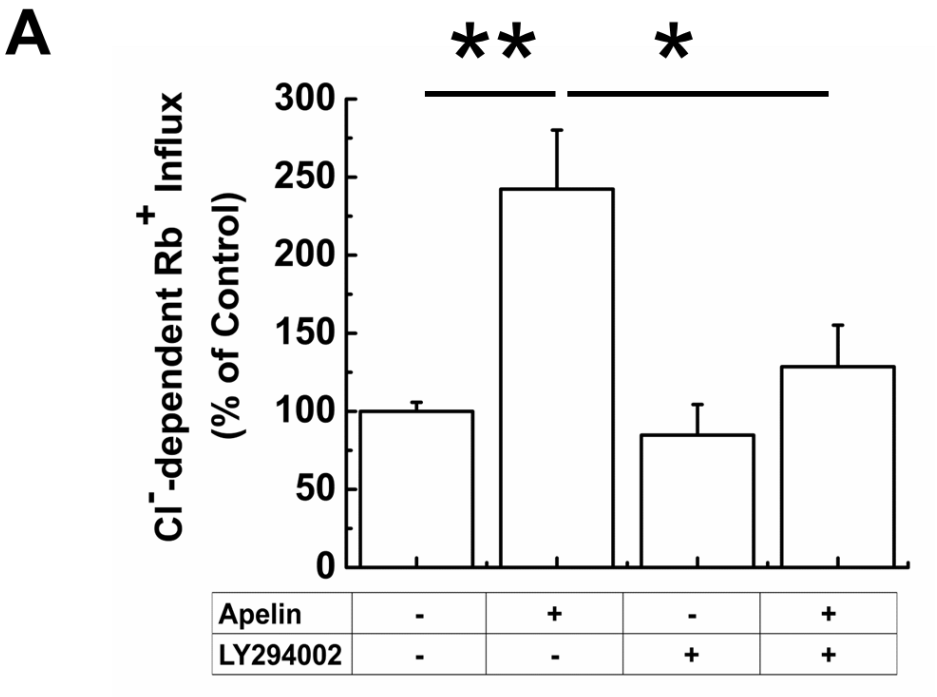
A
**
*
Cl-dependent Rb+ Influx
(% of Control)
300
250
200
150
100
50
0
Apelin - + - +
LY294002 - - + +

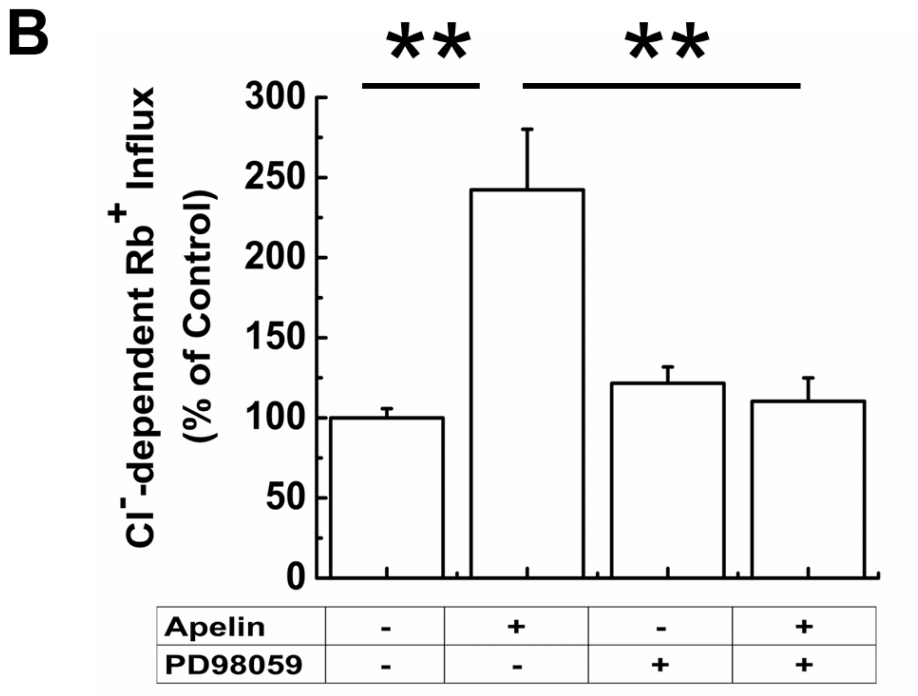
B
**
**
Cl-dependent Rb+ Influx
(% of Control)
300
250
200
150
100
50
0
Apelin - + - +
PD98059 - - + +

Figure 32.

Figure 32. Apelin-mediated activation of KCC occurs through a PI3K/Akt and MAPK pathways in synthetic VSMCs. (A) Apelin-mediated activation of KCC occurs through the PI3K/Akt pathway. KCC-mediated Rb^+ uptake by 24 h-serum deprived synthetic VSMCs was measured, according to Materials and Methods, in the presence or absence of 1 µM apelin and 10 µM of LY294002, an inhibitor of the PI3K/Akt pathway. LY294002 was present in preincubation and flux media. Apelin was added to flux solution. (B) Apelin-mediated activation of KCC occurs through a MAPK dependent pathway in synthetic VSMC. KCC-mediated Rb^+ uptake by 24h-serum-deprived synthetic VSMCs was measured in the presence or absence of 1 µM apelin and 10 µM of PD98059, an inhibitor of the MAPK pathway, in preincubation and flux. For both (A) and (B), experimental outcomes were normalized to the baseline control. Data represents mean ± standard error of two independent experiments done in triplicates. For each conditions, n = 6. *$p<0.05$ *vs* control group.

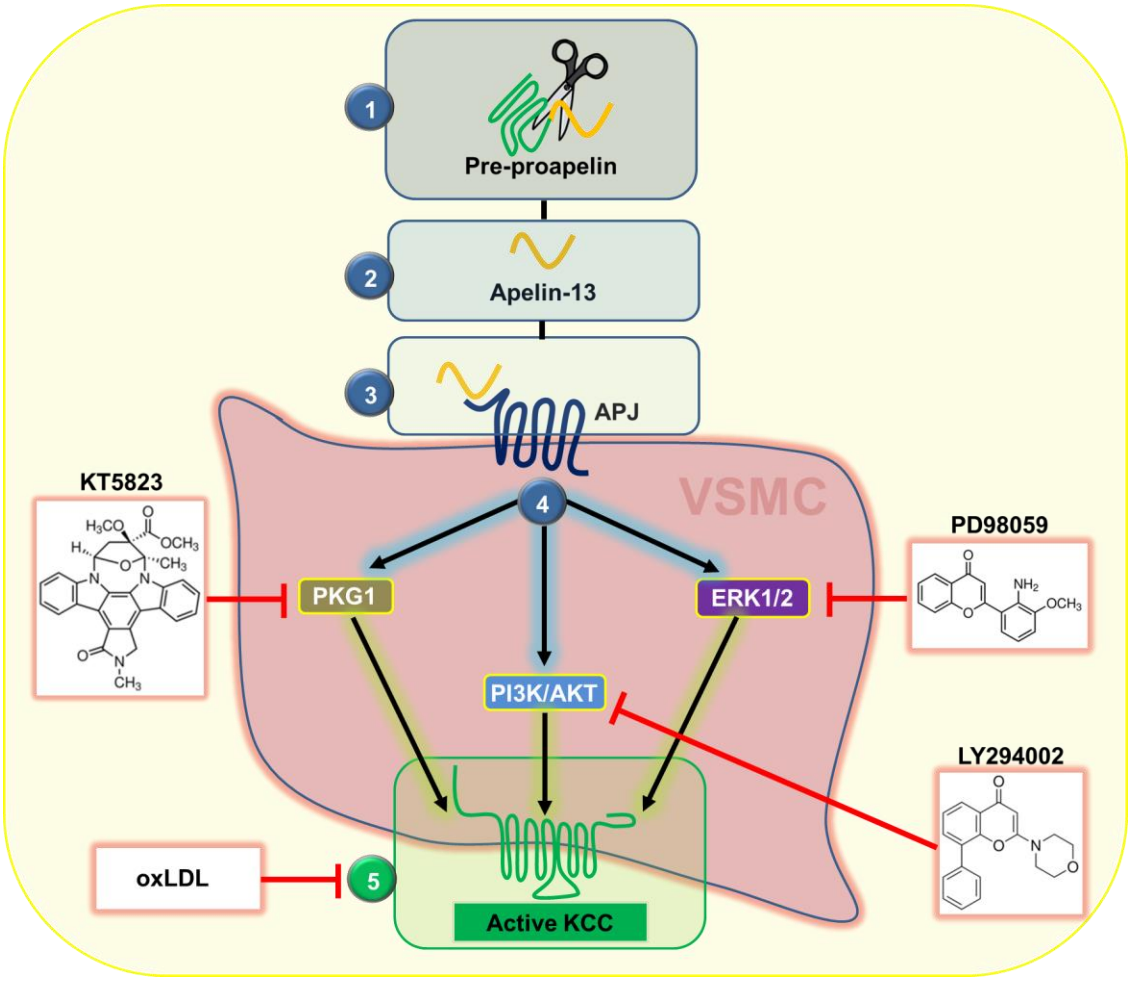

Figure 33. Proposed signal transduction pathway of K-Cl cotransport regulation by apelin in contractile and synthetic VSMCs. Apelin binds to its receptor APJ and elicits three signaling pathways. Whereas oxLDL inhibits K-Cl cotransport activity, in contractile VSMCs, apelin uses the NO-mediated pathway to sustain this mode of cotransport. In synthetic VSMCs, apelin uses the PI3K/Akt and MAPK-mediated pathways to activate K-Cl cotransport activity. The drugs KT5823, LY294002 and PD98059 block the NO, PI3K/Akt and MAPK pathways, respectively.

Chronic treatment with apelin does not change K-Cl cotransport activity in serum-starved VSMCs

Once we showed that acute treatment of apelin resulted in stimulation of K-Cl cotransport activity, we wondered if longer incubation times had the same effect. To this end, apelin was added to growth media before the flux time periods. As can be seen in **Figure 34**, serum-starved VSMCs were treated with 1 µM apelin for: 30 min, 1 h, 6 h, 12 h, 18 h or 24 h. Cells were rinsed thoroughly with BSS and K-Cl cotransport was compared to untreated cells (see Materials and Methods). As shown in **Figure 34**, no significance change in Rb^+ flux was observed between untreated and apelin-treated VSMCs. To rule out the possibility that lack of effect on KCC activity was due to apelin degradation, MALDI-TOF mass spectrometry analyses were carried out with the assistance of Dr. David Cool. After apelin reconstitution in deionized water at 50 microgram final stock concentration, and over one year of storage, no evidence for proteolysis was detectable. As seen in **Figure 35**, three peaks at monoisotropic mass of 1532, 1555 and 1578 corresponding to apelin and sodium adducts confirmed the apelin integrity in solution.

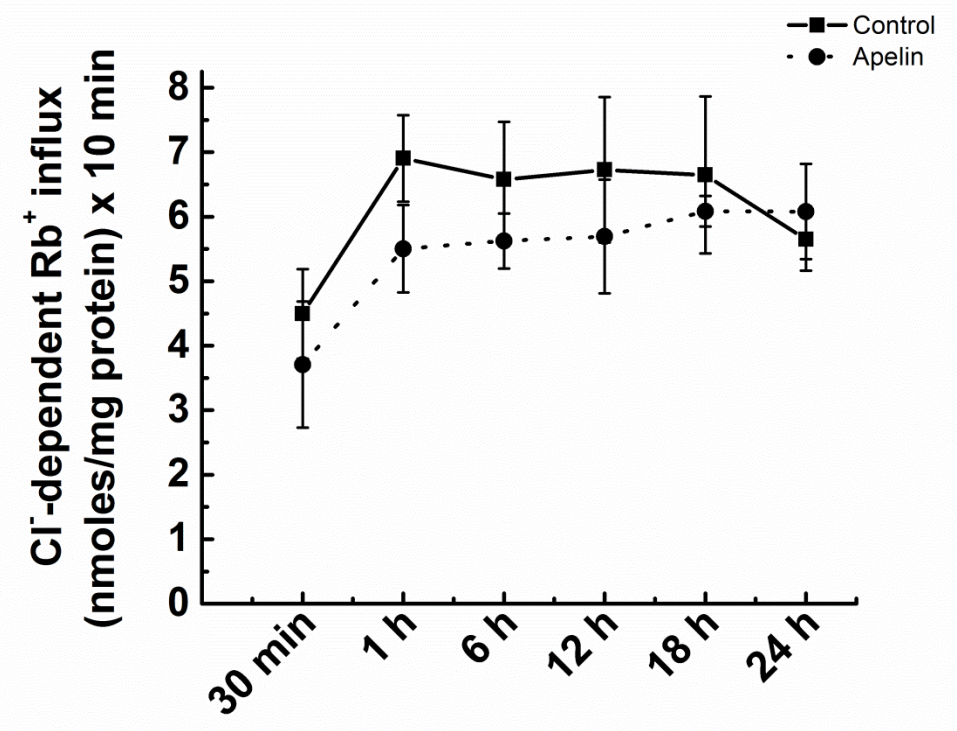

Figure 34. Time-course of chronic apelin incubation on K-Cl cotransport. Cells serum-deprived for 24 h were exposed to 1µM apelin during different time periods. After termination of apelin incubation, cells were washed 3 times with BSS solution and the flux experiment was carried out as described in Materials and Methods. Apelin was not present during the flux time. Ouabain (2 mM) and bumetanide (2 µM) were present during both the preincubation and flux. After 10 min of Rb^+ flux, no difference in KCC activity was observed between untreated (filled squares) and apelin-treated VSMCs (filled circles). Data shown is mean ± standard error of a representative experiment done in triplicates. For each condition, n = 3.

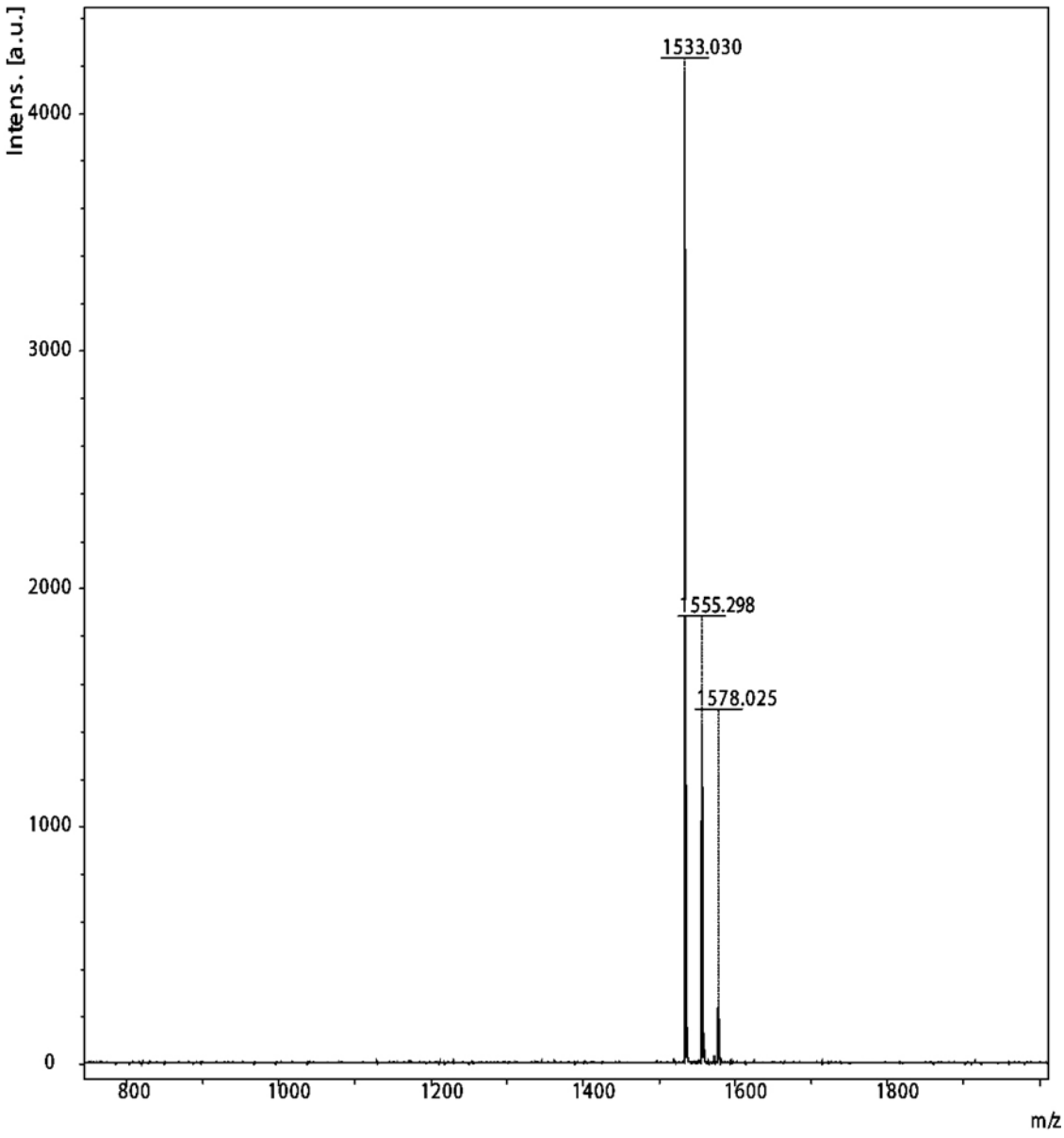
Intens. [a.u.]
4000
3000
2000
1000
0
1533.030
1555.298
1578.025
800
1000
1200
1400
1600
1800
m/z

Figure 35.

Figure 35. Mass spectrometry of water reconstituted apelin. Apelin, 50 micrograms, was mixed 1:1 with CHCA matrix and 1 microliter was spotted to a MALDI brushed steel plate. A Bruker Autoflex III MALDI-TOF was used to capture the data with laser intensity settings adjusted at 70%, gain to 4.0 and 3000 laser shots captured randomly around the spot. The data represent the expected mass of apelin at 1532 Da, and sodium adducts at 1555 and 1578 Da.

SPECIFIC AIM 3

To assess the factors, such as, serum, osmolality, ionic strength, VSMCs phenotypes on apelin-mediated effect on K-Cl cotransport activity. The above factors will shed light on possible variability of the response of K-Cl activity to apelin.

RESULTS: Specific Aim 3

Factors affecting apelin response: Variable effects on K-Cl cotransport activity.

During the determination of K-Cl cotransport activity, variability in the extent of activation after apelin treatment became evident. Being aware of several factors, such as the effect of serum deprivation, extracellular ionic content and osmolalities as determinants for changes in K-Cl cotransport, we determined whether serum deprivation and/or sodium-free media altered the apelin-mediated Rb^+ response in VSMCs (150, 182).

As shown in **Figure 36 (A and B)**, the absence of extracellular Na^+ prevented the apelin-mediated increase in K-Cl cotransport activity irrespective of serum deprivation, cell phenotype (synthetic and contractile) and extracellular osmolality. In addition, neither hypotonic incubation (known to activate K-Cl cotransport) nor apelin treatment resulted in changes in Rb^+ influx levels under these conditions. Furthermore, previously described inhibitory stimuli, such as, hypertonicity resulted in no change in K-Cl cotransport activity and similarly, apelin treatment had no effect in Rb^+ influx. To date, the role of extracelluar Na^+ in sustaining KCC activity and regulation remains unclear.

To further dissect the variability behind the apelin-mediated effect on K-Cl cotransport, the effect of extracellular Na^+ on serum-deprived and serum-fed

synthetic VSMCs was tested. As shown in **Figure 37**, the addition of external Na^+ did not sustain the previously shown apelin-mediated increase of Rb^+ influx. In contrast, the combination of serum and extracellular Na^+ allowed apelin to potentiate the K-Cl cotransport under hypotonicity and hypertonicity. Surprisingly, under isotonic conditions, apelin treatment did not result in changes of baseline Rb^+ influx (**Figure 37B**).

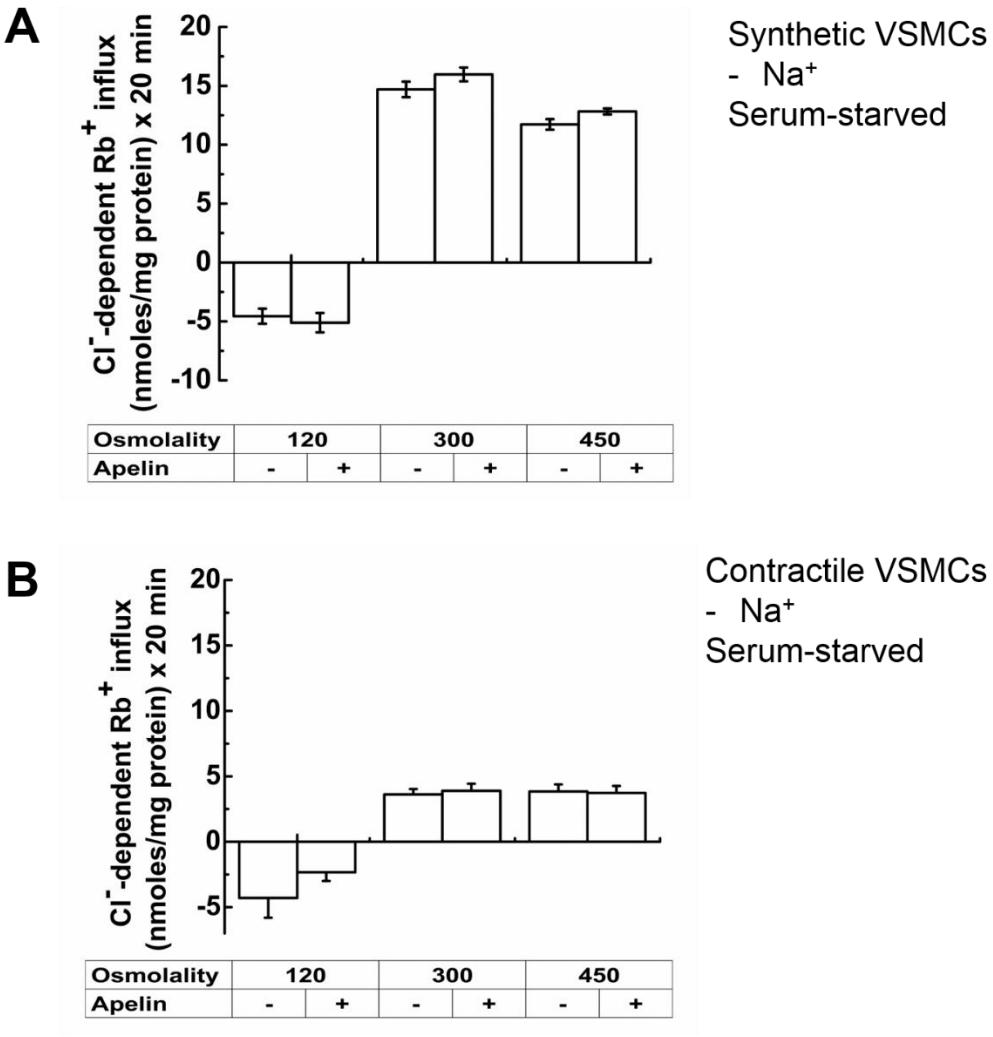
A
Cl-dependent Rb+ influx
(nmoles/mg protein) x 20 min
20
15
10
5
0
-5
-10
Osmolality
120
300
450
Apelin
- + - + - +
Synthetic VSMCs
- Na+
Serum-starved
B
Cl-dependent Rb+ influx
(nmoles/mg protein) x 20 min
20
15
10
5
0
-5
Osmolality
120
300
450
Apelin
- + - + - +
Contractile VSMCs
- Na+
Serum-starved

Figure 36.

Figure 36. Effect of apelin on KCC activity in primary cultures of rat aortic vascular smooth muscle cells (VSMCs) with respect to various osmolalities in the absence of Na^+ and serum. Panel (A) Synthetic VSMCs (passage 39), and Panel (B) Contractile VSMCs (passage 3). Rb^+ influx was determined from serum-starved cells at different osmolalities in Na^+-free solutions. Osmolality changes were achieved by adding NMDGCl and NMDGSf. Ouabain (2 mM) and bumetanide (2 µM) were present in preincubation and flux solution. Apelin (1 µM) was added during flux. The difference between Rb^+ influx in NMDGCl and NMDGSf was used to determine Na^+-independent KCC activity. Data represents mean ± standard error and for each condition n = 6.

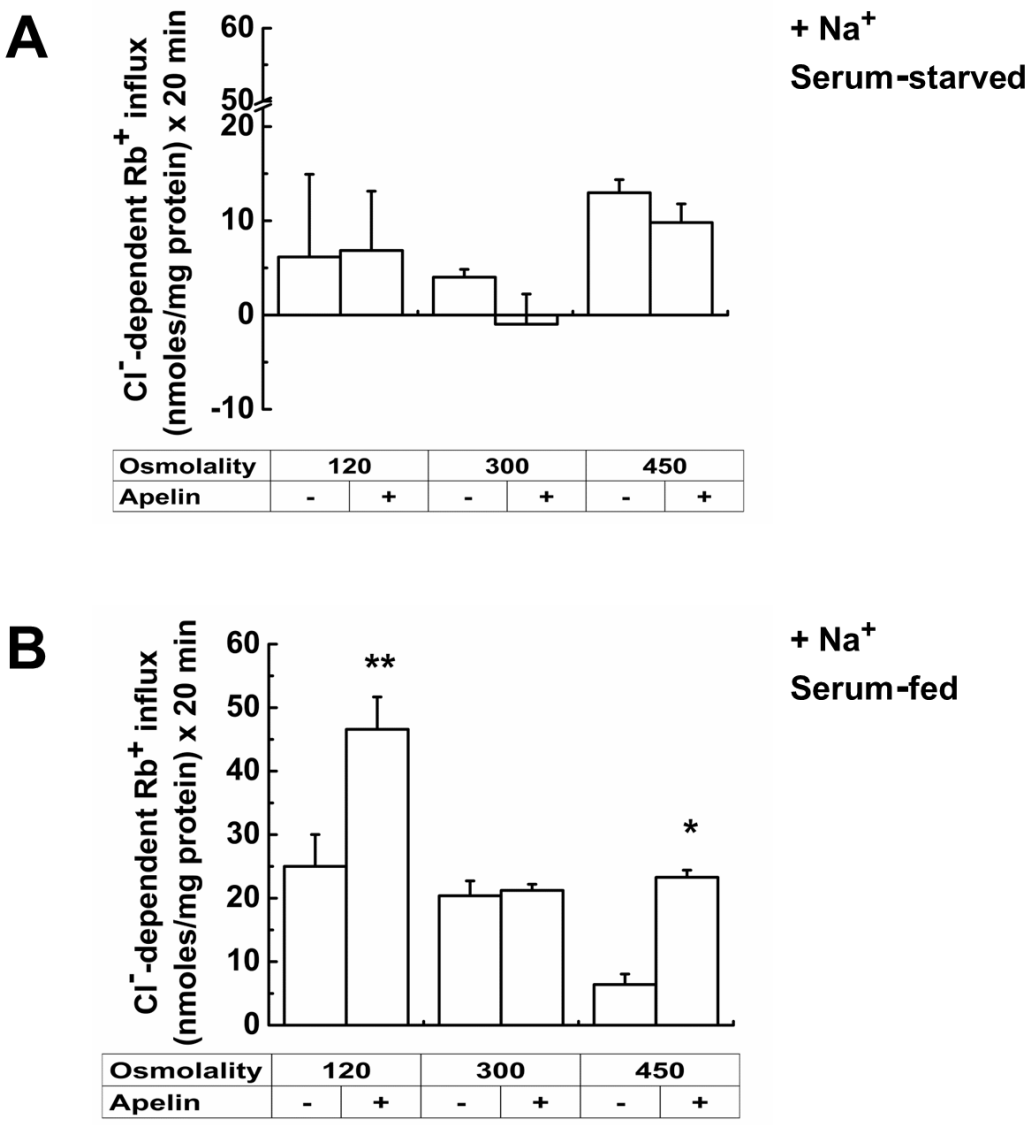
A
+ Na+
Serum-starved
Cl--dependent Rb+ influx
(nmoles/mg protein) x 20 min
60
50
20
10
0
-10
Osmolality 120 300 450
Apelin - + - + - +
B
+ Na+
Serum-fed
Cl--dependent Rb+ influx
(nmoles/mg protein) x 20 min
**
*
60
50
40
30
20
10
0
Osmolality 120 300 450
Apelin - + - + - +

Figure 37.

Figure 37. Effect of apelin on KCC activity with respect to various osmolalities in serum-starved and serum-fed VSMCs in the presence of external Na^+. KCC activity was measured from serum-starved and serum-fed (24 h) VSMCs (passage 11) in the presence of external Na^+ at different osmolalities (Panel A and B). NaCl and NaSf were used to increase the osmolality. Cells were exposed to various tonicities in the preincubation and flux media containing ouabain (2 mM) and bumetanide (5 µM). Apelin (1 µM) was added during flux. As shown in Panel (A) apelin treatment did not change KCC activity in serum-starved cells. In Panel (B) apelin treatment significantly increased KCC activity under hypo and hypertonicity. Data shown are mean ± standard error with n = 3 per conditions. *$p < 0.05$ *vs* control group.

Since incomplete inhibition of alternative K^+/Rb^+ transport mechanisms such as, the ouabain-sensitive Na^+/K^+ pump and/or bumetanide-sensitive Na^+-K^+-$2Cl^-$ cotransporter could be responsible for the apparent lack of apelin effect under isotonic conditions, we performed dose-response curves to rule out the possibility of residual Rb^+ transport with ouabain (2 mM) and bumetanide (2-5 µM) concentrations used so far. As shown in **Figure 38**, ouabain (2 mM) resulted in complete inhibition of the Na^+/K^+ pump. Addition of ouabain to the preincubation media did not result in any further inhibition of the ouabain-sensitive Rb^+ transport compared to the one observed during flux incubation period. As seen in **Figures 39A-C**, residual K^+/Rb^+ transport was detectable at 2 µM bumetanide. Therefore, higher bumetanide concentrations (up to 30 µM) will be required to fully inhibit Na^+-K^+-$2Cl^-$ cotransport activity in subsequent Rb^+ influx determinations.

Having determined the requirement of extracellular Na^+ and presence of serum in the growth media for the apelin-mediated increase in K-Cl cotransport, we reevaluated the osmolality-dependency of Rb^+ fluxes in VSMCs using 30 µM bumetanide (**Figure 40**). To our surprise, extracellular Na^+ was required for K-Cl cotransport to be activated and inhibited under hypotonicity and hypertonicity, respectively (**Figure 40A**). Presence of extracellular Na^+ and serum in the growth media resulted in activation and inhibition of K-Cl cotransport under hypo- and hypertonic conditions, respectively (**Figure 40B**). Simultaneous K-Cl cotransport inhibition and activation of Na^+-K^+-$2Cl^-$ mechanisms during increases in osmolality confirmed the physiological relevance of regulatory volume responses

necessary to properly control cell volume (**Figure 41**). To further confirm the coordinated activity of K^+ transport mechanisms (K-Cl cotransport *vs.* Na^+-K^+-$2Cl^-$); Na^+-K^+-$2Cl^-$ activity was assessed under the same conditions. As shown in **Figure 41A**, whereas increases in osmolality inhibited K-Cl cotransport, opposite regulation (activation) of Na^+-K^+-$2Cl^-$ was observed (**Figure 41B**). In other words, presence of extracellular Na^+ and serum in the growth media resulted in the expected activation of K-Cl and possibly inhibition of Na^+-K^+-$2Cl^-$ (**Figure 41A and B**). These results highlight the coordinate activity of cation chloride cotransporters (CCCs) to modulate intracellular Cl^- concentration and therefore cell volume.

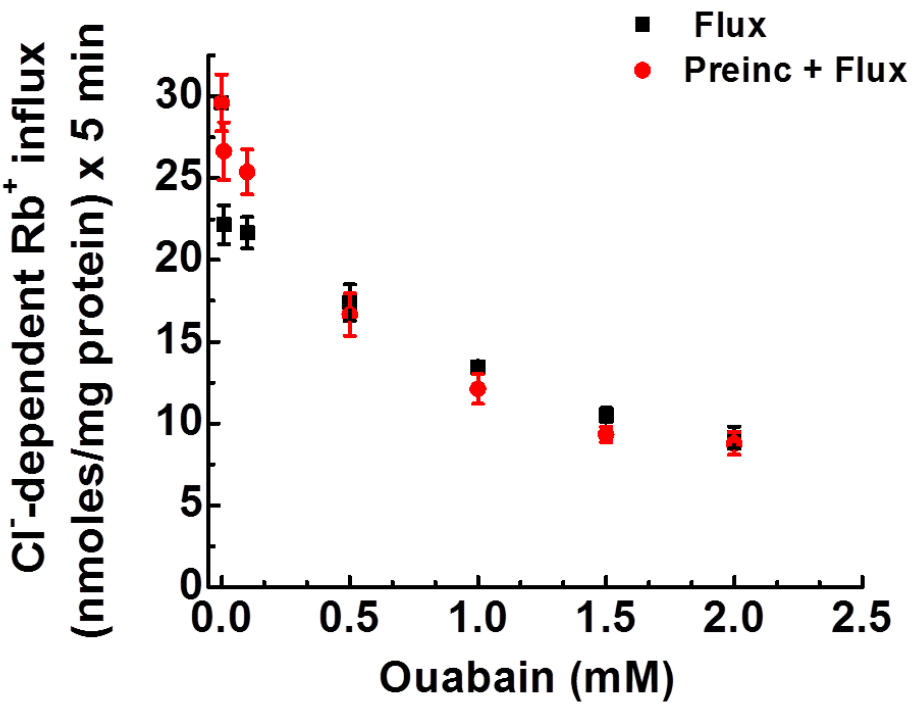

Figure 38. Ouabain dose-reponse curve. KCC activity was measured in isotonic condition in the presence of increasing concentration of ouabain ranging from 0-2 mM and in the presence of 5 µM bumetanide to inhibit Na^+-K^+-$2Cl^-$ cotransporter. Cl^--dependent Rb^+ influx (KCC) became stable by 2 mM ouabain and there was no difference in KCC activity when ouabain was present in flux (filled black squares) *vs*. preincubation and flux (filled red circles) at highest concentration used. Data represents mean ± standard error of a representative experiment with n = 3 per condition.

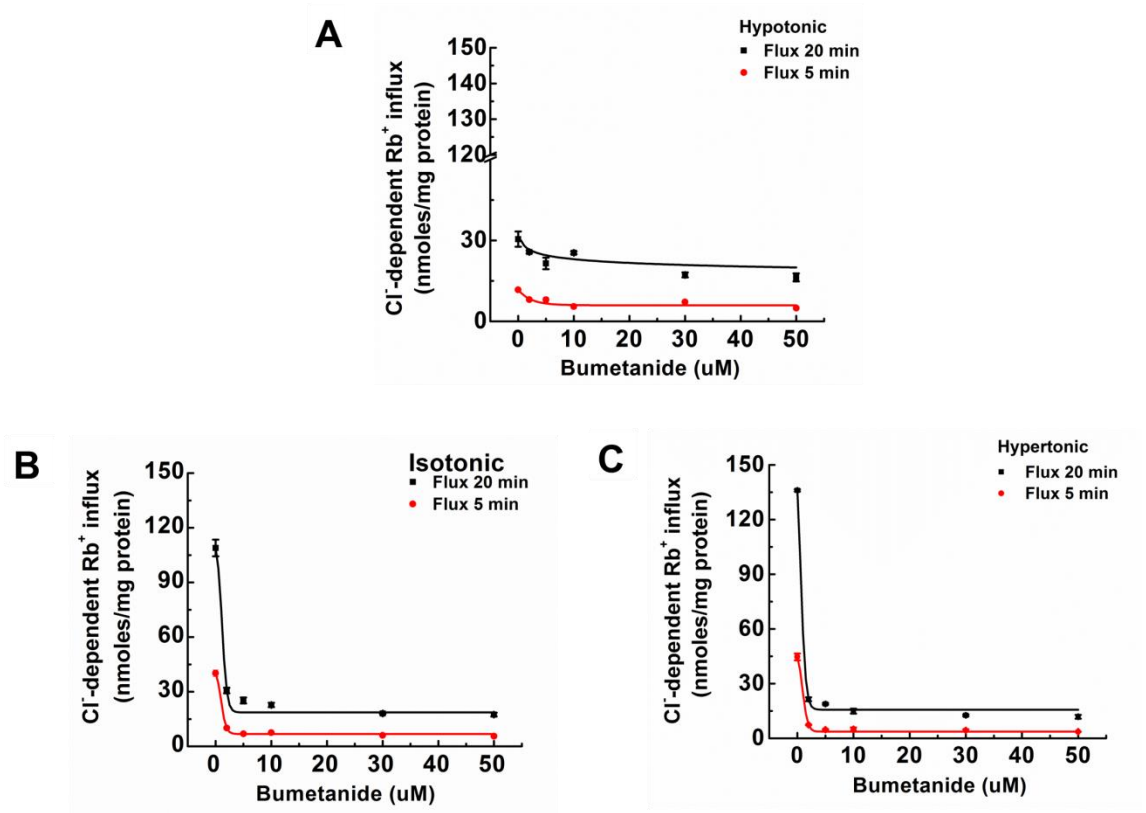

Figure 39. Bumetanide dose-response with respect to various osmolalities. Panel (A) Hypotonic conditions, Panel (B) Isotonic condition, and Panel (C) Hypertonic condition. NaCl and NaSf salts were used to increase the tonicity of external media. Confluent VSMCs were washed three times with BSS and flux experiment was carried out as described in Materials and Methods. Cl^--dependent Rb^+ influx, KCC, activity was assessed in the presence of bumetanide concentration ranging from 0-50 µM (present during preincubation + flux). Ouabain (2 mM) was present to inhibit the Na^+/K^+ pump. Flux was performed at 5 min and 20 min time period. The Rb^+ influx in Cl^- was subtracted from that in Sf^- media to yield the Cl^--dependent Rb^+ influx. Data represent mean ± error of three independent experiments with n = 3 per conditions.

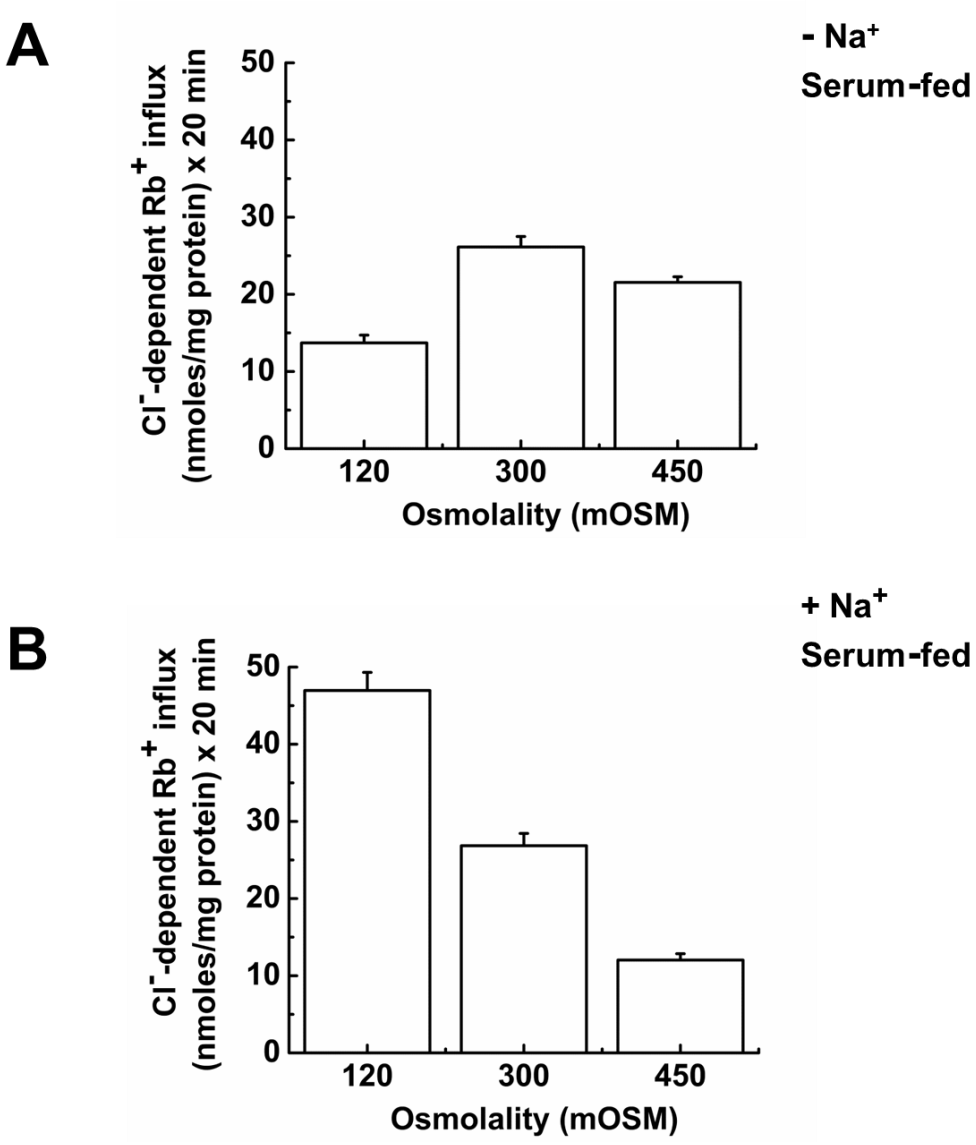
A
- Na+
Serum-fed
Cl--dependent Rb+ influx
(nmoles/mg protein) x 20 min
0
10
20
30
40
50
120
300
450
Osmolality (mOSM)
B
+ Na+
Serum-fed
Cl--dependent Rb+ influx
(nmoles/mg protein) x 20 min
0
10
20
30
40
50
120
300
450
Osmolality (mOSM)

Figure 40.

Figure 40. External Na^+ influences KCC sensitivity to osmoregulation. Serum-fed VSMCs were fluxed in the absence (Panel A) or presence (Panel B) of external Na^+ at different osmolalities. Changes in osmolality from solutions containing Na^+ were achieved by using NaCl and NaSf, whereas NMDGCl and NMDGSf were used for Na^+-free media. Ouabain (2 mM) and bumetanide (30 µM) was used to inhibit Na^+/K^+ pump and Na^+-K^+-$2Cl^+$. As shown in Panel B, KCC activity is differentially regulated according to changes in osmolality. In contrast, in Na^+-free media (Panel A), KCC activity was unresponsive to changes in osmolality. Data represents mean ± standard error of a representative experiment with n = 3 per condition.

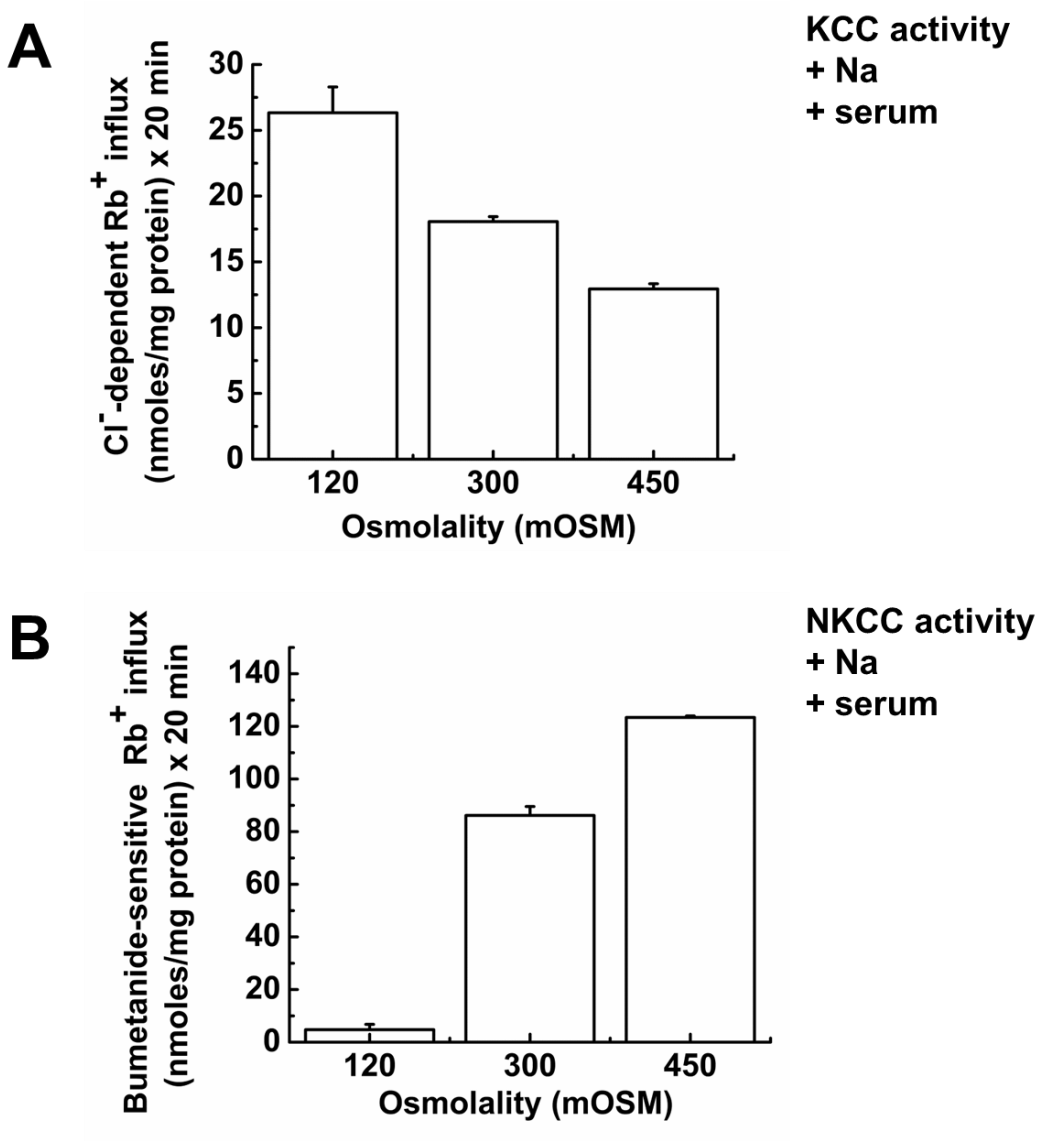
A
KCC activity
+ Na
+ serum
Cl-dependent Rb+ influx
(nmoles/mg protein) x 20 min
30
25
20
15
10
5
0
120
300
450
Osmolality (mOSM)
B
NKCC activity
+ Na
+ serum
Bumetanide-sensitive Rb+ influx
(nmoles/mg protein) x 20 min
140
120
100
80
60
40
20
0
120
300
450
Osmolality (mOSM)

Figure 41.

Figure 41. NKCC and KCC activation tightly and reciprocally regulated (Yin-Yang mechanism). To establish Yin-Yang canonical mechanism between NKCC and KCC along different tonicities (NaCl and NaSf were used to increase the tonicity of external media). VSMCs were grown in serum enriched media until subconfluency and Rb^+ influx was tested in the presence of external Na^+, and ouabain (2 mM) and bumetanide (30 µM) was used in preincubation and flux. Data represents mean ± standard error of three experiments with n = 3 per condition.

Apelin effect on K-Cl cotransport in serum-fed VSMCs under different osmolalities.

To further dissect the mechanism(s) behind the apelin-mediated increase in K-Cl cotransport, we treated subconfluent serum-fed VSMCs with apelin at different osmolalites by either modifying the ionic strength or keeping it constant (addition of sucrose). In previous **Figures 29 to 37A**, VSMCs were serum deprived for 24 h before being exposed to apelin. This time, Rb^+ influx was measured in apelin-treated VSMCs that were grown in serum containing media. Under constant ionic strength where sucrose was used to increase the extracellular osmolalities, the apelin response was not detectable (**Figure 42**). Thus, subsequent experiments were conducted under variable ionic strength conditions which resemble physiological challenges *in vivo*. To shed light into the mechanism(s) behind the lack of apelin effect under isotonic condition tested under 5 µM bumetanide (**Figure 37B**), 30 µM bumetanide was used on contractile VSMCs at different osmolalities obtained by modifying ionic strength. As shown in **Figure 43**, apelin treatment allowed increases in K-Cl cotransport in hypo- and hypertonic conditions. Interestingly, the extent of activation was considerably less when compared to synthetic VSMCs (**Figure 37B *vs* 43**). These results suggest that heterogeneous cultures of synthetic VSMCs might be unresponsive to apelin when cell integrity is not compromised by changes in osmolality (isotonic conditions). When similar assays were carried out using contractile VSMCs (**Figure 43**) a major difference in the apelin-mediated effect was observed. Under isotonic conditions, K-Cl cotransport activity in serum-fed contractile VSMCs was

stimulated by apelin treatment. Altogether these results suggest that contractile VSMCs under isotonic conditions might be more susceptible to apelin effects. These findings are in accordance with a more pronounced need in the responsiveness to apelin from contractile/healthy VSMCs to aid in the repair of damaged endothelium.

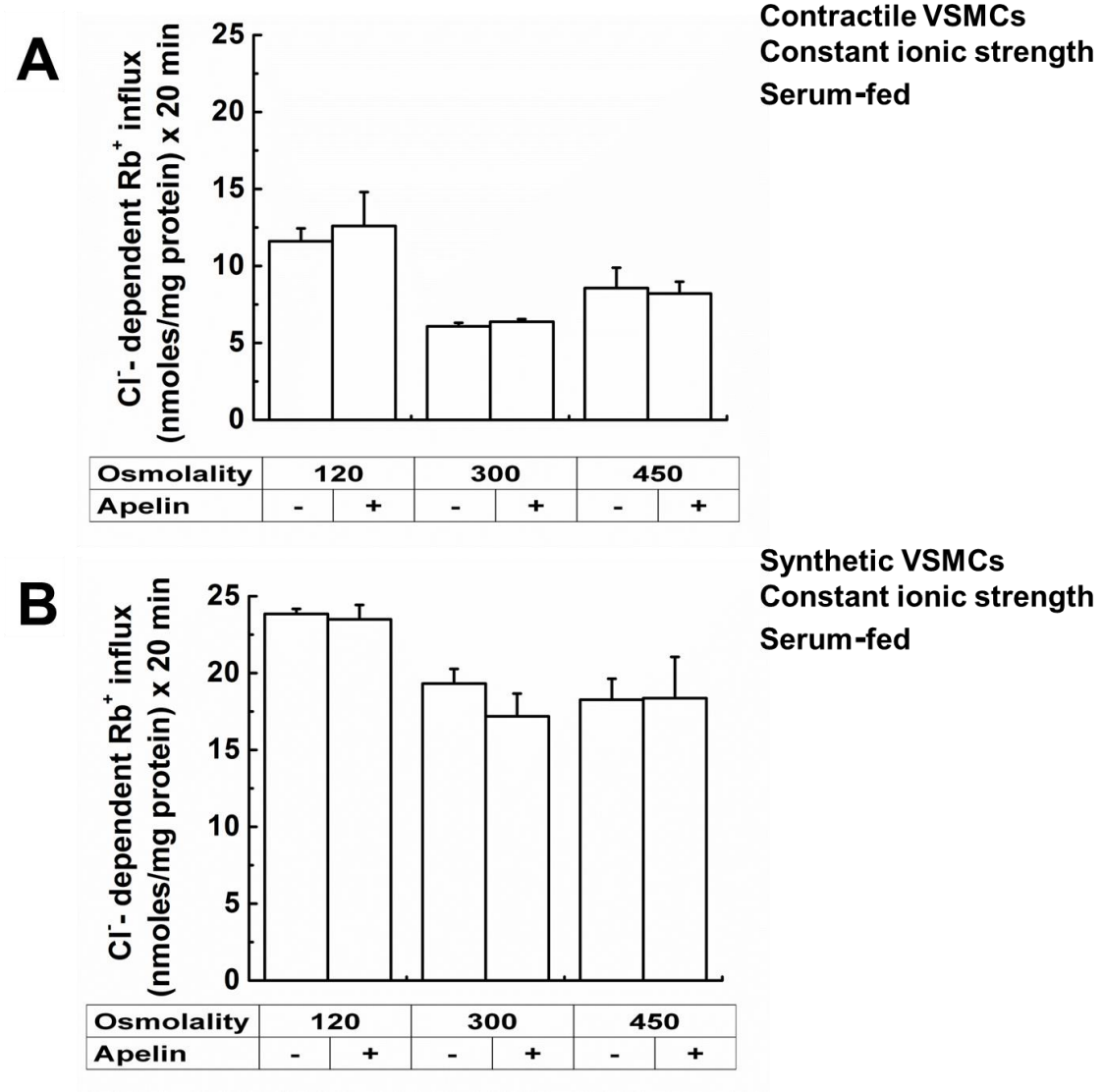

Figure 42. Effect of apelin in constant ionic strength. In serum-fed contractile (Panel A) and synthetic (Panel B) cells, KCC activity was measured in the presence or absence of apelin at different osmolalities. Sucrose was used to change the osmolality of the flux solution while keeping the concentration of other salts constant. As can be seen, apelin treatment did not change KCC activity under this condition. Data represents mean ± standard error of two independent experiments done in triplicates (n = 6).

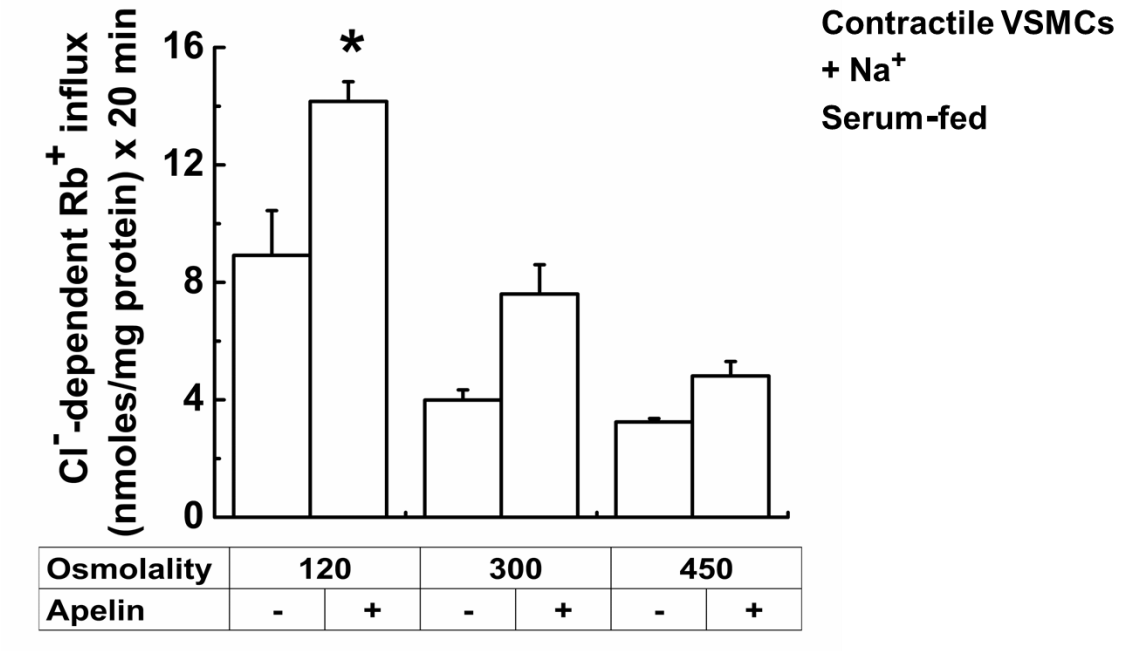

Figure 43. Effect of apelin on KCC activity in serum-fed contractile cells with respect to increase in external osmolality. Contractile VSMCs (passage 3) were grown in serum enriched media until subconfluency. Cells were then washed and exposed to different osmolalities (Hypotonic: 120 mOSM, Isotonic: 300 mOSM and Hypertonic: 450 mOSM) in the preincubation and flux media containing ouabain (2 mM) and bumetanide (30 µM). NaCl and NaSf salts were used to change the osmolalities of the external media. For each condition, n = 3 and the values are mean ± standard error. *$p < 0.05$ *vs* control group.

Apelin effect on K-Cl cotransport activity in synthetic VSMCs at different time point under hypotonic conditions

We then evaluated the kinetics of the effect of apelin in hypotonic conditions on K-Cl cotransport activity. VSMCs were grown until subconfluency in serum rich media and then apelin was added for 30 minutes, 1 hour, 12 hours, 18 hours and 24 hours before flux. Cells were then exposed to hypotonic media and Cl^--dependent Rb^+ influx was measured for 20 min in the presence of 1 µM apelin. As shown in **Figure 44**; apelin treatment resulted in significant increases on K-Cl cotransport at most time points tested. Interestingly, after 24 h of 1 µM apelin incubation; no significant increase in K-Cl cotransport was detected. It is possible that long exposure times result in APJ desensitization (internalization) and therefore absence of apelin effect on K-Cl cotransport activity. GPCRs like APJ can be desensitized following activation by agonists through phosphorylation by members of the GRKs (G-protein coupled receptor kinases (196). This mode of control of APJ remains to be further studied.

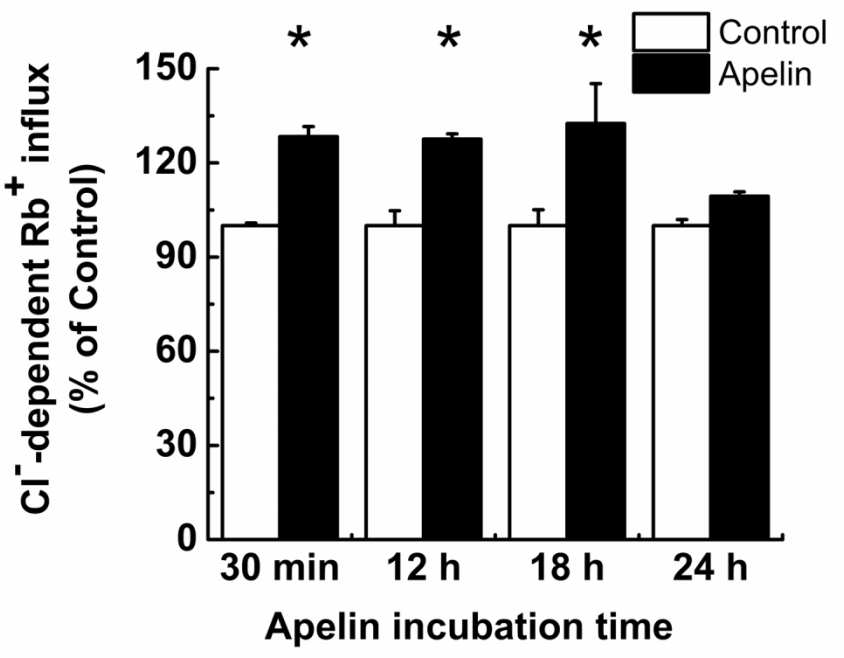

Figure 44. Effect of apelin in hypotonic conditions at different time points. Subconfluent VSMCs were incubated in the presence of 1 µM apelin for 30 min, 1 hour, 12 hours, 18 hours and 24 hours in a serum enriched growth media. Cells were then washed with BSS solution and flux measurement was carried out under hypotonic conditions in the presence of Ouabain (2 mM) and bumetanide (30 µM) to inhibit the pump and Na^+-K^+-$2Cl^-$ cotransport activity as described in MATERIALS AND METHODS. Apelin was added for additional 20 min during flux to the treatment groups. Each experimental outcome was normalized to its control. Apelin treatment resulted in significant increases of K-Cl cotransport activity in all time points tested except 24 hours. It is possible that APJ desensitization at 24 h could be the reason of absence of apelin stimulatory effect. Data represents mean ± standard error (n = 3 per conditions). *$p < 0.05$ *vs* control group.

Apelin regulatory effect on K-Cl cotransport activity during changes in osmolality in serum-fed synthetic phenotypes

VSMCs of synthetic passages are implicated in atherosclerosis. Thus, to assess apelin-induced K-Cl cotransport activity, VSMCs of various synthetic passages were examined. Urged by the observation that K-Cl cotransport could still be stimulated by apelin under hypertonic conditions (in which basal KCC activity is normally abrogated) (**Figure 37B and 43**) (91, 111), we examined whether manipulation of cell volume by shrinking and swelling could result in differences in the apelin response. Although we did not measure cell volume in our study, we did modulate external osmolality which would produce similar changes in cellular volume. **Figure 45** shows various conditions where apelin effects were tested during: a) cell swelling (hypotonicity), b) shrinkage (hypertonicity), c) shrinkage followed by swelling or d) swelling followed by shrinkage.

As can be seen in **Figure 45A**, under hypotonic conditions/cell swelling, apelin treatment further enhanced the activation of K-Cl cotransport by 54 % (*$p < 0.05$). Importantly, osmolarity shifts from hypertonicity to hypotonicity (shrinkage followed by swelling) did not affect the apelin stimulatory effect (74 % increase, **$p < 0.01$) on KCC activity. These findings strongly suggest that apelin might potentiate regulatory volume decrease (RVD) mechanisms. When preswollen VSMCs were shrunken by shifting them from hypotonicity to hypertonicity (swelling followed by shrinkage); apelin treatment failed to stimulate KCC activity (**Figure 45B**). Next we established whether VSMCs' progression to late synthetic states affected the apelin stimulatory effect in KCC activity during a shift from

hypertonicity to hypotonicity. As shown in **Figure 46A**, the apelin stimulatory effect was stronger in early synthetic VSMCs (passage number 7) when compared to later states (passage number 13 and 20). Similarly, and in accordance with **Figure 45B**; when pre-swollen VSMCs from different passage numbers were shifted to hypertonicity, apelin treatment failed to promote K-Cl cotransport (**Figure 46B**). The summaries of apelin response from contractile and synthetic VSMCs with respect to various factors are displayed in **Table 3**.

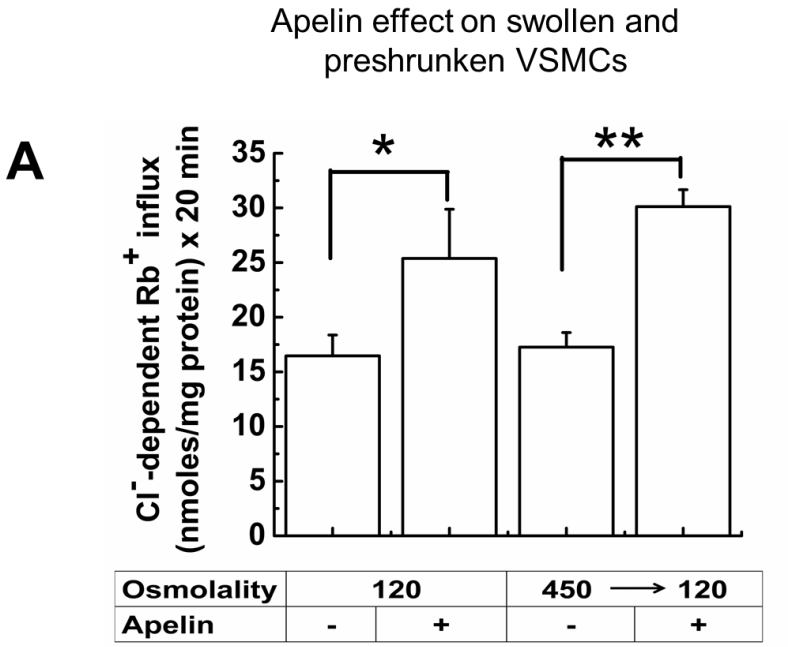
A
Apelin effect on swollen and preshrunken VSMCs
Cl⁻-dependent Rb⁺ influx (nmoles/mg protein) x 20 min
35
30
25
20
15
10
5
0
*
**
Osmolality
120
450 → 120
Apelin
-
+
-
+

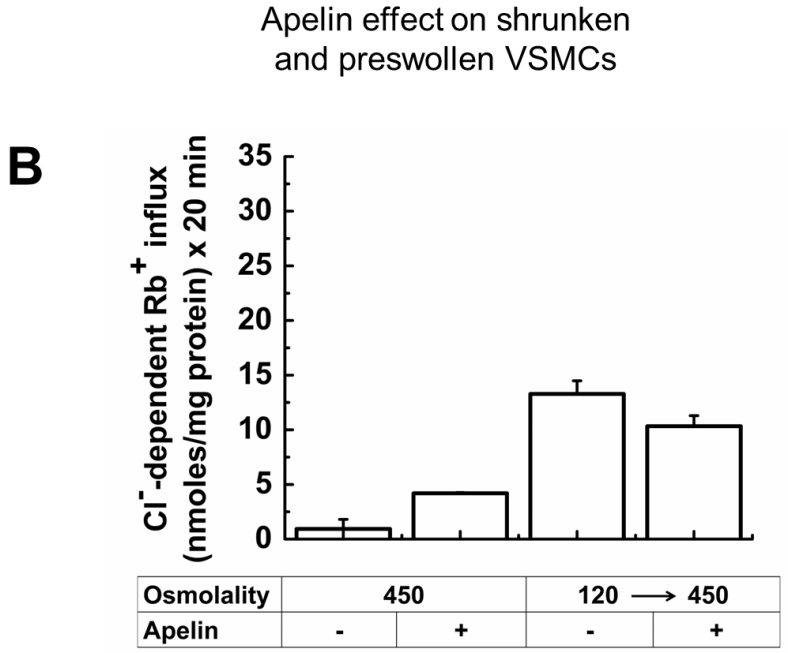
B
Apelin effect on shrunken and preswollen VSMCs
Cl⁻-dependent Rb⁺ influx (nmoles/mg protein) x 20 min
35
30
25
20
15
10
5
0
Osmolality
450
120 → 450
Apelin
-
+
-
+

Figure 45.

Figure 45. Apelin enhances KCC sensitivity with changes in external osmolality. KCC-mediated Rb^+ influx was measured in synthetic serum-fed VSMCs (passage 7). Cells were grown in serum enriched media and after reaching sub confluence, apelin was added for 6 h in the treatment group. Apelin was added for additional 20 min during flux; whereas, the control group contained no apelin. Panel (A). Apelin stimulated KCC activity in hypotonic condition (120 mOSM) and also in preshrunken cells that were first exposed to hypertonic solution (450 mOSM) during preincubation (10 min) and then in hypotonic solution (120 mOSM) during flux (20 min). Panel (B) Apelin stimulated KCC activity (borderline significant) under hypertonic conditions (450 mOSM) but lack of apelin response was observed in pre-swollen cells when the cells were transferred from hypotonic (120 mOSM) to hypertonic conditions (450 mOSM). Data represents mean ± standard error (n = 6 per conditions). *$p < 0.05$ *vs* control group.

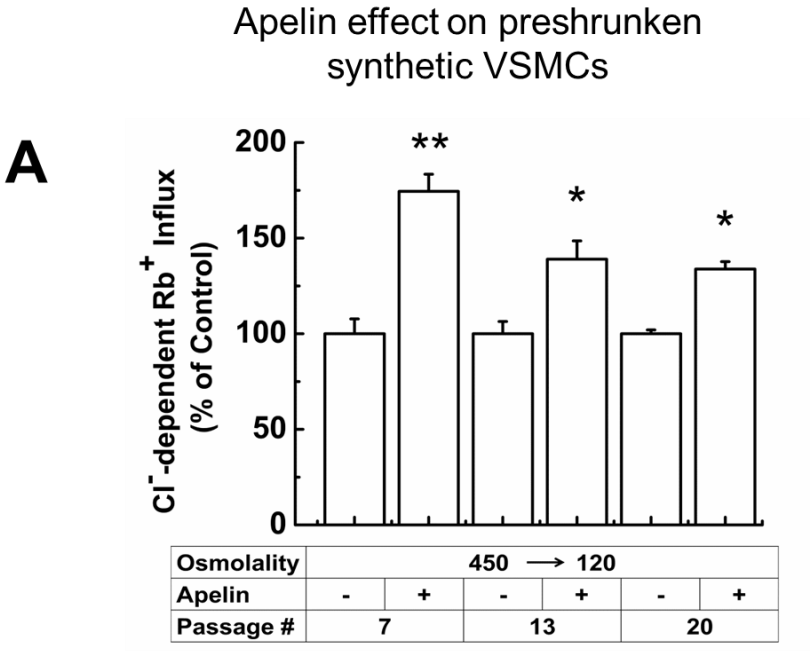
A
Apelin effect on preshrunken synthetic VSMCs
Cl⁻-dependent Rb⁺ Influx (% of Control)
200
150
100
50
0
**
*
*
Osmolality 450 → 120
Apelin - + - + - +
Passage # 7 13 20

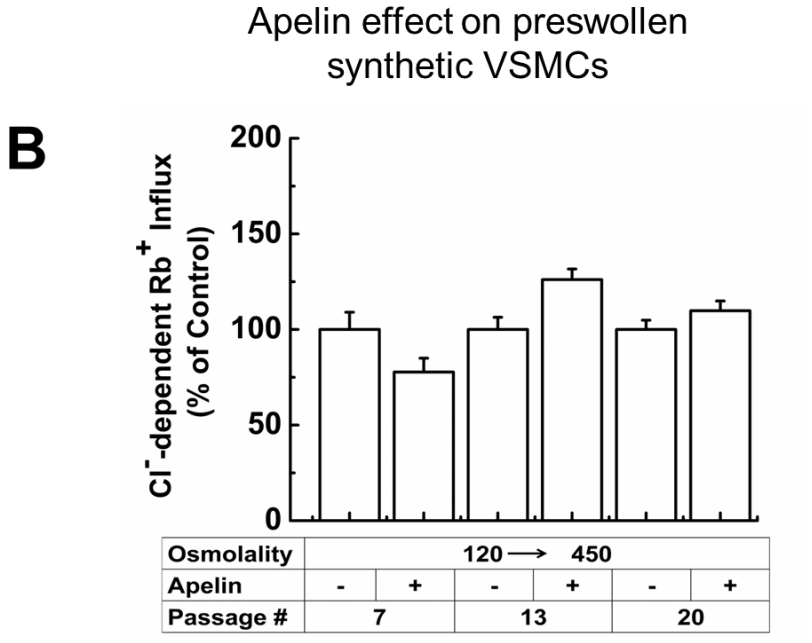
B
Apelin effect on preswollen synthetic VSMCs
Cl⁻-dependent Rb⁺ Influx (% of Control)
200
150
100
50
0
Osmolality 120 → 450
Apelin - + - + - +
Passage # 7 13 20

Figure 46.

Figure 46. Apelin response in preshrunken cells is passage-dependent and absent in preswollen cells. Cells were grown in serum enriched media and after reaching sub confluence, apelin was added for 6 h in the treatment group. Furthermore, apelin was present for additional 20 min during flux; whereas, the control group contained no apelin. Panel (A) Percent (%) apelin-mediated increase in KCC activity in pre-shrunken cells subsequently swollen (cells that were first exposed to hypertonic solution during preincubation (10 min) and then in hypotonic solution (20 min) during flux (450 → 120 mOSM), and Panel (B) Percent (%) apelin-mediated increase or decrease in KCC activity in pre-swollen cells subsequently shrunken (cells that were first exposed to hypotonic solution during preincubation and then in hypertonic solution during flux (120 → 450 mOSM). For each VSMCs passage, apelin response was normalized to that of the control. Data represents mean ± standard error of three independent experiments, n = 6 per conditions. *$p < 0.05$ *vs* control group.

In the presence of extracellular Na^+		Stimulation by apelin-13 at: 120 mOSM	300 mOSM	450 mOSM
Serum- starved VSMCs	Contractile	NO	YES	NO
	Synthetic	NO	YES	NO
Serum- fed VSMCs	Contractile	YES	YES	YES
	Synthetic	YES	NO	YES

In the absence of extracellular Na^+		Stimulation by apelin-13 at: 120 mOSM	300 mOSM	450 mOSM
Serum- starved VSMCs	Contractile	NO	NO	NO
	Synthetic	NO	NO	NO
Serum- fed VSMCs	Contractile	NO	NO	NO
	Synthetic	NO	NO	NO

	Stimulation by apelin-13 when transferred from : 450 mOSM → 120 mOSM	120 mOSM → 450 mOSM
Serum-fed Synthetic VSMCs	YES	NO

	Stimulation by apelin-13 at 120 mOSM during: (Growth media 24h) + (20 min flux)	(Growth media 1-18h) + (20 min flux)
Serum-fed Synthetic VSMCs	NO	YES

	Stimulation by apelin-13 during: Growth media 24h prior flux	Flux media 20-40 min
Serum-starved Synthetic VSMCs	NO	YES

Table 3. **Summary of apelin effect on K-Cl cotransport in VSMCs**. Under isotonic conditions, acute treatment of apelin-13 in serum-starved VSMCs stimulated KCC activity in the presence of extracellular sodium. In the absence of serum deprivation (serum-fed cells) apelin-13 treatment significantly increased K-Cl cotransport in contractile VSMCs. In contrast, in synthetic VSMCs, apelin-13 did not promote KCC activity under isotonic conditions. Similarly, in the absence of extracellular sodium no stimulatory effect of apelin was observed. Stimulation of K-Cl cotransport activity can be observed in serum-fed synthetic VSMCs under hypotonic conditions when apelin is present in growth and flux media. This mode

of activation was not seen at longer incubation times (24 h) probably due to APJ desensitization. Finally, KCC activity from serum-fed synthetic VSMCs was up regulated when cells were transferred from hypertonic to hypotonic conditions. Importantly, apelin stimulated KCC activity only when apelin was present in the flux media (acute activation); no stimulation of K-Cl cotransport was seen after chronic apelin exposure times in serum-starved cells.

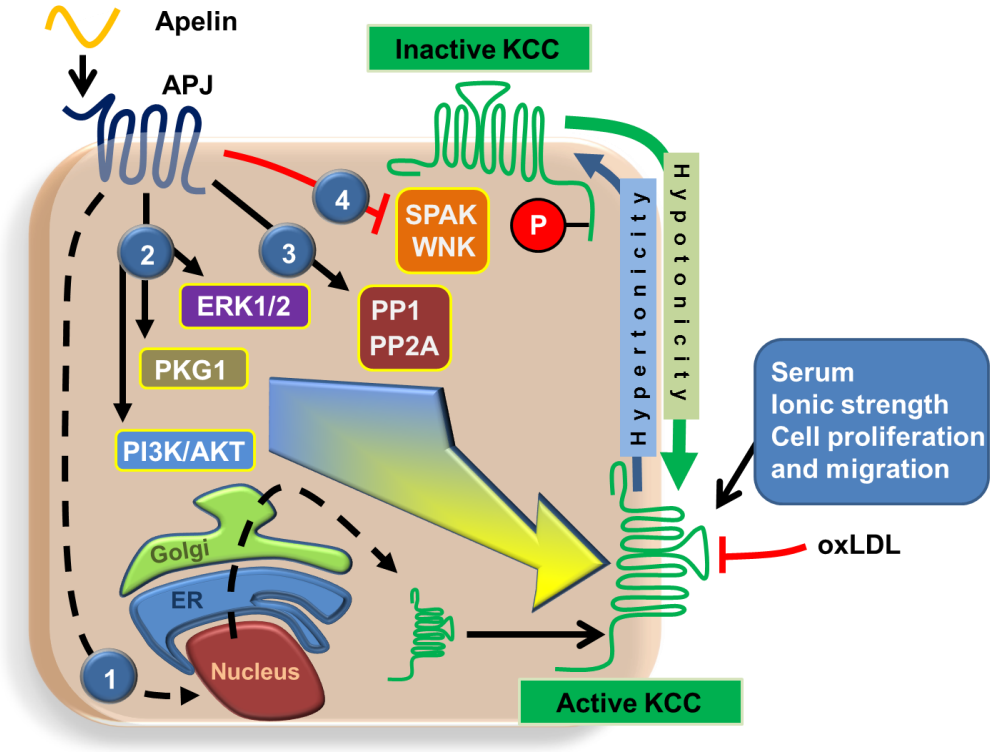

Figure 47. Schematic hypothetical representation of apelin regulation of K-Cl cotransport in VSMCs. In VSMCs, the binding of apelin-13 to its receptor APJ, activates K-Cl cotransport by increasing KCC protein expression and possibly increased membrane trafficking (1). Additionally, apelin-13 elicits the activation of several signaling cascades including PI3K/Akt, NO/cGMP/PKG1 and ERK1/2 to sustain KCC activation (2). Apelin-13-mediated activation of KCC occurs under both, hypertonicity and hypotonicity. In normal conditions, hypotonicity and RVD stimulate K-Cl cotransport through activation of protein phosphatases like PP1 and PP2A. It is possible that apelin administration results in PP1 and PP2A stimulation in order to sustain KCC activation (4). During hypertonicity, KCC activity is inhibited by phosphorylation events and activation of serine threonine kinases including WNK and SPAK (4). The apelin-13-

mediated activation of K-Cl cotransport is dependent on the presence of serum in the growth media, ionic strength and is central to control cell proliferation and migration which are required to sustain VSMCs phenotypic switching. Importantly, apelin-13 administration is able to rescue the oxLDL mediated inhibition of KCC.

DISCUSSION: Specific Aims 2 and 3

Apelin/APJ has emerged as an important regulator of cellular homeostasis and cardiovascular function. By targeting apelin/APJ, and subsequent stimulation of several signaling cascades such as the NO/cGMP/PKG, PI3K/Akt and ERK (1/2), a coordinated cardio-protective multicellular response takes place to repair and prevent further cell damage (53, 63, 197-199). Migration of VSMCs and their transition from contractile to synthetic states constitute initial steps to aid in the repair of atherosclerotic endothelium. Failure of VSMCs to switch back to contractile states accelerates lesion formation and results counterproductive due to possible increases in inflammatory processes (29). Although, further research is required to fully understand the inability of VSMCs to return to contractile states, in general, it has become evident that dysregulations in cell proliferation (mostly caused by high levels of growth factors, and uncontrolled uptake of oxLDL) are involved in the molecular pathogenesis of atherosclerosis (42, 47).

Several lines of evidence have pointed out that common signaling networks regulate the activity of KCC and the apelin-mediated cardio-protective effects (53, 105, 150, 157, 160, 184). Here we have provided evidence to support that electroneutral K-Cl cotransport in VSMCs is responsive to apelin via its membrane receptor APJ. Although differences were found in the APJ subcellular localization between synthetic (homogenously distributed) and contractile

VSMCs (perinuclear, localization), in general, the apelin receptor was found abundantly expressed in contractile and synthetic VSMCs (**Figure 28C-D**). Apelin treatment stimulated K-Cl cotransport irrespective of VSMCs phenotype. These results suggest a rapid trafficking of APJ to the membrane in order to elicit a comparable response in synthetic and contractile VSMCs. Although further experiments will be required to determine whether apelin could change the APJ subcellular localization, it is likely that increased APJ membrane trafficking facilitates apelin signaling in VSMCs (200, 201). In addition, further research will be required to confirm whether APJ is present in endosomes or any other subcellular compartment (202).

Our results also indicate an intricate overlap among several signaling cascades (NO/cGMP/PKG, PI3K/Akt and ERK1/2) to coordinate the apelin-mediated effects on KCC activity. Although selective inhibition of PKG, Akt and ERK1/2 completely prevented the apelin stimulatory-effect on the K-Cl cotransport in VSMCs (**Figures 31-32**); further examination will be required to determine the exact degree of contribution of each signaling cascade and their relevance to sustain vascular tone and endothelial function *in vivo*. Based on previous studies by our laboratory and others, in which PKG expression has proven to be absent in synthetic VSMCs (132), it is possible that differential regulation of KCCs' activity might occur within VSMCs phenotypes. Contractile VSMCs could be more dependent on the NO/cGMP/PKG pathway to respond to apelin, whereas in synthetic VSMCs, apelin could elicit its effects mostly through PI3K/Akt and ERK1/2 signaling cascades. It remains to be studied whether apelin treatment

results in an increase of KCCs expression/turnover, more efficiently trafficking to the plasma membrane or posttranslational modifications that promote an increase in KCCs activity. For years it has been recognized that phosphorylation/dephosphorylation events greatly determine the activity of NKCCs and KCCs. Consistent with their coordinated role in modulating intracellular chloride concentration, reciprocal modes of activation govern their activity. Increased activity of serine threonine kinases such as members of the WNK family (WNK 1-4) and Ste20 (SPAK and OSR1) enhance NKCCs activity and decrease KCCs function. Similarly, up regulation of protein phosphatases (PP1 and PP2B) inhibit NKCCs and activate KCCs. Therefore, it is likely that dephosphorylation of serine and threonine residues within the KCCs carboxy terminus constitute final events in the apelin stimulatory effect on KCCs (146).

Studies have shown that apelin and oxLDL have opposite effects on cardiovascular function. In CVD low levels of circulating apelin have been observed (203). Similarly, it has been recently shown that low plasma apelin concentrations constitute a risk to develop atrial fibrillation (204). Even though atherosclerosis is caused and sustained by a plethora of factors, the increasing evidence pointing out apelin administration as a remarkable protective therapy against atherosclerotic lesions is fully supported by our observations. Here we showed that apelin treatment restored the oxLDL-inhibitory effect on KCCs activity in contractile VSMCs (**Figure 31B**). Since high levels of oxLDL have shown in one hand to promote an increase in KCC1 mRNA expression (166) and simultaneously inhibit K-Cl cotransport in our studies (**Figure 31B**), it has not

escaped our notice that the increased mRNA levels for KCC could be part of a compensatory mechanism to attempt restore VSMCs' migration and normal cell volume.

Perhaps the most intriguing findings in these studies constitute the variability in the apelin-mediated effect on K-Cl cotransport. These differences were related to changes in external Na^+, serum and phenotypic states. In summary, serum-fed cells in the presence of external Na^+ displayed activation of K-Cl cotransport under hypo- and hypertonic conditions. In the absence of extracellular Na^+, no stimulatory effect by apelin was observed. To date it remains to be determined how extracellular Na^+ could be modulating the originally described sodium independent K-Cl cotransport.

Additionally, our data highlights apelin's role to modulate KCC activity in response to changes in extracellular osmolality (**Figures 37B, 43-45**). In both, synthetic and contractile VSMCs, apelin treatment resulted in further stimulation under hypotonic/swelling conditions (**Figure 37B and 43-44**). Studies have shown that hypotonic stimuli result in cell swelling and decreased lumen diameters (205). Noteworthy, hypotonic conditions also promote KCC activation; all of the above highlights increase in KCC activity as responsible for the apelin-mediated cardioprotective effects. The above has clinical implications since increased K-Cl cotransport and therefore vasorelaxation are commonly seen after exposure to hydralazine (HYZ), a vasodilator that has been shown to reduce tension of the vascular smooth muscle through increase in K-Cl cotransport activity (152). The effect of hydralazine can be mirrored to the apelin

response under hypotonic stimuli in VSMCs. Altogether our findings highlight increases in KCC activity as important effectors in sustaining normal vascular tone.

Under hypertonic/shrinking conditions, apelin treatment significantly increased KCCs activity and bypassed the osmolality-mediated inhibition of KCCs in synthetic VSMCs (**Figure 37B**). To our knowledge, this is the first time an extracellular stimulus bypasses the osmolality-mediated regulation on KCCs activity. Studies have shown that cell shrinkage results in increased lumen diameters and thus, stimulation of apelin response in hypertonic condition might be beneficial in maintenance of vessel relaxation *in vivo* (206). Consistently, absence of stimulation by apelin was observed when pre-swollen VSMCs were exposed to hypertonic media (shifted from 120 to 450 mOSM). In contrast, when pre-shrunken VSMCs were exposed to hypotonic stimuli (shifted from 450 to 120 mOSM); apelin treatment resulted in significant increase of KCCs. Based on published reports, it is likely that serine and threonine residues within KCCs carboxy terminus constitute final targets in the apelin stimulatory effect on KCCs (146, 207). Altogether these findings place apelin as a master regulator of cell volume and highlight its role during osmosensing processes.

KCC is involved in ionic balance and cellular homeostasis. Apelin and its receptor are also implicated in fluid homeostasis (52, 64, 72). The mechanisms by which apelin promotes fluid and cellular homeostasis by regulating ion transporters are less understood. Thus, the third specific aim of the thesis sought to test the hypothesis that apelin may promote cellular homeostasis through its

action on KCC and by modulating its transport activity. This homeostatic mechanism is important for overall vascular function. Finally, the close association between cell proliferation and volume regulation suggests that K-Cl cotransport activity and its regulation by apelin, are both important to confer protection against atherosclerosis. A better understanding of apelin effects on K-Cl cotransport will help design a more powerful therapeutic approach to treat atherosclerosis-linked cardiovascular diseases.

CONCLUSION

The work presented in this thesis offers compelling evidence supporting that apelin/APJ constitutes an important modulator of electroneutral K-Cl cotransport in rat aortic vascular smooth muscle cells. Increased K-Cl cotransport activity, measured by atomic absorption spectrometry, was determined under isotonic condition, in both contractile and synthetic VSMCs when exposed to 1 µM of the most abundant form of apelin found in the circulatory system (apelin-13). In contrast, no stimulatory effect on K-Cl cotransport was observed when apelin was present in serum-free growth media before flux measurements.

By using selective inhibitors of PKG, PI3K and MAPK signaling pathways, such as KT5823, LY294002, and PD98059, we demonstrated that under isotonic conditions, apelin-13 increased K-Cl cotransport in serum-starved VSMCs through activation of those signaling cascades. Our data also suggests differences in expression and subcellular localization of APJ among VSMCs phenotypes. APJ total expression was decreased in synthetic VSMCs. Its expression appeared more diffused and cytoplasmic when compared to contractile VSMCs where a more localized and perinuclear immunolocalization could be observed.

We showed that K-Cl cotransport in VSMCs is dramatically impaired (~ 70 % of inhibition) by oxLDLs, a known promoter of vascular lesions and atherosclerosis

progression. Importantly, apelin treatment prevented the oxLDL-mediated inhibition of K-Cl cotransport since similar activation was observed in response to apelin. These findings are in accordance with the protective roles of apelin against cardiovascular disease (CVD).

However, variability in the apelin response was observed among VSMCs phenotypes. K-Cl cotransport activity is more prone to activation by apelin in serum-fed compared to serum-starved VSMCs. Besides, extracellular sodium was required for apelin to modulate KCC activity. Additionally, apelin's role in controlling K-Cl cotransport proved to be of central importance since stimulation of KCC activity was enhanced under hypotonic and hypertonic conditions. Similar stimulatory effect of apelin was observed when pre-shrunken VSMCs were swollen. In sum, these results highlight apelin's role in controlling cellular homeostasis and place KCC activity as an important therapeutic target) and potential mediator in the apelin-conferred protection against CVD.

In addition, we found that expression levels of cytoskeletal protein markers like α-actin, vimentin, and desmin decreased in late synthetic stages. Finally we also showed that both, the apparent Rb^+ and Cl^- affinities and V_{max} values of KCC increased in late synthetic VSMCs compared to earlier states. Consistently, increased protein expression of KCC1 and KCC4 were observed in late synthetic VSMCs compared to earlier states. These results point out that the functional properties of KCC may be involved and required to sustain VSMCs phenotypic switching and their transition to a diseased state during CVD, perhaps as a

compensatory mechanism trying to overcome the ravages of this serious disease.

REFERENCES

1. Mathers CD, Lopez AD, Murray CJL. The burden of disease and mortality by condition: Data, methods, and results for 2001. In: Lopez AD, Mathers CD, Ezzati M, Jamison DT, Murray CJL, editors. Global Burden of Disease and Risk Factors. Washington (DC): The International Bank for Reconstruction and Development/The World Bank Group; 2006.

2. Roger VL, Go AS, Lloyd-Jones DM, Benjamin EJ, Berry JD, Borden WB, et al. Heart disease and stroke statistics--2012 update: A report from the american heart association. Circulation. 2012 Jan 3;125(1):e2-e220.

3. Lloyd-Jones D, Adams R, Carnethon M, De Simone G, Ferguson TB, Flegal K, et al. Heart disease and stroke statistics--2009 update: A report from the american heart association statistics committee and stroke statistics subcommittee. Circulation. 2009 Jan 27;119(3):480-6.

4. Lloyd-Jones D, Adams R, Carnethon M, De Simone G, Ferguson TB, Flegal K, et al. Heart disease and stroke statistics--2009 update: A report from the american heart association statistics committee and stroke statistics subcommittee. Circulation. 2009 Jan 27;119(3):480-6.

5. The 10 leading causes of death in the world, 2000 and 2011. fact sheet no. 310 [Internet].: World Health Organization; 2013 [updated July 2013; cited January 17, 2014.]. Available from: http://www.who.int/mediacentre/factsheets/fs310/en/.

6. Barton M. Mechanisms and therapy of atherosclerosis and its clinical complications. Curr Opin Pharmacol. 2013 Apr;13(2):149-53.

7. Mallika V, Goswami B, Rajappa M. Atherosclerosis pathophysiology and the role of novel risk factors: A clinicobiochemical perspective. Angiology. 2007 Oct-Nov;58(5):513-22.

8. Madamanchi NR, Vendrov A, Runge MS. Oxidative stress and vascular disease. Arterioscler Thromb Vasc Biol. 2005 Jan;25(1):29-38.

9. Enis DR, Shepherd BR, Wang Y, Qasim A, Shanahan CM, Weissberg PL, et al. Induction, differentiation, and remodeling of blood vessels after transplantation of bcl-2-transduced endothelial cells. Proc Natl Acad Sci U S A. 2005 Jan 11;102(2):425-30.

10. Timpl R. Macromolecular organization of basement membranes. Curr Opin Cell Biol. 1996 Oct;8(5):618-24.

11. Zalewski A, Shi Y, Johnson AG. Diverse origin of intimal cells: Smooth muscle cells, myofibroblasts, fibroblasts, and beyond? Circ Res. 2002 Oct 18;91(8):652-5.

12. Wight TN. The extracellular matrix and atherosclerosis. Curr Opin Lipidol. 1995 Oct;6(5):326-34.

13. Rensen SS, Doevendans PA, van Eys GJ. Regulation and characteristics of vascular smooth muscle cell phenotypic diversity. Neth Heart J. 2007;15(3):100-8.

14. Lang F, Busch GL, Zempel G, Ditlevsen J, Hoch M, Emerich U, et al. Ca2+ entry and vasoconstriction during osmotic swelling of vascular smooth muscle cells. Pflugers Arch. 1995 Dec;431(2):253-8.

15. Anderson RG. The caveolae membrane system. Annu Rev Biochem. 1998;67:199-225.

16. Goldberg GS, Valiunas V, Brink PR. Selective permeability of gap junction channels. Biochim Biophys Acta. 2004 Mar 23;1662(1-2):96-101.

17. Gabbiani G, Schmid E, Winter S, Chaponnier C, de Ckhastonay C, Vandekerckhove J, et al. Vascular smooth muscle cells differ from other smooth muscle cells: Predominance of vimentin filaments and a specific alpha-type actin. Proc Natl Acad Sci U S A. 1981 Jan;78(1):298-302.

18. Tang DD, Anfinogenova Y. Physiologic properties and regulation of the actin cytoskeleton in vascular smooth muscle. J Cardiovasc Pharmacol Ther. 2008 Jun;13(2):130-40.

19. Tang DD. Intermediate filaments in smooth muscle. Am J Physiol Cell Physiol. 2008 Apr;294(4):C869-78.

20. Lincoln TM, Cornwell TL, Komalavilas P, Boerth N. Cyclic GMP-dependent protein kinase in nitric oxide signaling. Methods Enzymol. 1996;269:149-66.

21. Lincoln TM, Dey NB, Boerth NJ, Cornwell TL, Soff GA. Nitric oxide--cyclic GMP pathway regulates vascular smooth muscle cell phenotypic modulation: Implications in vascular diseases. Acta Physiol Scand. 1998 Dec;164(4):507-15.

22. Lincoln TM, Wu X, Sellak H, Dey N, Choi CS. Regulation of vascular smooth muscle cell phenotype by cyclic GMP and cyclic GMP-dependent protein kinase. Front Biosci. 2006 Jan 1;11:356-67.

23. Kudryavtseva O, Aalkjaer C, Matchkov VV. Vascular smooth muscle cell phenotype is defined by Ca2+-dependent transcription factors. FEBS J. 2013 Nov;280(21):5488-99.

24. Lincoln TM, Cornwell TL. Towards an understanding of the mechanism of action of cyclic AMP and cyclic GMP in smooth muscle relaxation. Blood Vessels. 1991;28(1-3):129-37.

25. Lincoln TM, Dey NB, Boerth NJ, Cornwell TL, Soff GA. Nitric oxide--cyclic GMP pathway regulates vascular smooth muscle cell phenotypic modulation: Implications in vascular diseases. Acta Physiol Scand. 1998 Dec;164(4):507-15.

26. Matchkov VV, Kudryavtseva O, Aalkjaer C. Intracellular ca(2)(+) signalling and phenotype of vascular smooth muscle cells. Basic Clin Pharmacol Toxicol. 2012 Jan;110(1):42-8.

27. Louis SF, Zahradka P. Vascular smooth muscle cell motility: From migration to invasion. Exp Clin Cardiol. 2010 Winter;15(4):e75-85.

28. Rudijanto A. The role of vascular smooth muscle cells on the pathogenesis of atherosclerosis. Acta Med Indones. 2007 Apr-Jun;39(2):86-93.

29. Gomez D, Owens GK. Smooth muscle cell phenotypic switching in atherosclerosis. Cardiovasc Res. 2012 Jul 15;95(2):156-64.

30. Worth NF, Rolfe BE, Song J, Campbell GR. Vascular smooth muscle cell phenotypic modulation in culture is associated with reorganisation of contractile and cytoskeletal proteins. Cell Motil Cytoskeleton. 2001 Jul;49(3):130-45.

31. Brown MS, Goldstein JL. Receptor-mediated endocytosis: Insights from the lipoprotein receptor system. Proc Natl Acad Sci U S A. 1979 Jul;76(7):3330-7.

32. Brown MS, Goldstein JL. A receptor-mediated pathway for cholesterol homeostasis. Science. 1986 Apr 4;232(4746):34-47.

33. John W. Kimball. Endocytosis. In: Kimball's Biology Pages. 6th ed. Dubuque, Iowa: Wm. C. Brown; 1994.

34. Schwartz CJ, Kelley JL, Nerem RM, Sprague EA, Rozek MM, Valente AJ, et al. Pathophysiology of the atherogenic process. Am J Cardiol. 1989 Oct 3;64(13):23G-30G.

35. Holvoet P, Mertens A, Verhamme P, Bogaerts K, Beyens G, Verhaeghe R, et al. Circulating oxidized LDL is a useful marker for identifying patients with coronary artery disease. Arterioscler Thromb Vasc Biol. 2001 May;21(5):844-8.

36. Toshima S, Hasegawa A, Kurabayashi M, Itabe H, Takano T, Sugano J, et al. Circulating oxidized low density lipoprotein levels. A biochemical risk marker for coronary heart disease. Arterioscler Thromb Vasc Biol. 2000 Oct;20(10):2243-7.

37. Hodis HN, Kramsch DM, Avogaro P, Bittolo-Bon G, Cazzolato G, Hwang J, et al. Biochemical and cytotoxic characteristics of an in vivo circulating oxidized low density lipoprotein (LDL-). J Lipid Res. 1994 Apr;35(4):669-77.

38. Levitan I, Shentu TP. Impact of oxLDL on cholesterol-rich membrane rafts. J Lipids. 2011;2011:730209.

39. Boullier A, Bird DA, Chang MK, Dennis EA, Friedman P, Gillotre-Taylor K, et al. Scavenger receptors, oxidized LDL, and atherosclerosis. Ann N Y Acad Sci. 2001 Dec;947:214,22; discussion 222-3.

40. Mehta JL, Li D. Identification, regulation and function of a novel lectin-like oxidized low-density lipoprotein receptor. J Am Coll Cardiol. 2002 May 1;39(9):1429-35.

41. Steinberg D. Low density lipoprotein oxidation and its pathobiological significance. J Biol Chem. 1997 Aug 22;272(34):20963-6.

42. Levitan I, Volkov S, Subbaiah PV. Oxidized LDL: Diversity, patterns of recognition, and pathophysiology. Antioxid Redox Signal. 2010 Jul 1;13(1):39-75.

43. Glukhova MA, Kabakov AE, Frid MG, Ornatsky OI, Belkin AM, Mukhin DN, et al. Modulation of human aorta smooth muscle cell phenotype: A study of muscle-specific variants of vinculin, caldesmon, and actin expression. Proc Natl Acad Sci U S A. 1988 Dec;85(24):9542-6.

44. Kocher O, Gabbiani F, Gabbiani G, Reidy MA, Cokay MS, Peters H, et al. Phenotypic features of smooth muscle cells during the evolution of experimental carotid artery intimal thickening. biochemical and morphologic studies. Lab Invest. 1991 Oct;65(4):459-70.

45. Proudfoot D, Shanahan C. Human vascular smooth muscle cell culture. Methods Mol Biol. 2012;806:251-63.

46. Chahine MN, Blackwood DP, Dibrov E, Richard MN, Pierce GN. Oxidized LDL affects smooth muscle cell growth through MAPK-mediated actions on nuclear protein import. J Mol Cell Cardiol. 2009 Mar;46(3):431-41.

47. Chien MW, Chien CS, Hsiao LD, Lin CH, Yang CM. OxLDL induces mitogen-activated protein kinase activation mediated via PI3-kinase/Akt in vascular smooth muscle cells. J Lipid Res. 2003 Sep;44(9):1667-75.

48. Lincoln TM, Dey N, Sellak H. Invited review: CGMP-dependent protein kinase signaling mechanisms in smooth muscle: From the regulation of tone to gene expression. J Appl Physiol. 2001 Sep;91(3):1421-30.

49. Pitkin SL, Maguire JJ, Kuc RE, Davenport AP. Modulation of the apelin/APJ system in heart failure and atherosclerosis in man. Br J Pharmacol. 2010 Aug;160(7):1785-95.

50. Kalea AZ, Batlle D. Apelin and ACE2 in cardiovascular disease. Curr Opin Investig Drugs. 2010 Mar;11(3):273-82.

51. Chun HJ, Ali ZA, Kojima Y, Kundu RK, Sheikh AY, Agrawal R, et al. Apelin signaling antagonizes ang II effects in mouse models of atherosclerosis. J Clin Invest. 2008 Oct;118(10):3343-54.

52. O'Carroll AM, Lolait SJ, Harris LE, Pope GR. The apelin receptor APJ: Journey from an orphan to a multifaceted regulator of homeostasis. J Endocrinol. 2013 Sep 11;219(1):R13-35.

53. Yu XH, Tang ZB, Liu LJ, Qian H, Tang SL, Zhang DW, et al. Apelin and its receptor APJ in cardiovascular diseases. Clin Chim Acta. 2014 Jan 20;428:1-8.

54. Tatemoto K, Hosoya M, Habata Y, Fujii R, Kakegawa T, Zou MX, et al. Isolation and characterization of a novel endogenous peptide ligand for the human APJ receptor. Biochem Biophys Res Commun. 1998 Oct 20;251(2):471-6.

55. Van Coillie E, Proost P, Van Aelst I, Struyf S, Polfliet M, De Meester I, et al. Functional comparison of two human monocyte chemotactic protein-2 isoforms, role of the amino-terminal pyroglutamic acid and processing by CD26/dipeptidyl peptidase IV. Biochemistry. 1998 Sep 8;37(36):12672-80.

56. O'Dowd BF, Heiber M, Chan A, Heng HH, Tsui LC, Kennedy JL, et al. A human gene that shows identity with the gene encoding the angiotensin receptor is located on chromosome 11. Gene. 1993 Dec 22;136(1-2):355-60.

57. Devic E, Rizzoti K, Bodin S, Knibiehler B, Audigier Y. Amino acid sequence and embryonic expression of msr/apj, the mouse homolog of xenopus X-msr and human APJ. Mech Dev. 1999 Jun;84(1-2):199-203.

58. O'Carroll AM, Selby TL, Palkovits M, Lolait SJ. Distribution of mRNA encoding B78/apj, the rat homologue of the human APJ receptor, and its endogenous ligand apelin in brain and peripheral tissues. Biochim Biophys Acta. 2000 Jun 21;1492(1):72-80.

59. Carpene C, Dray C, Attane C, Valet P, Portillo MP, Churruca I, et al. Expanding role for the apelin/APJ system in physiopathology. J Physiol Biochem. 2007 Dec;63(4):359-73.

60. Grisk O. Apelin and vascular dysfunction in type 2 diabetes. Cardiovasc Res. 2007 Jun 1;74(3):339-40.

61. Andersen CU, Hilberg O, Mellemkjaer S, Nielsen-Kudsk JE, Simonsen U. Apelin and pulmonary hypertension. Pulm Circ. 2011 Jul-Sep;1(3):334-46.

62. Qin D, Zheng XX, Jiang YR. Apelin-13 induces proliferation, migration, and collagen I mRNA expression in human RPE cells via PI3K/Akt and MEK/Erk signaling pathways. Mol Vis. 2013 Nov 7;19:2227-36.

63. Liu C, Su T, Li F, Li L, Qin X, Pan W, et al. PI3K/Akt signaling transduction pathway is involved in rat vascular smooth muscle cell proliferation induced by apelin-13. Acta Biochim Biophys Sin (Shanghai). 2010 Jun 15;42(6):396-402.

64. Lee DK, Cheng R, Nguyen T, Fan T, Kariyawasam AP, Liu Y, et al. Characterization of apelin, the ligand for the APJ receptor. J Neurochem. 2000 Jan;74(1):34-41.

65. Reaux A, De Mota N, Skultetyova I, Lenkei Z, El Messari S, Gallatz K, et al. Physiological role of a novel neuropeptide, apelin, and its receptor in the rat brain. J Neurochem. 2001 May;77(4):1085-96.

66. Losano G, Penna C, Cappello S, Pagliaro P. Activity of apelin and APJ receptors on myocardial contractility and vasomotor tone]. Ital Heart J Suppl. 2005 May;6(5):272-8.

67. Losano GA. On the cardiovascular activity of apelin. Cardiovasc Res. 2005 Jan 1;65(1):8-9.

68. Kuba K, Zhang L, Imai Y, Arab S, Chen M, Maekawa Y, et al. Impaired heart contractility in apelin gene-deficient mice associated with aging and pressure overload. Circ Res. 2007 Aug 17;101(4):e32-42.

69. Kasai A, Shintani N, Oda M, Kakuda M, Hashimoto H, Matsuda T, et al. Apelin is a novel angiogenic factor in retinal endothelial cells. Biochem Biophys Res Commun. 2004 Dec 10;325(2):395-400.

70. Cox CM, D'Agostino SL, Miller MK, Heimark RL, Krieg PA. Apelin, the ligand for the endothelial G-protein-coupled receptor, APJ, is a potent angiogenic factor required for normal vascular development of the frog embryo. Dev Biol. 2006 Aug 1;296(1):177-89.

71. Masri B, Morin N, Cornu M, Knibiehler B, Audigier Y. Apelin (65-77) activates p70 S6 kinase and is mitogenic for umbilical endothelial cells. FASEB J. 2004 Dec;18(15):1909-11.

72. De Mota N, Lenkei Z, Llorens-Cortes C. Cloning, pharmacological characterization and brain distribution of the rat apelin receptor. Neuroendocrinology. 2000 Dec;72(6):400-7.

73. Kang Y, Kim J, Anderson JP, Wu J, Gleim SR, Kundu RK, et al. Apelin-APJ signaling is a critical regulator of endothelial MEF2 activation in cardiovascular development. Circ Res. 2013 Jun 21;113(1):22-31.

74. Barnes G, Japp AG, Newby DE. Translational promise of the apelin--APJ system. Heart. 2010 Jul;96(13):1011-6.

75. Adragna NC, Di Fulvio M, Lauf PK. Regulation of K-cl cotransport: From function to genes. J Membr Biol. 2004 Oct 1;201(3):109-37.

76. Gamba G. Molecular physiology and pathophysiology of electroneutral cation-chloride cotransporters. Physiol Rev. 2005 Apr;85(2):423-93.

77. Lang F. Mechanisms and significance of cell volume regulation. J Am Coll Nutr. 2007 Oct;26(5 Suppl):613S-23S.

78. Reus L. Cell volume regulation in nonrenal epithelia. Ren Physiol Biochem. 1988 May-Oct;11(3-5):187-201.

79. Cossins AR, Gibson JS. Volume-sensitive transport systems and volume homeostasis in vertebrate red blood cells. J Exp Biol. 1997 Jan;200(Pt 2):343-52.

80. Kerrigan MJ, Hook CS, Qusous A, Hall AC. Regulatory volume increase (RVI) by in situ and isolated bovine articular chondrocytes. J Cell Physiol. 2006 Nov;209(2):481-92.

81. Bildin VN, Yang H, Fischbarg J, Reinach PS. Effects of chronic hypertonic stress on regulatory volume increase and na-K-2Cl cotransporter expression in cultured corneal epithelial cells. Adv Exp Med Biol. 1998;438:637-42.

82. Bonanno JA, Klyce SD, Cragoe EJ,Jr. Mechanism of chloride uptake in rabbit corneal epithelium. Am J Physiol. 1989 Aug;257(2 Pt 1):C290-6.

83. Geck P, Pietrzyk C, Burckhardt BC, Pfeiffer B, Heinz E. Electrically silent cotransport on na+, K+ and cl- in ehrlich cells. Biochim Biophys Acta. 1980 Aug 4;600(2):432-47.

84. Lauf PK, Theg BE. A chloride dependent K+ flux induced by N-ethylmaleimide in genetically low K+ sheep and goat erythrocytes. Biochem Biophys Res Commun. 1980 Feb 27;92(4):1422-8.

85. Dunham PB, Stewart GW, Ellory JC. Chloride-activated passive potassium transport in human erythrocytes. Proc Natl Acad Sci U S A. 1980 Mar;77(3):1711-5.

86. Jennings ML, Adame MF. Direct estimate of 1:1 stoichiometry of K(+)-cl(-) cotransport in rabbit erythrocytes. Am J Physiol Cell Physiol. 2001 Sep;281(3):C825-32.

87. Lauf PK, Adragna NC. A thermodynamic study of electroneutral K-cl cotransport in pH- and volume-clamped low K sheep erythrocytes with normal and low internal magnesium. J Gen Physiol. 1996 Oct;108(4):341-50.

88. Gillen CM, Brill S, Payne JA, Forbush B,3rd. Molecular cloning and functional expression of the K-cl cotransporter from rabbit, rat, and human. A new member of the cation-chloride cotransporter family. J Biol Chem. 1996 Jul 5;271(27):16237-44.

89. Adragna NC, Lauf PK. K-cl cotransport function and its potential contribution to cardiovascular disease. Pathophysiology. 2007 Dec;14(3-4):135-46.

90. Adragna NC, Lauf,Peter K. (Eric Delpire and Kerstin Piechotta). Cell volume and signaling. In: Peter K. Lauf and Norma C. Adragna, editor. Advances in experimental medicine and biology. New York: Springer Science+Business Media; 2004. p. 444,43-53.

91. Hoffmann EK, Lambert IH, Pedersen SF. Physiology of cell volume regulation in vertebrates. Physiol Rev. 2009 Jan;89(1):193-277.

92. Payne JA, Forbush B,3rd. Molecular characterization of the epithelial na-K-cl cotransporter isoforms. Curr Opin Cell Biol. 1995 Aug;7(4):493-503.

93. Lytle C, Forbush B,3rd. The na-K-cl cotransport protein of shark rectal gland. II. regulation by direct phosphorylation. J Biol Chem. 1992 Dec 15;267(35):25438-43.

94. Delpire E, Gullans SR. Cell volume and K+ transport during differentiation of mouse erythroleukemia cells. Am J Physiol. 1994 Feb;266(2 Pt 1):C515-23.

95. Gamba G, Miyanoshita A, Lombardi M, Lytton J, Lee WS, Hediger MA, et al. Molecular cloning, primary structure, and characterization of two members of the mammalian electroneutral sodium-(potassium)-chloride cotransporter family expressed in kidney. J Biol Chem. 1994 Jul 1;269(26):17713-22.

96. Gamba G, Saltzberg SN, Lombardi M, Miyanoshita A, Lytton J, Hediger MA, et al. Primary structure and functional expression of a cDNA encoding the thiazide-sensitive, electroneutral sodium-chloride cotransporter. Proc Natl Acad Sci U S A. 1993 Apr 1;90(7):2749-53.

97. Isenring P, Jacoby SC, Forbush B,3rd. The role of transmembrane domain 2 in cation transport by the na-K-cl cotransporter. Proc Natl Acad Sci U S A. 1998 Jun 9;95(12):7179-84.

98. Isenring P, Forbush B,3rd. Ion and bumetanide binding by the na-K-cl cotransporter. importance of transmembrane domains. J Biol Chem. 1997 Sep 26;272(39):24556-62.

99. Isenring P, Jacoby SC, Chang J, Forbush B. Mutagenic mapping of the na-K-cl cotransporter for domains involved in ion transport and bumetanide binding. J Gen Physiol. 1998 Nov;112(5):549-58.

100. Darman RB, Forbush B. A regulatory locus of phosphorylation in the N terminus of the na-K-cl cotransporter, NKCC1. J Biol Chem. 2002 Oct 4;277(40):37542-50.

101. Delpire E, Gagnon KB. SPAK and OSR1, key kinases involved in the regulation of chloride transport. Acta Physiol (Oxf). 2006 May-Jun;187(1-2):103-13.

102. Di Fulvio M, Lauf PK, Adragna NC. The NO signaling pathway differentially regulates KCC3a and KCC3b mRNA expression. Nitric Oxide. 2003 Nov;9(3):165-71.

103. Di Fulvio M, Lincoln TM, Lauf PK, Adragna NC. Protein kinase G regulates potassium chloride cotransporter-4 [corrected] expression in primary cultures of rat vascular smooth muscle cells. J Biol Chem. 2001 Jun 15;276(24):21046-52.

104. Di Fulvio M, Lauf PK, Adragna NC. Nitric oxide signaling pathway regulates potassium chloride cotransporter-1 mRNA expression in vascular smooth muscle cells. J Biol Chem. 2001 Nov 30;276(48):44534-40.

105. Di Fulvio M, Lauf PK, Shah S, Adragna NC. NONOates regulate KCl cotransporter-1 and -3 mRNA expression in vascular smooth muscle cells. Am J Physiol Heart Circ Physiol. 2003 May;284(5):H1686-92.

106. Payne JA, Stevenson TJ, Donaldson LF. Molecular characterization of a putative K-cl cotransporter in rat brain. A neuronal-specific isoform. J Biol Chem. 1996 Jul 5;271(27):16245-52.

107. Delpire E, Lauf PK. Kinetics of cl-dependent K fluxes in hyposmotically swollen low K sheep erythrocytes. J Gen Physiol. 1991 Feb;97(2):173-93.

108. Delpire E, Lauf PK. Kinetics of cl-dependent K fluxes in hyposmotically swollen low K sheep erythrocytes. J Gen Physiol. 1991 Feb;97(2):173-93.

109. Sarkadi B, Parker JC. Activation of ion transport pathways by changes in cell volume. Biochim Biophys Acta. 1991 Dec 12;1071(4):407-27.

110. Delpire E, Lauf PK. Trans effects of cellular K and cl on ouabain-resistant rb(K) influx in low K sheep red blood cells: Further evidence for asymmetry of K-cl cotransport [corrected. Pflugers Arch. 1991 Nov;419(5):540-2.

111. Jennings ML, al-Rohil N. Kinetics of activation and inactivation of swelling-stimulated K+/Cl- transport. the volume-sensitive parameter is the rate constant for inactivation. J Gen Physiol. 1990 Jun;95(6):1021-40.

112. Kahle KT, Rinehart J, Lifton RP. Phosphoregulation of the na-K-2Cl and K-cl cotransporters by the WNK kinases. Biochim Biophys Acta. 2010 Dec;1802(12):1150-8.

113. Kahle KT, Gimenez I, Hassan H, Wilson FH, Wong RD, Forbush B, et al. WNK4 regulates apical and basolateral cl- flux in extrarenal epithelia. Proc Natl Acad Sci U S A. 2004 Feb 17;101(7):2064-9.

114. Kahle KT, Rinehart J, de Los Heros P, Louvi A, Meade P, Vazquez N, et al. WNK3 modulates transport of cl- in and out of cells: Implications for control of cell volume and neuronal excitability. Proc Natl Acad Sci U S A. 2005 Nov 15;102(46):16783-8.

115. Kahle KT, Rinehart J, Ring A, Gimenez I, Gamba G, Hebert SC, et al. WNK protein kinases modulate cellular cl- flux by altering the phosphorylation state of the na-K-cl and K-cl cotransporters. Physiology (Bethesda). 2006 Oct;21:326-35.

116. Gagnon KB, England R, Delpire E. Volume sensitivity of cation-cl-cotransporters is modulated by the interaction of two kinases: Ste20-related proline-alanine-rich kinase and WNK4. Am J Physiol Cell Physiol. 2006 Jan;290(1):C134-42.

117. Delpire E, Gagnon KB. SPAK and OSR1: STE20 kinases involved in the regulation of ion homoeostasis and volume control in mammalian cells. Biochem J. 2008 Jan 15;409(2):321-31.

118. Lauf PK, Adragna NC. K-cl cotransport: Properties and molecular mechanism. Cell Physiol Biochem. 2000;10(5-6):341-54.

119. Kramhoft B, Lambert IH, Hoffmann EK, Jorgensen F. Activation of cl-dependent K transport in ehrlich ascites tumor cells. Am J Physiol. 1986 Sep;251(3 Pt 1):C369-79.

120. Lauf PK, Bauer J, Adragna NC, Fujise H, Zade-Oppen AM, Ryu KH, et al. Erythrocyte K-cl cotransport: Properties and regulation. Am J Physiol. 1992 Nov;263(5 Pt 1):C917-32.

121. Ellory JC, Dunham PB, Logue PJ, Stewart GW. Anion-dependent cation transport in erythrocytes. Philos Trans R Soc Lond B Biol Sci. 1982 Dec 1;299(1097):483-95.

122. Lauf PK. Thiol-dependent passive K/Cl transport in sheep red cells: II. loss of cl- and N-ethylmaleimide sensitivity in maturing high K+ cells. J Membr Biol. 1983;73(3):247-56.

123. Logue P, Anderson C, Kanik C, Farquharson B, Dunham P. Passive potassium transport in LK sheep red cells. modification by N-ethyl maleimide. J Gen Physiol. 1983 Jun;81(6):861-85.

124. Bauer J, Lauf PK. Thiol-dependent passive K/Cl transport in sheep red cells: III. differential reactivity of membrane SH groups with N-ethylmaleimide and iodoacetamide. J Membr Biol. 1983;73(3):257-61.

125. Mount DB, Mercado A, Song L, Xu J, George AL,Jr, Delpire E, et al. Cloning and characterization of KCC3 and KCC4, new members of the cation-chloride cotransporter gene family. J Biol Chem. 1999 Jun 4;274(23):16355-62.

126. Mount DB, Delpire E, Gamba G, Hall AE, Poch E, Hoover RS, et al. The electroneutral cation-chloride cotransporters. J Exp Biol. 1998 Jul;201(Pt 14):2091-102.

127. Watanabe M, Wake H, Moorhouse AJ, Nabekura J. Clustering of neuronal K+-cl- cotransporters in lipid rafts by tyrosine phosphorylation. J Biol Chem. 2009 Oct 9;284(41):27980-8.

128. Uvarov P, Ludwig A, Markkanen M, Soni S, Hubner CA, Rivera C, et al. Coexpression and heteromerization of two neuronal K-cl cotransporter isoforms in neonatal brain. J Biol Chem. 2009 May 15;284(20):13696-704.

129. Blaesse P, Guillemin I, Schindler J, Schweizer M, Delpire E, Khiroug L, et al. Oligomerization of KCC2 correlates with development of inhibitory neurotransmission. J Neurosci. 2006 Oct 11;26(41):10407-19.

130. Holtzman EJ, Kumar S, Faaland CA, Warner F, Logue PJ, Erickson SJ, et al. Cloning, characterization, and gene organization of K-cl cotransporter from pig and human kidney and C. elegans. Am J Physiol. 1998 Oct;275(4 Pt 2):F550-64.

131. Gillen CM, Forbush B,3rd. Functional interaction of the K-cl cotransporter (KCC1) with the na-K-cl cotransporter in HEK-293 cells. Am J Physiol. 1999 Feb;276(2 Pt 1):C328-36.

132. Di Fulvio, M., Lincoln, T.M., Lauf, P.K., Adragna, N.C. Protein kinase G regulates potassium chloride cotransporter-3 expression in primary cultures of rat vascular smooth muscle cells. The Journal of Biological Chemistry. 2001;276(24):21046-21052.

133. Wei WC, Akerman CJ, Newey SE, Pan J, Clinch NW, Jacob Y, et al. The potassium chloride cotransporter 2 (KCC2) promotes cervical cancer cell migration and invasion by an ion transport-independent mechanism. J Physiol. 2011 Sep 19.

134. Chen YF, Chou CY, Ellory JC, Shen MR. The emerging role of KCl cotransport in tumor biology. Am J Transl Res. 2010 Jun 18;2(4):345-55.

135. Hiki K, D'Andrea RJ, Furze J, Crawford J, Woollatt E, Sutherland GR, et al. Cloning, characterization, and chromosomal location of a novel human K+-cl- cotransporter. J Biol Chem. 1999 Apr 9;274(15):10661-7.

136. Race JE, Makhlouf FN, Logue PJ, Wilson FH, Dunham PB, Holtzman EJ. Molecular cloning and functional characterization of KCC3, a new K-cl cotransporter. Am J Physiol. 1999 Dec;277(6 Pt 1):C1210-9.

137. Adragna NC, Ferrell CM, Zhang J, Di Fulvio M, Temprana CF, Sharma A, et al. Signal transduction mechanisms of K+-cl- cotransport regulation and relationship to disease. Acta Physiol (Oxf). 2006 May-Jun;187(1-2):125-39.

138. Lauf PK, Di Fulvio M, Srivastava V, Sharma N, Adragna NC. KCC2a expression in a human fetal lens epithelial cell line. Cell Physiol Biochem. 2012;29(1-2):303-12.

139. Rivera C, Voipio J, Payne JA, Ruusuvuori E, Lahtinen H, Lamsa K, et al. The K+/Cl- co-transporter KCC2 renders GABA hyperpolarizing during neuronal maturation. Nature. 1999 Jan 21;397(6716):251-5.

140. Rivera C, Li H, Thomas-Crusells J, Lahtinen H, Viitanen T, Nanobashvili A, et al. BDNF-induced TrkB activation down-regulates the K+-cl- cotransporter KCC2 and impairs neuronal cl- extrusion. J Cell Biol. 2002 Dec 9;159(5):747-52.

141. Khirug S, Ahmad F, Puskarjov M, Afzalov R, Kaila K, Blaesse P. A single seizure episode leads to rapid functional activation of KCC2 in the neonatal rat hippocampus. J Neurosci. 2010 Sep 8;30(36):12028-35.

142. Canessa M. Red cell volume-related ion transport systems in hemoglobinopathies. Hematol Oncol Clin North Am. 1991 Jun;5(3):495-516.

143. Canessa M, Romero JR, Lawrence C, Nagel RL, Fabry ME. Rate of activation and deactivation of K:Cl cotransport by changes in cell volume in hemoglobin SS, CC and AA red cells. J Membr Biol. 1994 Dec;142(3):349-62.

144. Boettger T, Hubner CA, Maier H, Rust MB, Beck FX, Jentsch TJ. Deafness and renal tubular acidosis in mice lacking the K-cl co-transporter Kcc4. Nature. 2002 Apr 25;416(6883):874-8.

145. Adragna NC, Chen Y, Delpire E, Lauf PK, Morris M. Hypertension in K-cl cotransporter-3 knockout mice. Adv Exp Med Biol. 2004;559:379-85.

146. Rinehart J, Maksimova YD, Tanis JE, Stone KL, Hodson CA, Zhang J, et al. Sites of regulated phosphorylation that control K-cl cotransporter activity. Cell. 2009 8/7;138(3):525-36.

147. Vale C, Schoorlemmer J, Sanes DH. Deafness disrupts chloride transporter function and inhibitory synaptic transmission. J Neurosci. 2003 Aug 20;23(20):7516-24.

148. Adragna NC, Zhang J, Di Fulvio M, Lincoln TM, Lauf PK. KCl cotransport regulation and protein kinase G in cultured vascular smooth muscle cells. J Membr Biol. 2002 May 15;187(2):157-65.

149. Zhang J, Lauf PK, Adragna NC. PDGF activates K-cl cotransport through phosphoinositide 3-kinase and protein phosphatase-1 in primary cultures of vascular smooth muscle cells. Life Sci. 2005 Jul 15;77(9):953-65.

150. Zhang J, Lauf PK, Adragna NC. Platelet-derived growth factor regulates K-cl cotransport in vascular smooth muscle cells. Am J Physiol Cell Physiol. 2003 Mar;284(3):C674-80.

151. Ferrell CM, Lauf PK, Wilson BA, Adragna NC. Lithium and protein kinase C modulators regulate swelling-activated K-cl cotransport and reveal a complete phosphatidylinositol cycle in low K sheep erythrocytes. J Membr Biol. 2000 Sep 1;177(1):81-93.

152. Adragna NC, White RE, Orlov SN, Lauf PK. K-cl cotransport in vascular smooth muscle and erythrocytes: Possible implication in vasodilation. Am J Physiol Cell Physiol. 2000 Feb;278(2):C381-90.

153. Garg UC, Hassid A. Nitric oxide-generating vasodilators and 8-bromo-cyclic guanosine monophosphate inhibit mitogenesis and proliferation of cultured rat vascular smooth muscle cells. J Clin Invest. 1989 May;83(5):1774-7.

154. Pollman MJ, Yamada T, Horiuchi M, Gibbons GH. Vasoactive substances regulate vascular smooth muscle cell apoptosis. countervailing influences of nitric oxide and angiotensin II. Circ Res. 1996 Oct;79(4):748-56.

155. Murad F. What are the molecular mechanisms for the antiproliferative effects of nitric oxide and cGMP in vascular smooth muscle? Circulation. 1997 Mar 4;95(5):1101-3.

156. Shen MR, Chou CY, Ellory JC. Swelling-activated taurine and K+ transport in human cervical cancer cells: Association with cell cycle progression. Pflugers Arch. 2001 Mar;441(6):787-95.

157. Hsu YM, Chou CY, Chen HH, Lee WY, Chen YF, Lin PW, et al. IGF-1 upregulates electroneutral K-cl cotransporter KCC3 and KCC4 which are differentially required for breast cancer cell proliferation and invasiveness. J Cell Physiol. 2007 Mar;210(3):626-36.

158. Shen MR, Chou CY, Hsu KF, Hsu YM, Chiu WT, Tang MJ, et al. KCl cotransport is an important modulator of human cervical cancer growth and invasion. J Biol Chem. 2003 Oct 10;278(41):39941-50.

159. Shen MR, Chou CY, Hsu KF, Liu HS, Dunham PB, Holtzman EJ, et al. The KCl cotransporter isoform KCC3 can play an important role in cell growth regulation. Proc Natl Acad Sci U S A. 2001 Dec 4;98(25):14714-9.

160. Shen MR, Lin AC, Hsu YM, Chang TJ, Tang MJ, Alper SL, et al. Insulin-like growth factor 1 stimulates KCl cotransport, which is necessary for invasion and proliferation of cervical cancer and ovarian cancer cells. J Biol Chem. 2004 Sep 17;279(38):40017-25.

161. Panet R, Atlan H. Bumetanide-sensitive Na+/K+/Cl- transporter is stimulated by phorbol ester and different mitogens in quiescent human skin fibroblasts. J Cell Physiol. 1990 Oct;145(1):30-8.

162. Sardet C, Counillon L, Franchi A, Pouyssegur J. Growth factors induce phosphorylation of the Na+/H+ antiporter, glycoprotein of 110 kD. Science. 1990 Feb 9;247(4943):723-6.

163. Schwab A. Ion channels and transporters on the move. News Physiol Sci. 2001 Feb;16:29-33.

164. Wei WC, Akerman CJ, Newey SE, Pan J, Clinch NW, Jacob Y, et al. The potassium-chloride cotransporter 2 promotes cervical cancer cell migration and invasion by an ion transport-independent mechanism. J Physiol. 2011 Nov 15;589(Pt 22):5349-59.

165. Becchetti A, Arcangeli A. Integrins and ion channels in cell migration: Implications for neuronal development, wound healing and metastatic spread. Adv Exp Med Biol. 2010;674:107-23.

166. Sukhanov S, Hua Song Y, Delafontaine P. Global analysis of differentially expressed genes in oxidized LDL-treated human aortic smooth muscle cells. Biochem Biophys Res Commun. 2003 Jun 27;306(2):443-9.

167. Gagnon KBE. Localization and functional properties of KCC1 and KCC2, two isoforms of the K-C1 cotransporter, in the mammalian central nervous system. ; 2003.

168. Jones BA, Aly HM, Forsyth EA, Sidawy AN. Phenotypic characterization of human smooth muscle cells derived from atherosclerotic tibial and peroneal arteries. Journal of Vascular Surgery. 1996 11;24(5):883-91.

169. Boerth NJ, Dey NB, Cornwell TL, Lincoln TM. Cyclic GMP-dependent protein kinase regulates vascular smooth muscle cell phenotype. J Vasc Res. 1997 Jul-Aug;34(4):245-59.

170. Lauf PK. Thiol-dependent passive K/Cl transport in sheep red cells: II. loss of cl- and N-ethylmaleimide sensitivity in maturing high K+ cells. J Membr Biol. 1983;73(3):247-56.

171. Lauf PK, Misri S, Chimote AA, Adragna NC. Apparent intermediate K conductance channel hyposmotic activation in human lens epithelial cells. Am J Physiol Cell Physiol. 2008 Mar;294(3):C820-32.

172. Hannemann A, Flatman PW. Phosphorylation and transport in the na-K-2Cl cotransporters, NKCC1 and NKCC2A, compared in HEK-293 cells. PLoS One. 2011 Mar 25;6(3):e17992.

173. O'Brien WJ, Lingrel JB, Wallick ET. Ouabain binding kinetics of the rat alpha two and alpha three isoforms of the sodium-potassium adenosine triphosphate. Arch Biochem Biophys. 1994 Apr;310(1):32-9.

174. Juhaszova M, Blaustein MP. Na+ pump low and high ouabain affinity alpha subunit isoforms are differently distributed in cells. Proc Natl Acad Sci U S A. 1997 Mar 4;94(5):1800-5.

175. Lauf PK. Volume and anion dependency of ouabain-resistant K-rb fluxes in sheep red blood cells. Am J Physiol. 1988 Sep;255(3 Pt 1):C331-9.

176. Lauf PK. K+:Cl- cotransport: Sulfhydryls, divalent cations, and the mechanism of volume activation in a red cell. J Membr Biol. 1985;88(1):1-13.

177. Beamish JA, He P, Kottke-Marchant K, Marchant RE. Molecular regulation of contractile smooth muscle cell phenotype: Implications for vascular tissue engineering. Tissue Eng Part B Rev. 2010 Oct;16(5):467-91.

178. Slomp J, Gittenberger-de Groot AC, Glukhova MA, Conny van Munsteren J, Kockx MM, Schwartz SM, et al. Differentiation, dedifferentiation, and apoptosis of smooth muscle cells during the development of the human ductus arteriosus. Arterioscler Thromb Vasc Biol. 1997 May;17(5):1003-9.

179. Gabbiani G, Schmid E, Winter S, Chaponnier C, de Ckhastonay C, Vandekerckhove J, et al. Vascular smooth muscle cells differ from other smooth muscle cells: Predominance of vimentin filaments and a specific alpha-type actin. Proc Natl Acad Sci U S A. 1981 Jan;78(1):298-302.

180. Mercado A, de los Heros P, Vazquez N, Meade P, Mount DB, Gamba G. Functional and molecular characterization of the K-cl cotransporter of xenopus laevis oocytes. Am J Physiol Cell Physiol. 2001 Aug;281(2):C670-80.

181. Gibson, J.S., Ellory, J.C., Adragna, N.C., Lauf, P.K. Pathophysiology of the K^+-Cl^- Cotransporters: Paths to discovery and overview. In: F. Javier Alvarez-Leefmans and Eric Delpire, editor. Physiology and Pathology of Chloride Transporters and Channels in the Nervous System. 1st ed. UK: Elsevier Inc.; 2009. p. 27.

182. Gagnon KB, Adragna NC, Fyffe RE, Lauf PK. Characterization of glial cell K-cl cotransport. Cell Physiol Biochem. 2007;20(1-4):121-30.

183. Capo-Aponte JE, Wang Z, Bildin VN, Iserovich P, Pan Z, Zhang F, et al. Functional and molecular characterization of multiple K-cl cotransporter isoforms in corneal epithelial cells. Exp Eye Res. 2007 Jun;84(6):1090-103.

184. Adragna NC, Zhang J, Di Fulvio M, Lincoln TM, Lauf PK. KCl cotransport regulation and protein kinase G in cultured vascular smooth muscle cells. J Membr Biol. 2002 May 15;187(2):157-65.

185. Jennings ML, Schulz RK. Okadaic acid inhibition of KCl cotransport. evidence that protein dephosphorylation is necessary for activation of transport by either cell swelling or N-ethylmaleimide. J Gen Physiol. 1991 Apr;97(4):799-817.

186. Starke LC, Jennings ML. K-cl cotransport in rabbit red cells: Further evidence for regulation by protein phosphatase type 1. Am J Physiol. 1993 Jan;264(1 Pt 1):C118-24.

187. Flatman PW, Adragna NC, Lauf PK. Role of protein kinases in regulating sheep erythrocyte K-cl cotransport. Am J Physiol. 1996 Jul;271(1 Pt 1):C255-63.

188. Carpenter CL. Actin cytoskeleton and cell signaling. Crit Care Med. 2000 Apr;28(4 Suppl):N94-9.

189. Suetsugu S, Takenawa T. Regulation of cortical actin networks in cell migration. Int Rev Cytol. 2003;229:245-86.

190. Schwab A, Nechyporuk-Zloy V, Fabian A, Stock C. Cells move when ions and water flow. Pflugers Arch. 2007 Jan;453(4):421-32.

191. Chen YF, Chou CY, Ellory JC, Shen MR. The emerging role of KCl cotransport in tumor biology. Am J Transl Res. 2010 Jun 18;2(4):345-55.

192. Rzucidlo, E.M. , Martin, K.A. and Powell, R.J. Regulation of vascular smooth muscle cells differentiation. JOURNAL OF VASCULAR SURGERY. June 2007;45(A):25A-32A.

193. Medhurst AD, Jennings CA, Robbins MJ, Davis RP, Ellis C, Winborn KY, et al. Pharmacological and immunohistochemical characterization of the APJ receptor and its endogenous ligand apelin. J Neurochem. 2003 Mar;84(5):1162-72.

194. Jay MT, Chirico S, Siow RC, Bruckdorfer KR, Jacobs M, Leake DS, et al. Modulation of vascular tone by low density lipoproteins: Effects on L-arginine transport and nitric oxide synthesis. Exp Physiol. 1997 Mar;82(2):349-60.

195. Chikani G, Zhu W, Smart EJ. Lipids: Potential regulators of nitric oxide generation. Am J Physiol Endocrinol Metab. 2004 Sep;287(3):E386-9.

196. Kamal FA, Travers JG, Blaxall BC. G protein-coupled receptor kinases in cardiovascular disease: Why "where" matters. Trends Cardiovasc Med. 2012 Nov;22(8):213-9.

197. Cudnoch Jedrzejewska A, Czarzasta K, Gomolka R, Szczepanska Sadowska E. The role of apelin in pathogenesis of cardiovascular diseases and metabolic disorders. Kardiol Pol. 2011;69 Suppl 3:89-93.

198. Zeng XJ, Zhang LK, Wang HX, Lu LQ, Ma LQ, Tang CS. Apelin protects heart against ischemia/reperfusion injury in rat. Peptides. 2009 Jun;30(6):1144-52.

199. Simpkin JC, Yellon DM, Davidson SM, Lim SY, Wynne AM, Smith CC. Apelin-13 and apelin-36 exhibit direct cardioprotective activity against ischemia-reperfusion injury. Basic Res Cardiol. 2007 Nov;102(6):518-28.

200. Kleinz MJ, Skepper JN, Davenport AP. Immunocytochemical localisation of the apelin receptor, APJ, to human cardiomyocytes, vascular smooth muscle and endothelial cells. Regul Pept. 2005 Mar 30;126(3):233-40.

201. Lee DK, Lanca AJ, Cheng R, Nguyen T, Ji XD, Gobeil F,Jr, et al. Agonist-independent nuclear localization of the apelin, angiotensin AT1, and bradykinin B2 receptors. J Biol Chem. 2004 Feb 27;279(9):7901-8.

202. El Messari S, Iturrioz X, Fassot C, De Mota N, Roesch D, Llorens-Cortes C. Functional dissociation of apelin receptor signaling and endocytosis: Implications for the effects of apelin on arterial blood pressure. J Neurochem. 2004 Sep;90(6):1290-301.

203. Tasci I, Dogru T, Naharci I, Erdem G, Yilmaz MI, Sonmez A, et al. Plasma apelin is lower in patients with elevated LDL-cholesterol. Exp Clin Endocrinol Diabetes. 2007 Jul;115(7):428-32.

204. Falcone C, Buzzi MP, D'Angelo A, Schirinzi S, Falcone R, Rordorf R, et al. Apelin plasma levels predict arrhythmia recurrence in patients with persistent atrial fibrillation. Int J Immunopathol Pharmacol. 2010 Jul-Sep;23(3):917-25.

205. Shi XL, Wang GL, Zhang Z, Liu YJ, Chen JH, Zhou JG, et al. Alteration of volume-regulated chloride movement in rat cerebrovascular smooth muscle cells during hypertension. Hypertension. 2007 Jun;49(6):1371-7.

206. Schiff JD, Overweg NI. Effects of increasing osmolality on rat ileal smooth muscle. Pflugers Arch. 1980 Dec;389(1):75-9.

207. de Los Heros P, Kahle KT, Rinehart J, Bobadilla NA, Vazquez N, San Cristobal P, et al. WNK3 bypasses the tonicity requirement for K-cl cotransporter activation via a phosphatase-dependent pathway. Proc Natl Acad Sci U S A. 2006 Feb 7;103(6):1976-81.